

Eddy covariance and scintillation measurements of atmospheric exchange processes over different types of vegetation

Promotor:

Dr. ir. J. Goudriaan

Persoonlijk hoogleraar bij de leerstoelgroep theoretische productie-
ecologie

Co-promotor:

Dr. ir. A.F.G. Jacobs

Universitair hoofddocent bij de leerstoelgroep meteorologie &
luchtkwaliteit

1108-201, 2394

J.P. Nieveen

**EDDY COVARIANCE AND SCINTILLATION
MEASUREMENTS OF ATMOSPHERIC EXCHANGE
PROCESSES OVER DIFFERENT TYPES OF VEGETATION**

Proefschrift

ter verkrijging van de graad van doctor
op gezag van de rector magnificus
van de Landbouwniversiteit Wageningen,
dr. C.M. Karssen,
in het openbaar te verdedigen op
woensdag 7 april 1999
des namiddags te vier uur in de Aula.

bn 903909

CIP-DATA KONINKLIJKE BIBLIOTHEEK DEN HAAG

Nieveen, J.P.

Eddy covariance and scintillation measurements of atmospheric exchange processes over different types of vegetation. / J.P. Nieveen.- [S.l.:s.n.]

Thesis Landbouwniversiteit Wageningen. – With ref. – With summary in Dutch.

ISBN 90-5808-028-5

Subject headings: Meteorological measurements; peat bog / CO₂ / Scintillation measurements



- Cover page by Theo Nieveen
- This study was carried out at the Meteorology and Air Quality Group of the Wageningen Agricultural University, the Netherlands. Funding for this work was supported by the Netherlands Organisation for Scientific Research under project number 753-06-234.

BIBLIOTHEEK
LANDEBOUWUNIVERSITEIT
WAGENINGEN

Stellingen behorend bij het proefschrift van Joost Nieveen

EDDY COVARIANCE AND SCINTILLATION MEASUREMENTS OF ATMOSPHERIC EXCHANGE PROCESSES OVER DIFFERENT TYPES OF VEGETATION

1. De uitwisseling van kooldioxide van veengebieden met de atmosfeer wordt in hoge mate bepaald door het bodemklimaat (*Dit proefschrift*).
2. Het parametriseren van atmosferische uitwisselingsprocessen van veengebieden voor klimaatmodellen is door de grote mondiale verscheidenheid een uitdagende opdracht (*Dit proefschrift*).
3. Langjarige eddy-covariantie metingen van de uitwisseling van kooldioxide van ecosystemen leveren een grotere toegevoegde waarde als micrometeorologen, plantfysiologen, biochemici, modellers en experimentalisten meer samenwerken (*Baldocchi, D.D., Valentini, R., Running, S., Oechel, W. and Dahlman, R.: 1996, 'Strategies for measuring and modelling carbon dioxide and water vapour fluxes over terrestrial ecosystems', Global Change Biology., 2, 159-168*).
4. Het gebruik van de 940 nm golflengte voor de scintillometer met grote openingshoek kan vooral onder (bijna) neutrale en stabiele atmosferische omstandigheden tot aanzienlijke fouten leiden bij het bepalen van de structuurparameter van temperatuur uit de structuurparameter van brekingsindex (*Dit proefschrift*).
5. De uit de zeventiger jaren stammende gewasfactoren voor het bepalen van de "potentiële" gewasverdamping uit de referentieverdamping volgens Makkink zijn nodig aan een algemene periodieke keuring toe.
6. De gemoedstoestand "druk-druk-druk" is geen psychisch probleem maar een probleem voor en door de maatschappij.
7. Een sterke reductie van het gebruik van de hoeveelheid chemische gewasbeschermingsmiddelen in de landbouw kan bereikt worden door rekening te houden met de (verwachte) weersomstandigheden (*Wartena, L. en Bouma, E.: 1998, Agrarisch weerboek; Optimaal inspelen op alle weersomstandigheden, Roodbont, Zutphen, pp. 176*).
8. De enige oplossing voor de uitbreiding van Schiphol is het verplaatsen van de omliggende woonkernen naar de Flevopolder.

VOORWOORD

-
-
-

Het is gelukt! Bijna vijf en half jaar na aanvang en 3 veldexperimenten verder is het resultaat een 122 pagina's tellend proefschrift. Hoewel in de laatste paar jaren het werk sterk individueel is geweest, is de inbreng van een aanzienlijk aantal mensen onmisbaar geweest.

Voor experimenteel werk is technische ondersteuning onontbeerlijk. Daarom Teun Jansen, Willy Hillen, Frits Antonysen, Dick Welgraven en Bert Heusinkveld bedankt voor: het opzetten en toerusten van masten, het betere draai- en freeswerk, vlonders en dekzeilen, AD630jes, PCAD, soldeertin en het nodige sjouwwerk, kortom jullie inzet en vakmanschap. Volgende keer weer op een droge ondergrond. Bert en Frits wil ik extra bedanken voor respectievelijk hun inventiviteit en vocale levensbeschouwing tijdens de talloze retourtjes Appelscha. Gerrie van den Brink en Kees van den Dries bedankt voor het scheppen van belangrijke randvoorwaarden voor het project.

Voor de dagelijkse bijstand gaat alle eer naar mijn copromotor, Adrie Jacobs. Jouw vertrouwen, 'kritische woorden' en optimisme hebben mij zelfvertrouwen gegeven om mijn doel te bereiken; prima joh. Mijn promotor, Jan Goudriaan, wil ik bedanken voor zijn inspirerende en heldere commentaar op mijn werk. Graag had ik nog iets langer en intensiever willen samenwerken, maar liet de situatie dat niet toe.

Naast de begeleiding van hogere hand, heb ook te kort samengewerkt met Cor Jacobs en Rushdi El-Kilani, die beide als Postdocs bij het SLIMM project betrokken zijn geweest. Corretje bedankt en Rushdi Al-Hamedo le ALLAH bedankt. In dit kader wil ik ook Wim Kohsiek bedanken voor zijn enthousiasme en inzicht.

New Zealand has played and plays an important role in my life. My contacts with the Hort Research Environmental Physics Group during my MSc degree has lead to three cooperative field experiments on the Purerua Peninsula and near the Ahipara settlement (great surf). Therefore, I would like to say 'cheers for everything' to Mark Astill and Phil Prendergast. A special word of gratitude goes to Alan Green. Thanks mate for your

enthusiasm, for being a colleague and most of all for being a friend.

Duivendaal is een prima stek geweest de afgelopen vijf en een half jaar. Ondanks alle perikelen is de sfeer er één geweest die mij zeer aansprak. Daarvoor heeft iedereen zijn eigen bijdrage geleverd, dus: Job, Berenice, Anne-Wim, Henk, Leo, Jon, Michaël, Ad, Ton, Rolf, Bart, Anne, Bas, Reinder, Wouter, Oscar, Arjan en Arnold ook jullie bedankt.

CONTENTS

-
-
-

LIST OF SYMBOLS AND ABBREVIATIONS V

1. GENERAL INTRODUCTION 1

1.1. Background 1
1.2. From canopy to global scales 2
1.3. The SLIMM project 4
 1.3.1. General 4
 1.3.2. The contribution and objectives of the WAU 6
1.4. Organisation of the thesis 6

**2. DIURNAL AND SEASONAL VARIATION OF CARBON DIOXIDE
EXCHANGE FROM A FORMER TRUE RAISED BOG 8**

Global Change Biology, 4 (8): 823–834, 1998

2.1. Introduction 8
2.2. Material and Methods 9
 2.2.1. Site description 9
 2.2.2. Instrumentation 10
 2.2.3. Data acquisition and –processing 12
 2.2.4. Plant measurements 13
2.3. Results 13
 2.3.1. Leaf area index 13
 2.3.2. Diurnal CO₂ exchange 14

2.3.3. Seasonal variations of CO ₂ exchange	16
2.3.3.1. Carbon balance.....	16
2.3.3.2. Daytime CO ₂ flux densities	18
2.3.3.3. Nighttime CO ₂ flux densities; respiration.....	18
2.3.4. Effect of light on CO ₂ exchange	20
2.3.5. Effect of vapour pressure deficit on CO ₂ exchange.....	21
2.4. Discussion.....	23
Acknowledgements.....	24

3. THE EFFECT OF SURFACE COVER, VAPOUR PRESSURE DEFICIT AND TEMPERATURE ON THE CARBON DIOXIDE AND WATER VAPOUR FLUX DENSITIES OF A DISTURBED RAISED PEAT BOG25

Submitted to Agricultural and Forest Meteorology, 1998

3.1. Introduction.....	25
3.2. Materials and methods	27
3.2.1. Site description.....	27
3.2.2. Instrumentation	28
3.2.3. Data acquisition and –processing.....	29
3.2.3. The leaf area index.....	30
3.3. Results and discussion	31
3.3.1. Seasonal variation of environmental conditions and LAI.....	31
3.3.2. Variation of CO ₂ and latent heat exchange due to the local climate and vegetation	32
3.3.2.1. Seasonal variation of diurnal CO ₂ flux densities	32
3.3.2.2. Seasonal variation of diurnal latent heat flux densities	35
3.3.3. Net CO ₂ exchange and transpiration versus stomatal closure and surface temperature	37
3.3.4. Relationship between CO ₂ flux density and latent heat flux density.....	43
3.3.4.1. Relationship between CO ₂ flux density and temperature	43
3.3.4.2. Water use efficiency.....	45
3.3.5. Surface resistance.....	46
3.3.6. Atmospheric coupling.....	47
3.4. Summary and conclusions	49

Acknowledgements	50
4. THE SCINTILLATION TECHNIQUE	51
4.1. Introduction	51
4.2. Atmospheric turbulence	52
4.3. Propagation of light through a turbulent atmosphere and the Large Aperture Scintillometer	53
4.4. From scintillation to the refractive index structure parameter	55
4.5. The large aperture scintillometer	56
4.6. Estimation of the sensible heat flux density from C_n^2	56
4.7. The effect of absorption fluctuations	59
5. MEASURING SENSIBLE HEAT FLUX OVER PASTURE USING THE C_T^2-PROFILE METHOD	61
<i>Boundary-Layer Meteorology, 1999 (In press)</i>	
5.1. Introduction	61
5.2. Theory	63
5.3. Experimental	64
5.3.1. Site description and weather conditions	64
5.3.2. Data collection and instrumentation	66
5.4. Results and discussion	67
5.4.1. Scaling C_T^2 with height	67
5.4.2. Comparing the profile and eddy covariance methods	69
5.5. Summary	71
Acknowledgments	72
6. USING A LARGE APERTURE SCINTILLOMETER TO MEASURE ABSORPTION AND REFRACTIVE INDEX FLUCTUATIONS	75
<i>Boundary-Layer Meteorology, 87, 101-116, 1998</i>	
6.1. Introduction	75
6.2. Theory	77

6.3. The calculation of C_n^2 and C_Q^2	81
6.4. Experimental	82
6.4.1. Site description.....	82
6.4.2. Large aperture scintillometer	83
6.4.3. Instrumentation and data collection	83
6.5. Results and discussion	84
6.6. Conclusions.....	89
Acknowledgements.....	90
7. GENERAL CONCLUSIONS AND RECOMMENDATIONS	91
7.1. Introduction.....	91
7.2. Eddy covariance measurements.....	91
7.3. Scintillation measurements	92
SUMMARY	95
SAMENVATTING	101
REFERENCES.....	107
CURRICULUM VITAE.....	121

LIST OF SYMBOLS

-
-
-

Abbreviations and acronyms

<i>ABL</i>	Atmospheric Boundary–Layer
<i>EM</i>	Electro Magnetic
<i>GCM</i>	General Circulation Model
<i>IBL</i>	Internal Boundary–Layer
<i>IPCC</i>	Intergovernmental Panel on Climate Change
<i>IRGA</i>	InfraRed Gas Analyser
<i>LAI</i>	Leaf Area Index
<i>LAS</i>	Large Aperture Scintillometer
<i>LT</i>	Local Time
<i>PAR</i>	Photosynthetically Active Radiation
<i>RASS</i>	Radio Acoustic Sounding System
<i>SLIMM</i>	Surface Layer Integration Measurements and Modelling
<i>SODAR</i>	Sound Detection and Ranging technique
<i>UTC</i>	Universal Time Co–ordinated
<i>WAU</i>	Wageningen Agricultural University

Symbol	Description	Unit
<i>Greek</i>		
β	Bowen ratio	[–]
β	Total absorption coefficient for a band of absorption lines, with subscript:	[–]
	– <i>i</i> absorption coefficient of single absorption line	
	– <i>c</i> continuum absorption	
γ	Psychrometer ‘constant’ (0.67 at 20 °C)	[hPa K ⁻¹]
χ	Logarithmic amplitude of the optical wave	[–]
ΔS	Integrated energy storage term over the canopy	[W m ⁻²]
ϵ	Surface emissivity	[–]
κ	Von Karman constant (0.4)	[–]
λ	Optical wavelength	[m]
λ	Latent heat of vaporisation (2.46 x 10 ⁶)	[J kg ⁻¹]
λE	Latent heat flux density, with subscript:	[W m ⁻²]
	– <i>ec</i> measured by the eddy covariance technique	
ξ	Geometric mean of z_H/L_o and z_L/L_o	[–]

ρ	Density of air	$[\text{kg m}^{-3}]$
σ	Boltzman constant (5.67×10^{-8})	$[\text{W m}^{-2} \text{K}^{-4}]$
σ^2	Variance, with subscript:	$[-]$
	$-\chi$ the logarithmic amplitude	$[-]$
	$-\ln I$ the logarithmic intensity	$[-]$
	$-I$ the intensity	$[\text{W}^2 \text{m}^{-4}]$
Φ	Three dimensional spatial power spectrum	$[\text{m}^3]$
ψ	Integrated stability function	$[-]$
Ω	Decoupling factor (McNaughton & Jarvis, 1983)	$[-]$

General

A	Wavelength dependent constant, with subscript:	$[-]$
	$-T$ for temperature	
	$-Q$ for humidity	
b_{Qi}	The relation between the absorption line shape and the humidity	$[-]$
B	Wavelength dependent constant, with subscript:	$[-]$
	$-T$ for temperature	
	$-Q$ for humidity	
c_A	Empirical constant derived from the Kansas data	$[-]$
c_B	Empirical constant derived from the Kansas data	$[-]$
C_n^2	Refractive index structure parameter, with subscript:	$[\text{m}^{-2/3}]$
	$-I$ imaginary part due to absorption	
	$-R$ real part due to refraction	
C_p	Heat capacity of air at constant pressure (1005)	$[\text{J kg}^{-1} \text{K}^{-1}]$
C_Q^2	Humidity structure parameter	$[\text{kg}^2 \text{m}^{-6} \text{m}^{-2/3}]$
C_T^2	Temperature structure parameter, with subscript:	$[\text{K m}^{-2/3}]$
	$-H$ measured at upper height	
	$-L$ measured at lower height	
D	Atmospheric vapour pressure deficit at a reference height	$[\text{Pa}]$
D	Aperture diameter	$[\text{m}]$
d	Displacement height	$[\text{m}]$
$D_n(r)$	Refractive index structure function	$[-]$
E	Evaporation rate	$[\text{kg m}^{-2} \text{s}^{-1}]$
F_c	CO ₂ flux density	$[\text{mg m}^{-2} \text{s}^{-1}]$
G	Soil heat flux density	$[\text{W m}^{-2}]$
g	gravitational acceleration (9.81)	$[\text{m s}^{-2}]$
H	Sensible heat flux density, with subscript:	$[\text{W m}^{-2}]$
	$-ec$ measured by the eddy covariance technique	
	$-sc$ obtained by the scintillation technique	
I	Light intensity fluctuations	
k	Optical wave number ($2\pi\lambda^{-1}$)	$[\text{m}^{-1}]$
K	Atmospheric wave number	$[\text{m}^{-1}]$
L	Optical propagation path length	$[\text{m}]$
L_o	Obukhov length	$[\text{m}]$
l_o	Inner scale of turbulence	$[\text{m}]$
L_o	Outer scale of turbulence	$[\text{m}]$
LAI	Leaf area index	$[\text{m}^2 \text{m}^{-2}]$
n	Refractive index of the air	$[-]$
P	Atmospheric pressure	$[\text{Pa}]$

<i>PAR</i>	Photosynthetically active radiation	$[\mu\text{mol m}^{-2} \text{s}^{-1}]$
<i>Q*</i>	Humidity scaling parameter	$[\text{kg m}^{-3}]$
<i>Q₁₀</i>	Ratio of the rate at one temperature to that at a temperature 10 degrees lower	$[-]$
<i>r</i>	Distance within the inertial subrange	$[\text{m}]$
<i>r_a</i>	Aerodynamic resistance	$[\text{s m}^{-1}]$
<i>r_{aM}</i>	Aerodynamic resistance to momentum transport	$[\text{s m}^{-1}]$
<i>R</i>	Aperture radius, with subscript: <i>-t</i> transmitter <i>-r</i> receiver	$[\text{m}]$
<i>Rd</i>	Total respiration, expressed in CO ₂	$[\text{mg m}^{-2} \text{s}^{-1}]$
<i>Rn</i>	Net radiation	$[\text{W m}^{-2}]$
<i>Rs</i>	Incoming global radiation	$[\text{W m}^{-2}]$
<i>r_s</i>	Bulk surface resistance	$[\text{s m}^{-1}]$
<i>r_{sc}</i>	Ratio of two heights	$[-]$
<i>r_{TQ}</i>	Correlation coefficient between temperature and humidity	$[-]$
<i>s</i>	Rate of change of the saturated vapour pressure with temperature	$[\text{hPa K}^{-1}]$
<i>T</i>	Air temperature	$[\text{°C}]$
<i>T*</i>	Temperature scaling parameter	$[\text{K}]$
<i>T_a</i>	Air temperature at a reference level	$[\text{°C}]$
<i>T_{opt}</i>	Optimum temperature for photosynthesis	$[\text{°C}]$
<i>T_s</i>	Soil temperature at a reference depth	$[\text{°C}]$
<i>T_{surface}</i>	Surface temperature	$[\text{°C}]$
<i>u</i>	Horizontal wind speed at a reference height	$[\text{m s}^{-1}]$
<i>u*</i>	Friction velocity	$[\text{m s}^{-1}]$
<i>v</i>	Horizontal wind speed perpendicular to the propagation path	$[\text{m s}^{-1}]$
<i>W(z)</i>	Spatial weighting-function for $C_n^2(z)$ along the propagation path	$[-]$
<i>W_{χ(f)}</i>	Temporal spectral density of the log amplitude fluctuations with subscript: <i>-I</i> imaginary part due to absorption <i>-R</i> real part due to refraction	$[\text{s}]$
<i>z</i>	Reference height, with subscript: <i>-H</i> upper height <i>-L</i> lower height	$[\text{m}]$
<i>z₀</i>	Roughness length	$[\text{m}]$

CHAPTER I

-
-
-

GENERAL INTRODUCTION

1.1. Background

The exchange of energy and mass is of crucial importance to life on earth. Energy is the driving force for the biogeochemical cycles of e.g. carbon and water, which in turn play important roles in the functioning of our weather and climate. In the carbon cycle, carbon dioxide is fixed by the biosphere into carbohydrates, using solar energy and releasing oxygen to the atmosphere. Vice versa, oxidation of organic compounds supplies energy to the biosphere, releasing carbon dioxide back into the atmosphere at the expense of oxygen. In the water cycle, water vapour is transferred from the biosphere to the atmosphere by evaporation. Global redistribution of both latent and sensible energy as generated at the surface results in the atmospheric circulation of air i.e. weather and climate (Schmugge & André, 1991). In the process, latent energy is released and precipitation will transport water from the atmosphere back to the biosphere.

Also, atmospheric carbon dioxide and water vapour are strong absorbers of infrared radiation. This prevents the earth from cooling to a much lower equilibrium temperature as would result from the balance of absorbed solar (short wave) radiation and the emitted terrestrial (long wave) radiation. This so-called 'greenhouse effect' has received much attention over the past decades, as an increase in these radiatively active gases will probably cause a global rise in temperature and other shifts in climate forcing. The fact is the concentrations of green house gases, such as carbon dioxide, have significantly increased. Since the industrial revolution, the carbon dioxide concentration in the atmosphere has grown from 280 ppm to 360 ppm (Cowan *et al.*, 1994). By the end of the next century this figure may again have doubled as predicted by the International Panel on Climate Change (IPCC) (Houghton *et al.*, 1995).

Sound comprehension of the energy and mass cycles and their effect on climate

dynamics is crucial to understanding, predicting and anticipating ecological changes due to possible future climate perturbations (Baldocchi *et al.*, 1996). Direct and long-term flux density measurements of greenhouse gases from ecosystems provide means to supply such fundamental knowledge. These data could then be used to calculate the annual net exchange of for example carbon dioxide and water vapour from these ecosystems, and understand the biological and climate processes responsible for the exchange at canopy scale (Wolfsy *et al.*, 1993; Baldocchi *et al.*, 1996; Tans *et al.*, 1996). For the global cycles, however, extrapolating from canopy flux density measurements to global cycles leads to practical and theoretical problems (Jarvis & McNaughton, 1986; Parry *et al.*, 1988) as the interactions between different spatial scales become important (Garratt, 1993; Jacobs, 1994).

1.2. From canopy to global scales

Climate refers to a long-term mean state of the atmosphere over a range of spatial scales (Garratt, 1992), interacting through complex non-linear feedback mechanisms (e.g. Shuttleworth, 1988; Jacobs, 1994). At the canopy scale the surface energy balance (e.g. Garratt, 1992) is given by:

$$R_n - G = H + \lambda E + \Delta S. \quad (1.1)$$

Here R_n is the net radiation, G the soil heat flux density, H the sensible heat flux density, λE the latent heat flux density and ΔS the integrated energy storage term over the canopy, all expressed in [W m^{-2}]. Generally, ΔS is neglected, but could become important in special cases, such as during nighttime exchange processes (Jacobs *et al.*, 1996). The redistribution of the available energy ($R_n - G$) in sensible and latent heat depends on the soil, surface and atmospheric conditions and is related to the exchange of carbon dioxide and other trace gases through micrometeorological, biogeochemical and eco-physiological principles (e.g. Schimel *et al.*, 1991, Baldocchi & Meyers, 1997).

The soil-vegetation-atmosphere exchange of water vapour and carbon dioxide from different types of homogeneous (vegetated) surfaces has been and still is a primary research topic in meteorology, plant physiology and hydrology. In the early days, plant physiologists focussed on stomatal control of carbon dioxide and water vapour exchange, where the first experiments date back to the eighteenth century (Jarvis & McNaughton, 1986). Meteorologists, on the other hand, approached these processes from a physical rather than a physiological angle. The state of the atmospheric boundary layer (*ABL*) was believed to be the

driving force for the surface exchange processes, first demonstrated by Thornthwaite (Jarvis & McNaughton, 1986). Today, many environmental and plant related factors have been shown to influence stomatal behaviour and with it the exchange carbon dioxide and water vapour at canopy scale (see e.g. Meidner & Mansfield, 1968; Ruimy *et al.* 1995; Farquhar *et al.* 1980; Lösch & Tenhunen, 1981; Schulze *et al.*, 1987).

Often stomatal response demonstrates a highly non-linear relationship with these factors. For example, stomata generally close at low and open at high light intensities (Meidner & Mansfield, 1968). At the same time, the stomatal sensitivity to low light intensities is often greater than at high intensities (Burrows & Millthorpe, 1976) depending on the physiological and growth conditions of the canopy and other environmental factors (Ruimy *et al.*, 1995). Furthermore, complex feedback mechanisms between these factors can enhance or reduce stomatal response to a single factor. For instance, surface temperature and vapour pressure deficit, are often closely related. High surface temperatures increase the speed of stomatal movement and the final size of the stomatal aperture (Meidner & Mansfield, 1968; Burrows & Millthorpe, 1976), for some species even above the optimum temperature for photosynthesis (Schulze & Hall, 1982), for many plant species above 30 °C (Farquhar *et al.*, 1980; Lösch & Tenhunen, 1981). At the same time, high surface temperatures often coincide with high vapour pressure deficits which in turn can reduce carbon dioxide uptake due to an reduction in stomatal conductance (Lösch & Tenhunen, 1981; Grantz, 1990; Jacobs *et al.*, 1996). The interaction of environmental and plant related factors, thus, have a large impact on the exchange of mass and energy from the canopy and with it on the local climate.

In sparsely vegetated surfaces, interaction between the composing surface elements such as small plants, grassy patches and bare soil lead to more complicated conditions affecting the local climate. Besides the relations described above, advection and the positioning of the instruments become important experimental issues (Verhoef, 1995). Interaction effects of the individual patches only disappear higher up in the surface layer, well above the canopy elements (Van den Hurk, 1996). Depending on the horizontal scale of larger inhomogeneities other than described above, the *ABL* could be affected, and with it, the regional climate. Shuttleworth (1988) and later Raupach (1991) distinguished two classes of larger scale heterogeneous surfaces depending on the horizontal scale, 'disorganised' or 'microscale heterogeneity' and 'organised' or 'mesoscale heterogeneity', respectively.

In case of the so-called microscale heterogeneities (~1 km), the surface changes are disorganised at a scale less than 10 km (Shuttleworth, 1988). Here local advection becomes of major importance to the measurements of surface flux densities. Sudden changes in surface

characteristics lead to the development of an Internal Boundary Layer (*IBL*) in which the flow adapts to the new surface (e.g. Kaimal & Finnigan, 1994; Kroon & De Bruin, 1993; Bink, 1996) and surface fluxes are not in equilibrium with the underlying surface. An increase or decrease in drag when passing from one patch to the other enhances or reduces the exchange of momentum and indirectly the flux densities of heat and gases from the surface to the atmosphere (Claussen & Klaassen, 1992; Klaassen & Claussen, 1995). At the landscape scale (~1–10 km), much of the variability in flux densities of the individual surface patches are smoothed out within the *ABL* (Raupach, 1991; Kruijt, 1994, Wieringa, 1986). However, the areally averaged flux densities are not expected to be a simple average of the equilibrium flux densities from the individual patches (Mason, 1988; Klaassen, 1992).

For the so-called mesoscale heterogeneity, the organised surface patches (> 10 km) develop independent *ABL*'s, each with its own characteristics fully adapted to the underlying surface (André *et al.*, 1986; Raupach, 1991). Here nature- or land-use changes could affect the *ABL* flux densities, together with the climate at the scale of the changes (Garratt, 1992). For example, a decrease in transpiration will cause a relatively dry and warm *ABL*. At the same time a warmer *ABL* will increase the vapour pressure deficit stimulating transpiration. Thus, interactions of non-linear processes at different scales govern the exchange of heat and gases from the surface. As Jacobs (1994) pointed out, the regional scale (horizontal scale ~10-100 km) with mesoscale heterogeneity provides the link between global scale and local processes.

1.3. The SLIMM project

1.3.1. General

The Surface Layer Integration Measurements and Modelling (SLIMM) project was set up to investigate the soil-vegetation-atmosphere exchange of momentum, heat and carbon dioxide at the landscape scale (~10 km). At this scale the exchange processes are highly non-linear (Mason, 1988; Klaassen, 1992) due to interaction between the composing elements of the landscape. This co-operative research project between the Free University of Amsterdam, the University of Groningen and the Wageningen Agricultural University (WAU), took place during 1994 and 1995 in the north of the Netherlands (Lat. 53°00' N, Long. 6°23' W, Alt.+11 m) as indicated in Figure 1.1. Three patches with horizontal scales of a kilometre were chosen on a SW to NE transect, along the prevailing wind direction.



Figure 1.1: Location of the experimental area in the north of the Netherlands (Lat. 53°00' N, Long. 6°23' W, Alt. +11 m) as indicated by the solid square.

These patches contained three main types of surface cover, namely: peat bog tussock grassland, a mixed coniferous-deciduous forest and an agricultural/horticultural area as shown in Figure 1.2.

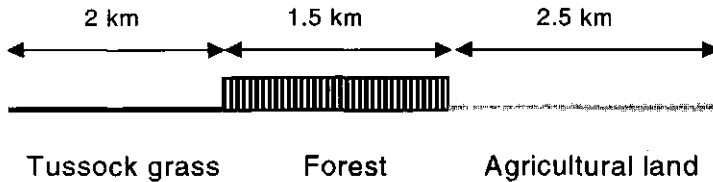


Figure 1.2: Position and typical dimensions of the 3 measuring sites. From the Southwest to the Northeast we find a peat bog tussock grassland (Wageningen Agricultural University), a mixed coniferous/deciduous forest (University of Groningen) and agricultural/horticultural land (Free University of Amsterdam), respectively.

Over these sites, the local flux densities of radiation, momentum and heat, both sensible and latent were measured using the eddy covariance and/or Bowen ratio technique. For an evaluation of the areally averaged flux densities, *ABL* observations were made using a Radio Acoustic Sounding System (*RASS*) and Sound Detection and Ranging (*SODAR*) technique. Combination of the local and *ABL* measurements should then result in a new averaging concept for scaling up local observations to areal averages for General Circulation Models (*GCM*'s) based on the concept of 'blending height' (Wieringa, 1986).

1.3.2. The contribution and objectives of the WAU

The site of *WAU* was located at Southwest site of the SW to NE transect. The so-called Fochteloöer area is one of the largest peat bog relicts in the Netherlands. Since 1985, 1700 hectares of this peat bog were dammed to increase the water table that should result in regeneration of the original peat bog ecosystem. Underneath the tussock grassland surface, a saturated, dark-brown layer of peat presented itself. In this area instruments were set up to determine the exchange processes between the surface and the atmosphere.

Apart from the peat bog experiment, two short scintillation experiments were carried out over pasture in co-operation with the Environmental Physics Group of the Horticultural Research Institute in Kerikeri, New Zealand.

The main objectives were:

- Direct and continuous long-term measurements of the surface flux densities of radiation, momentum, heat, water vapour and carbon dioxide to study the effect of biological and climatic processes that regulate carbon dioxide exchange of this ecosystem at the canopy scale.
- Long-term eddy covariance measurements of the water vapour and carbon dioxide flux densities to study the effect of plant related and environmental conditions on the interaction of carbon dioxide and water vapour exchange.
- To study the possibilities of the large aperture scintillation technique to measure the spatially averaged momentum and sensible heat flux density.
- To study the ability of the large aperture scintillation technique to produce reliable measurements of the scattering process due to refractive index fluctuations.

1.4. Organisation of the thesis

In Chapter 2 detailed information is given on the experimental site and instruments used during the experimental period in 1994 and 1995. Besides, a thorough description is given of the canopy structure during the growing season of the year. The complete data set is used to study the general effect of temperature, leaf area index, light and vapour pressure deficit on the exchange of carbon dioxide during various periods of the year. Some general relationships are deduced that might be used to study the effect of future perturbations in climate and ecology or to fill gaps in the data set. Finally the ecosystem carbon balance is established for a limited period of time under the current climate conditions.

Chapter 3 reports on the interaction between flux densities of carbon dioxide and water vapour from the canopy. For a selection of months, the monthly averaged course of carbon dioxide and water vapour flux densities are shown. Special attention is paid to the interaction of temperature and vapour pressure deficit and its effect on the surface flux densities during the summer period. The influence of the surface cover and leaf area index is expressed in terms of surface resistance, water use efficiency and the Ω decoupling factor of Jarvis & McNaughton (1986).

A short introduction to the scintillation technique is given in Chapter 4. It deals with the basic principles of propagation of electromagnetic radiation through a turbulent medium. The resulting scintillation of light is processed by a scintillometer and is represented as the refractive index structure parameter C_n^2 . From C_n^2 , the sensible heat flux density can be obtained. However to do so, compromising point measurements must be incorporated.

Chapter 5 addresses the prospect of obtaining the spatial averaged momentum and sensible heat flux densities from two large aperture scintillometers at different heights. A limitation of the current scintillation methods is that none provide kilometre scale path-averaged sensible heat flux without incorporating compromising point measurements of the friction velocity u_* or alternatively the average wind speed combined with a measure of the roughness length. The presumption that such measurements are representative of the entire transect usually holds for homogeneous surface cover but may not be valid for 'disorganised' or 'microscale heterogeneity' terrain. To assert scintillometers can determine path-averaged flux densities at landscape scales, and for them to successfully characterise surface flux densities over a heterogeneous surface will require resolution of this issue.

Chapter 6 focuses on the scintillation technique and its ability to measure the areally averaged flux density of sensible heat. In the operating bandwidth of the large aperture scintillometer, around 940 nm, the refractive index of the atmosphere is most sensitive to temperature fluctuations. Unfortunately, numerous absorption lines of water vapour around this wavelength cause extra scintillation. This effect is shown for the first time for infrared wavelengths. It causes an apparent increase in the observed sensible heat flux density especially during near neutral and stable conditions.

In chapter 7, the general conclusions are given, including some recommendations for future research.

CHAPTER 2

-
-
-

DIURNAL AND SEASONAL VARIATION OF CARBON DIOXIDE EXCHANGE FROM A FORMER TRUE RAISED BOG

JOOST P. NIEVEEN, COR M.J. JACOBS AND ADRIE F.G. JACOBS

*Department of Meteorology, Wageningen Agricultural University, Duivendaal 2, 6701AP
Wageningen, The Netherlands*

Global Change Biology, 4 (8): 823-834, 1998

2.1. Introduction

The global budget of radiatively active gases such as carbon dioxide (CO₂) is at present not fully understood. Because knowledge of this budget is essential in understanding climate dynamics and possible future climate changes, the global carbon budget has been identified by the Intergovernmental Panel on Climate Change (IPCC) as one of the priority research topics (Houghton *et al.*, 1995; see also Spence & Townsend, 1995). The strong need for direct and long-term measurements of CO₂ and water vapour exchange between miscellaneous ecosystems and the atmosphere was also emphasised at a Workshop on Strategies for Long-term Studies of CO₂ and Water Vapour Fluxes over Terrestrial Ecosystems (Baldocchi *et al.*, 1996).

Peat in the Northern Hemisphere's wetlands contains about one third of the world's carbon pool (Gorham, 1991). Lately, many regions in the arctic tundra have changed from sinks to sources for CO₂ (Oechel *et al.*, 1993) and although more and more information is available on the exchange of CO₂ over peatland ecosystems (e.g. Coyne & Kelley, 1975;

Oechel *et al.*, 1993; Neumann *et al.*, 1994; Beverland *et al.*, 1996), more is needed as results can not simply be generalised. Reasons for this are for example the different (soil) climate of the sites (e.g. arctic, subarctic or temperate with different water tables), the different types of vegetation (e.g. *Sphagnum* spp. or vascular plants) and the different measurement techniques (e.g. the chamber method and aerodynamic method).

In this paper we report on the CO₂ exchange of a former true raised bog, during a one and a half year experiment in the North of the Netherlands. The experiment was done within the framework of the Surface Layer Integration Measurements and Modelling project (SLIMM) (Vugts *et al.*, 1994). The eddy covariance technique, used in the experiment, allows the direct measurement of mass and energy transfer at a height above the surface resulting in a spatially integrated flux density. Data aggregated during this period can be used to get a better understanding of the biological and climatic processes that regulate CO₂ exchange of this ecosystem at the canopy scale. Also, they might be used to study the effect of future perturbations in climate and ecology of currently undisturbed true raised peat bogs.

2.2. Material and Methods

2.2.1. Site description

In the years 1994 and 1995, a meteorological field experiment was carried out in the Fochteloöer area, a disturbed raised peat bog in the north of the Netherlands (Lat. 53° 00' N, Long. 6°23' W, Alt. +11 m). Until 1980, Dutch peat bogs were used for fuel production and in an extensive part of the Netherlands peat was cut. For different reasons the Fochteloöer area was never largely affected by cutting, although drainage had a large impact on this peat bog ecosystem. Due to these influences, the area can be classified as peat relicts of a former true raised bog (Gore, 1983 and Schouwenaars & Vink, 1990). In 1985, the remaining area was dammed to increase the water table, which should result in regeneration of the peat bog.

Tussocks of varying dimensions covered the actual peat soil as schematically illustrated in Figure 2.1. The area taken by the individual tussocks differed from 20 cm² to more than 1 m². The average height of the tussocks is approximately 0.4 m. A layer (0.1 m) of dead organic material from the previous growing seasons covered the tussocks and the hollows in between. The dominating plant species around the experimental site was *Molinia caerulea* (> 75% of the vegetation) but in the Fochteloöer area other species such as: *Eriophorum vaginatum*, *Calluna vulgaris* and *Erica tetralix*, were also evident (Altenburg *et al.*, 1993). In sections that were permanently over-saturated *Sphagnum* spp. (<1% of the vegetation) were

present. In the hollows, shallow pools of open water could be observed. These differed in dimension from decimetres up to a few hundred metres. Many of these pools were strongly sheltered by the surrounding vegetation.

The growing season of *Molinia caerulea* extended from the beginning of May through to the end of October. During this period, green shoots grew up to a height of 1.2 m above the tussock. From November until the beginning of May, no green shoots were present. What was left above the tussock was the brownish surface of organic material and some brown shoots standing upright throughout the winter period. The tussocks were totally composed of organic material, mainly roots and decaying grass, with a gradual increase in density towards the base. Underneath the tussocks is a saturated dark brown layer of peat; the actual soil surface (Figure 2.1). The depth of this layer varied from 0 to 2.5 m. the measuring site this highly porous layer was about 0.3 m deep and at greater depth, a grey sandy loam was present. Throughout the seasons, the water table varied, depending on the weather, from 0 to 0.2 m below the tussock–soil interface but the soil remained saturated (Graham, 1995).

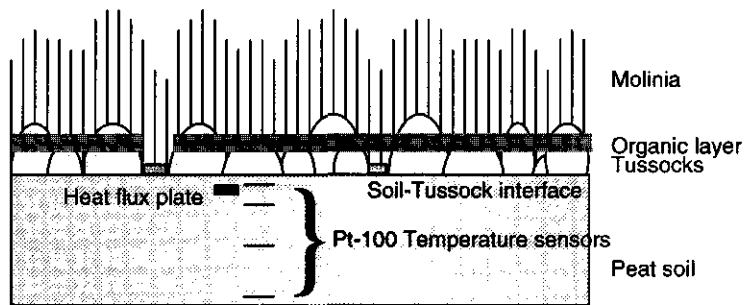


Figure 2.1: Side view of soil–plant–atmosphere interface at the experimental site. Also indicated are the positions of the Pt–100 temperature sensors (2.5, 20, 50, 100 cm) and the soil heat flux plate (5 cm) where the given depths are relative to the tussock – peat soil interface.

2.2.2. Instrumentation

Two six metre lattice towers were placed about 20 m apart at a representative location within the peat bog. The instruments were set up to determine the exchange processes of carbon dioxide, water vapour, momentum and heat. All were mounted on the two masts, except for the soil temperature and heat flux sensors that were placed 5 metres next to one of the masts (see Figure 2.1). Because of the isolated position of the site, the power supply was the limiting factor for the experiment and the main reason for gaps in the data set.

The exchange of CO₂ was measured using an eddy covariance system. A 3–D sonic

anemometer and a sampling tube, leading to closed path InfraRed CO₂/H₂O Gas Analyser (IRGA), were placed close together, 0.05 m apart (see Table 2.1 for details). The system was installed on an extendible tube at the top of the lattice tower. Flow distortion caused by the tower was therefore minimised.

Table 2.1: Overview of the sensors, types, manufacturers, heights from the soil surface and distance from the centre of the mast, used in the experiment

Object	Sensor	Type Manufacturer	Height/depth (m)	Distance (m)
Tower 1	Sonic anemometer	3-D-Solent Research, Gill Instruments Ltd., Lymington, UK	8.00	0
	Thermocouple	Copper-Constantan Dept. of Meteorology, WAU	7.95	0
	CO ₂ /H ₂ O Sampling tube	Polyethylene, 11.55 m Inner ø 0.004 m	8.00	0
	Net radiometer	Funk (or C.S.I.R.O) Middleton & Company Pty. Ltd., Australia	6.40	1.00
	Pyranometer	CM 10	6.40	0.80
	Incoming short wave Pyranometer	Kipp & Zonen, Delft, The Netherlands CM 10	6.40	0.80
	Reflected short wave Infrared gas analyser	Kipp & Zonen, Delft, The Netherlands LI-6262 CO ₂ /H ₂ O Analyser LI-COR Inc., Lincoln, Nebraska, USA	-	-
Tower 2	Pyrgeometer	CG 1	6.24	0.75
	Incoming long wave Pyrgeometer	Kipp & Zonen, Delft, The Netherlands CG 1	6.24	0.75
	Outgoing long wave	Kipp & Zonen, Delft, The Netherlands	-	-
	3 Psychrometers	-	2.01, 4.03,	0.66
	Southwest side	Dept. of Meteorology, WAU	6.09	-
	3 cup anemometers	-	2.01, 4.03,	0.90
	West side Wind vane	Dept. of Meteorology, WAU Dept. of Meteorology, WAU	6.09 6.50	0
Soil	4 Soil thermometers	Pt 100 Dept. of Meteorology, WAU	-0.025, -0.20, -0.50, -1.00	-
	1 Soil heat flux plate	WS 31-Cp TNO, Delft, The Netherlands	-0.05	-
Extra	Rain gauge	-	1.20	-
Data Logging	2 Data loggers	CR 21X Campbell Scientific Inc, Logan, Utah, USA	-	-
	Laptop computer	486-DX2 66 MHz Escom	-	-

For all wind directions the fetch was more than one kilometre. However, between 180–270° the terrain was slightly sloped. A pump was used to draw the air from the inlet to the IRGA at a rate of $10^{-4} \text{ m}^3 \text{ s}^{-1}$. The pump was placed in a way causing the pressure inside the sampling chambers to be slightly below atmospheric, but minimising the chance of condensation of water inside the tube. The IRGA ran in absolute mode and was re-calibrated every week. During this period the analyser's gain typically showed a 2 to 5% drift. The soda lime and magnesium perchlorate, used to keep the reference cell free of CO₂ and water

vapour, were changed every week. Every week, dry nitrogen from a cylinder was used as a zero calibration gas for CO₂ and water vapour, while dry air gas from a cylinder (400-ppm CO₂) was used as a second reference. An aspirated psychrometer was used as a second water vapour calibration.

A net radiometer and additional instruments for measuring the four components of the radiation balance were used and were distributed over the two masts to avoid shading effects. A soil temperature profile and the soil heat flux density were measured in the actual peat soil, but not in the organic layer between the soil surface and the atmosphere (see Figure 2.1). During the growing season, the leaf area index (*LAI*) was measured every week (see Section 2.4). Occasionally other measurements were performed, such as the heat conductivity of the soil, tussock and organic top layer with a thermal conductivity probe (Heusinkveld *et al.*, 1992). Table 2.1 lists the instruments and their position relative to the soil surface and the centre of the mast.

2.2.3. Data acquisition and -processing

All the instruments were sampled at 0.25 Hz, except for the eddy covariance system. Every 30 minutes the data were averaged and stored in data loggers for later processing. The 3-D sonic anemometer was sampled at 20.8 Hz. Analog inputs from the IRGA and thermocouple, connected to the sonic interface, were sampled at a lower frequency. The resolvable input frequency of the analog inputs was no faster than 5 Hz.

Raw data of the eddy covariance system was stored on a PC and processed later, using a first order recursive digital filter with a time constant of 200 seconds (McMillen, 1988). Here a moving average was subtracted from the every sample to get the fluctuating value of all the measured components. A software program (Van den Hurk, 1996) performed the necessary corrections, including: co-ordinate rotation (McMillen, 1986), Webb corrections (Webb *et al.*, 1980) and frequency response corrections (Moore, 1986), needed for the calculation of the half hour averaged flux densities. To test the quality of the data the power and co-spectra of the eddy covariance measurements were checked and the ability to close the surface energy balance. The latter, the available energy ($Rn-G$) versus the sum of the sensible heat (H) and latent heat (λE) flux density were excellently fitted with a linear regression line described by $Rn-G = 0.92(H+\lambda E)$ [$W\ m^{-2}$] ($R^2 = 0.91$; $N = 1641$).

2.2.4. Plant measurements

During the 1994-growing season, the course of leaf area index (*LAI*) was observed. For the measurements we used the amount of one-sided green leaf area per square metre of ground area for the determination of the *LAI*. In principle we measured, then multiplied, the areal density of the leaves by the mean area of the leaf.

The irregular surface and tussock structure made it necessary to carry out a large number of measurements that would average out small-scale variations. These data were obtained as follows. Three sampling patches were chosen, to perform the leaf area measurements. These patches were located about 50 m apart, surrounding the site. Each patch represented a typical feature of the soil surface, such as extremely wet, relatively dry or many pools of shallow open water and was sampled every three weeks. For the measurements, we only considered *Molinia caerulea*; the dominant plant species in the area (>75% of the vegetation) (Altenburg *et al.*, 1993).

To calculate the average leaf area unbiased from a patch, 100 shoots were picked. A hand-held scanner was used to determine the area of every individual leaf using a computer program giving an average leaf area. Furthermore, the average number of leaves from 25 plots of 0.09 m² were used to determine the average leaf density of the patch. The average leaf area was then multiplied by the average leaf density, to obtain the *LAI* for a particular patch as shown in Figure 2.2.

2.3. Results

2.3.1. Leaf area index

Figure 2.2 shows the measured course of the *LAI* of the three patches during the growing season of 1994 (Goedee, 1995). In this particular year the first green leaves became visible around the first of May (± 1 week). The maximum *LAI* of approximately 1.7, coincided with the flowering of the grass around mid August. After this stage the vegetation died off and by the end of October (± 1 week) all the green leaves had turned brown. The brown leaves partly stand upright and partly add to the layer of organic material covering the tussocks and hollows. The *LAI* was measured only during the growing season of 1994. For 1995 the assumption was made that the *LAI* followed the same trend, except for a different timing of the onset and end of the growing season and maximum *LAI*. The periods in which the first shoots became visible (± 1 week), the grass flowered (± 1 week) and the all leaves had turned

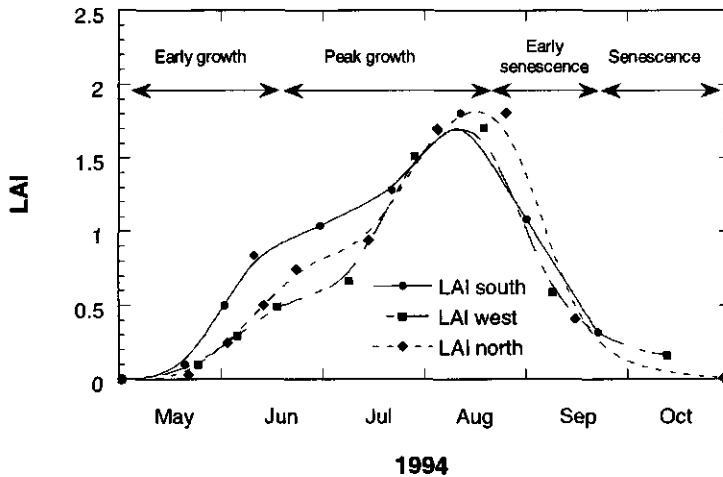


Figure 2.2: Course of the leaf area index (*LAI*) for three patches around experimental site during the growing season of 1994. Also indicated are the growth stages of *Molinia caerulea*.

brown (± 1 week) were recorded for 1995.

2.3.2. Diurnal CO_2 exchange

Figure 2.3 shows the net CO_2 flux density (F_c), the incoming global radiation (R_s) and the soil temperature at 2.5 cm and air temperature at 2 m for two representative days in the winter and summer of 1995 (Day 34 and 180 on the day of year calendar). Day 34 (solid circles Figure 2.3) is an example of a typical day in winter time. For this day the absence of green vegetation and therefore of photosynthesis, is clearly demonstrated. During day and night, the peat bog shows a small positive (upward) flux density of the order of $0.02 \text{ mg CO}_2 \text{ m}^{-2} \text{ s}^{-1}$ ($0.45 \text{ } \mu\text{mol CO}_2 \text{ m}^{-2} \text{ s}^{-1}$) with a maximum of $0.06 \text{ mg CO}_2 \text{ m}^{-2} \text{ s}^{-1}$ ($1.35 \text{ } \mu\text{mol CO}_2 \text{ m}^{-2} \text{ s}^{-1}$) and a net daily carbon dioxide flux density $2.0 \text{ g CO}_2 \text{ m}^{-2} \text{ d}^{-1}$ ($45 \text{ mmol CO}_2 \text{ m}^{-2} \text{ d}^{-1}$). R_s peaks around 14:00 h and has a maximum of 138 W m^{-2} ($314 \text{ } \mu\text{mol PAR m}^{-2} \text{ s}^{-1}$). The 2 m air temperature ranges from $0.5 \text{ }^\circ\text{C}$ during the night to $8 \text{ }^\circ\text{C}$ during daylight hours (07:00 – 16:30 h), while the 2.5 cm temperature of the actual peat soil hardly changes. The loss of CO_2 is probably solely caused by biochemical oxidation of organic matter, i.e. soil respiration. In contrast with other observations (e.g. Greco & Baldocchi, 1996), a diurnal pattern in respiration is almost absent. This can probably be explained by the fact that in our case the soil temperature is almost constant during day and night.

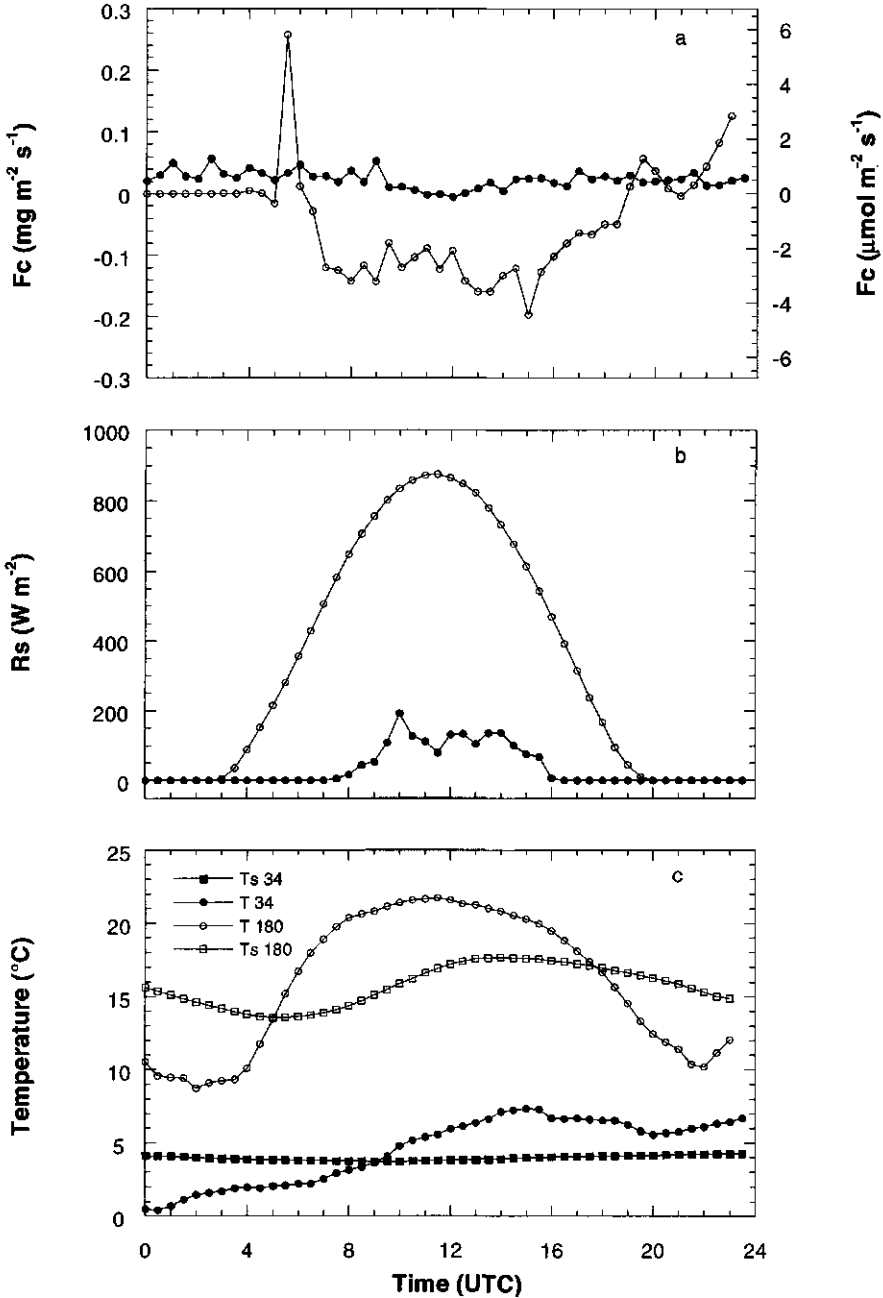


Figure 2.3: Diurnal course of: (a) The CO₂ flux density (F_c), (b) The incoming global radiation (R_s) and (c) The soil temperature at 2.5 cm and air temperature at 2 m for day 34 (solid circles/squares) and day 180 (open circles/squares). The CO₂ flux densities with a negative sign are directed downward from the atmosphere to the surface.

Day 180 (open circles Figure 2.3) displays a characteristic day during summer. The incoming global radiation peaks around 12:00 h with a maximum value of 875 W m^{-2} ($1990 \mu\text{mol PAR m}^{-2} \text{ s}^{-1}$). The estimated *LAI* on day 180 from Figure 2.1 is about 1, while the maximum daytime CO_2 flux density is $-0.20 \text{ mg CO}_2 \text{ m}^{-2} \text{ s}^{-1}$ ($-4.5 \mu\text{mol CO}_2 \text{ m}^{-2} \text{ s}^{-1}$). The net daily CO_2 flux density equals $-4.0 \text{ g CO}_2 \text{ m}^{-2} \text{ d}^{-1}$ ($-90 \text{ mmol CO}_2 \text{ m}^{-2} \text{ s}^{-1}$), i.e. a net gain of CO_2 . At 06:00 h *F_c* becomes negative (net CO_2 uptake). From 06:00 until 07:00 h, *F_c* increases (more negative) with increasing *R_s*, but shows no distinct trend from 07:00 h until 16:00 h as found by others (e.g. Neumann *et al.*, 1994). Towards the evening, *F_c* starts to diminish again (less negative) with decreasing *R_s* and becomes positive again around 19:00 h. The average nocturnal efflux of CO_2 on day 180 is $1.0 \mu\text{mol CO}_2 \text{ m}^{-2} \text{ s}^{-1}$ ($0.045 \text{ mg CO}_2 \text{ m}^{-2} \text{ s}^{-1}$), but shows a remarkable positive peak at 05:30 h. This phenomenon, which was observed quite regularly, could be explained as follows.

The CO_2 produced by the soil is released to the atmosphere, where turbulence, both mechanically and buoyancy driven, may effectively mix the CO_2 into the ambient air, causing an upward flux. However, under stable conditions the tussock surface and the atmosphere at the measuring height become de-coupled. As a result, there will be a build up of CO_2 as turbulent transport away from the surface is prevented. The observed peak in *F_c* at 05:30 h may therefore well be explained by the release of CO_2 respired during the previous hours. This release is related to a sudden increase in turbulence (*u_{*}* changes in one hour from 0.01 to 0.28 ms^{-1}) and the resulting transport of CO_2 away from the surface. Similar observations were made in forest canopies (e.g. Wofsy *et al.*, 1993; Greco & Baldocchi, 1996).

2.3.3. Seasonal variations of CO_2 exchange

2.3.3.1. Carbon balance

Figure 2.4 shows the seasonal variation in the net carbon dioxide flux density for the peat bog area, where the net monthly CO_2 flux density is calculated from the half hourly spatially averaged net daytime and nighttime flux densities. The hatched bars represent months with almost full data coverage, that is, all days without data gaps used to compute the average. The blank bars represent monthly averages based on limited data, e.g. only part of the month or scattered days within a month. Months with no data are also indicated. These were caused by power deficiency or malfunctioning of the IRGA. The assumption is made that the possible stored nocturnally respired CO_2 during periods with insufficient turbulent mixing, will

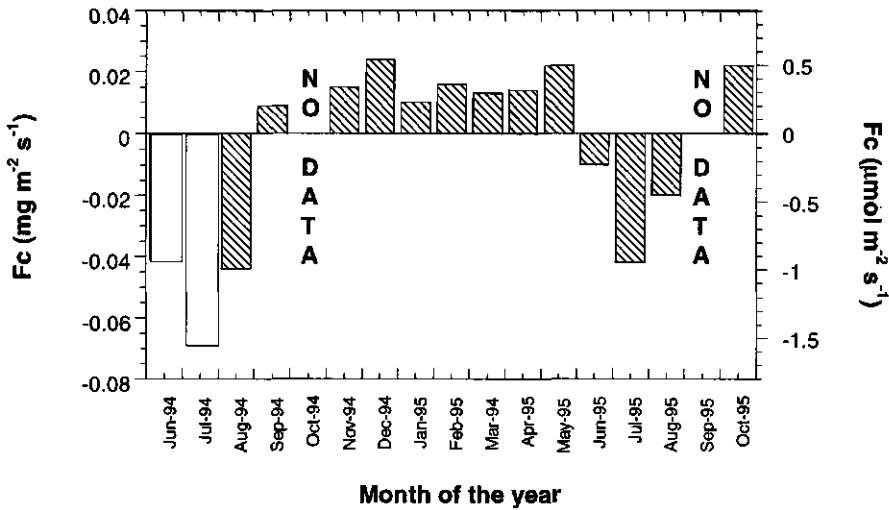


Figure 2.4: Monthly variation in the mean net CO₂ flux density from the disturbed peat bog. Open bars indicate averages from a limited number of data.

eventually be mixed and therefore be incorporated in the net CO₂ flux density.

During 3 months (June, July & August) of the year the peat bog behaved as a sink of CO₂. During this period the average daytime uptake of CO₂ by the vegetation was larger than the average respiratory losses of CO₂ by the plant and soil. The difference in the net release of CO₂ during August 94 and 95 probably reflects the effect of the inter-annual variability of the environmental conditions on the carbon balance. Such conditions include soil water status, soil and air temperature and the development of the vegetation. Both the 2 m air temperature and 2.5 cm soil temperature were on average 2 degrees higher in August 1995. This might have led to higher soil and plant respiration (see Section 2.3.3.3). The rest of the year, from September until May, the peat bog was a source of CO₂. The monthly averaged net exchange rates, ranged from -0.068 mg CO₂ m⁻² s⁻¹ (-1.5 μmol CO₂ m⁻² s⁻¹) in July 1994 to 0.024 mg CO₂ m⁻² s⁻¹ (0.54 μmol CO₂ m⁻² s⁻¹) in December 1994. From November 1994 to November 1995, the area released approximately 97 g CO₂ m⁻² y⁻¹ (265 kg C ha⁻¹ y⁻¹), i.e. during this period the peat bog behaved as a source of CO₂. Oechel et al. (1993) reported on whole-ecosystem CO₂ flux density measurements in Alaska over 5 seasons using a chamber method. The ecosystems investigated by these authors also showed a net release of CO₂ during this period, ranging from 34 g C m⁻² y⁻¹ for the wet coastal tundra sites to 156 g C m⁻² y⁻¹ for the drier tussock tundra sites. They subscribed the change from CO₂ sink to CO₂ source to enhanced drainage, and soil aeration and a decrease in the water table. The values found in their study are similar to ours. Beverland et al. (1996) on the other hand, estimated the annual

carbon exchange from a Scottish peatland ecosystem using the conditional-sampling technique to be $-41 \text{ g C m}^{-2} \text{ y}^{-1}$, i.e. a sink of CO_2 . Coyne and Kelley (1975) also measured a net uptake of carbon of $-40 \text{ g C m}^{-2} \text{ y}^{-1}$ for wet meadow tundra in Barrow, Alaska.

2.3.3.2. Daytime CO_2 flux densities

Maximum flux densities of about $-0.5 \text{ mg CO}_2 \text{ m}^{-2} \text{ s}^{-1}$ ($-11 \text{ } \mu\text{mol CO}_2 \text{ m}^{-2} \text{ s}^{-1}$) were observed in July and August 1995, but average daytime peak values were about $-0.33 \text{ mg CO}_2 \text{ m}^{-2} \text{ s}^{-1}$ ($-7.4 \text{ } \mu\text{mol CO}_2 \text{ m}^{-2} \text{ s}^{-1}$) in July and somewhat lower about $-0.30 \text{ mg CO}_2 \text{ m}^{-2} \text{ s}^{-1}$ ($-6.8 \text{ } \mu\text{mol CO}_2 \text{ m}^{-2} \text{ s}^{-1}$) in August. Average peak exchange rates compare with values observed in other peatland studies. For example, Beverland *et al.* (1996) found peak values for F_c between -0.12 and $-0.37 \text{ mg CO}_2 \text{ m}^{-2} \text{ s}^{-1}$ (-2.8 and $-8.3 \text{ } \mu\text{mol CO}_2 \text{ m}^{-2} \text{ s}^{-1}$) in a tussock like blanket bog in the north of Scotland. Shurpali *et al.* (1995) found $-0.24 \text{ mg CO}_2 \text{ m}^{-2} \text{ s}^{-1}$ ($-5.4 \text{ } \mu\text{mol CO}_2 \text{ m}^{-2} \text{ s}^{-1}$) from an open peatland in north central Minnesota, USA. However, measurements by Neumann *et al.* (1994) showed about 50% lower average peak downward flux densities ($-0.17 \text{ mg CO}_2 \text{ m}^{-2} \text{ s}^{-1}$; $-3.8 \text{ } \mu\text{mol CO}_2 \text{ m}^{-2} \text{ s}^{-1}$) over a raised open bog at the Kinosho Lake in Canada using the eddy covariance technique.

Our values are only 10% of values reported for closed agricultural crops (e.g. Baldocchi, 1994) and well-watered deciduous forest (e.g. Greco & Baldocchi, 1996) and about 25% of values reported for grasslands (e.g. Kim & Verma, 1990). June and September showed average daytime peaks in F_c of about $-0.2 \text{ mg CO}_2 \text{ m}^{-2} \text{ s}^{-1}$ ($-4.5 \text{ } \mu\text{mol CO}_2 \text{ m}^{-2} \text{ s}^{-1}$), while the peaks in F_c in May and October were about $-0.055 \text{ mg CO}_2 \text{ m}^{-2} \text{ s}^{-1}$ ($-1.2 \text{ } \mu\text{mol CO}_2 \text{ m}^{-2} \text{ s}^{-1}$). Daytime flux densities during the late autumn and winter season (November – February), showed no uptake of CO_2 by the vegetation. Here the soil will be the only contributor to CO_2 exchange. This will be the subject of next section.

2.3.3.3. Nighttime CO_2 flux densities; respiration

Total respiration (R_d) from a soil-canopy system is a combination of soil, plant and root CO_2 release. Emissions of CO_2 from the soil result from biochemical oxidation of organic matter, which is highly influenced by temperature. Maximum respiration rates measured at the Fochtelöer site, when no green vegetation was present, ranged between 0.025 and $0.16 \text{ mg CO}_2 \text{ m}^{-2} \text{ s}^{-1}$ (25 and $157 \text{ mg C m}^{-2} \text{ h}^{-1}$). The corresponding range of soil temperatures measured at a depth of 2.5 cm was between 1 to $12 \text{ }^\circ\text{C}$. Here both daytime and nighttime flux

densities were used for the analysis. Similar values to ours (6.8 to 115 mg C m⁻² h⁻¹) were found by Chapman and Thurlow (1996) for a hill blanket peat bog in Scotland using a closed chamber system in a soil temperature range between 1 and 14 °C. Smaller values (4.6 – 28.5 mg C m⁻² h⁻¹) were found by Svenson (1980) for a subarctic mire and by Silvola (1986) (21–41 mg C m⁻² h⁻¹) for reclaimed mires in Finland. The latter, however, showed a 100% increase in CO₂ release due to drainage of the mire.

Minimum half hourly averaged values of soil respiration of about 0.01 mg CO₂ m⁻² s⁻¹ (9.8 mg C m⁻² h⁻¹) were observed in January 1995 at a 2.5 cm soil temperature near 1 °C ($u_* > 0.2 \text{ ms}^{-1}$). A minimum of 0.0069 mg CO₂ m⁻² s⁻¹ (6.8 mg C m⁻² h⁻¹) at 1 °C soil temperature was found for soil respiration during winter from a hill blanket peat bog with a vegetation of mixed grasses and heather in Scotland using a closed chamber system (Chapman & Thurlow, 1996). In the period between July and August, when the 2.5 cm soil temperatures ranged between 11 and 20 °C, the average nocturnal CO₂ emission (plant and soil respiration) was about 0.10 mg CO₂ m⁻² s⁻¹ (2.25 μmol CO₂ m⁻² s⁻¹), with a maximum of 0.45 mg CO₂ m⁻² s⁻¹ (10.1 μmol CO₂ m⁻² s⁻¹). The midday 2 m air temperature during the same period was generally 25 °C. Similar respiration rates were observed by others: 0.09 – 0.19 mg CO₂ m⁻² s⁻¹ (2.0 and 4.3 μmol CO₂ m⁻² s⁻¹) in an open peatland ecosystem in Minnesota, USA with average air temperatures from 18 to 24 °C (Shurpali *et al.*, 1995); 0.1 mg CO₂ m⁻² s⁻¹ (2.2 μmol CO₂ m⁻² s⁻¹) in a tussock tundra in Alaska (Oberbauer *et al.*, 1991); 0.028 – 0.083 mg CO₂ m⁻² s⁻¹ (0.63 – 4.3 μmol CO₂ m⁻² s⁻¹) in a *Sphagnum papillosum* fen in Ilomantsi, Finland with an air temperature of 10 to 20 °C (Silvola *et al.*, 1992).

The relation between soil temperature at 2.5 cm and soil respiration is shown in Figure 2.5. Here only half hourly averaged nocturnal CO₂ flux densities were used where the 8 m average wind speed, u , exceeded 4 m s⁻¹ ($u_* > 0.2 \text{ m s}^{-1}$), to ensure sufficient turbulent mixing. The nocturnal flux densities incorporate both soil and plant respiration, where the soil is the only contributor during the absence of green vegetation. The soil temperature dependence of soil respiration is based on a so called Q_{10} response function. This function is depicted by the exponential fitted line in Figure 2.5 and from it a Q_{10} of 4.8 can be obtained for the peat bog area in a temperature range between 0 and 20 °C. In the upper temperature regions, plant respiration may also contribute to the nocturnal efflux of CO₂ and may cause more scatter of the data in this region.

This Q_{10} is in the same range as values found by others: e.g. $Q_{10} = 5.1$ for a peat bog with mainly *Calluna vulgaris* and mixed grasses and 6.1 for *Sphagnum* dominated peat bog

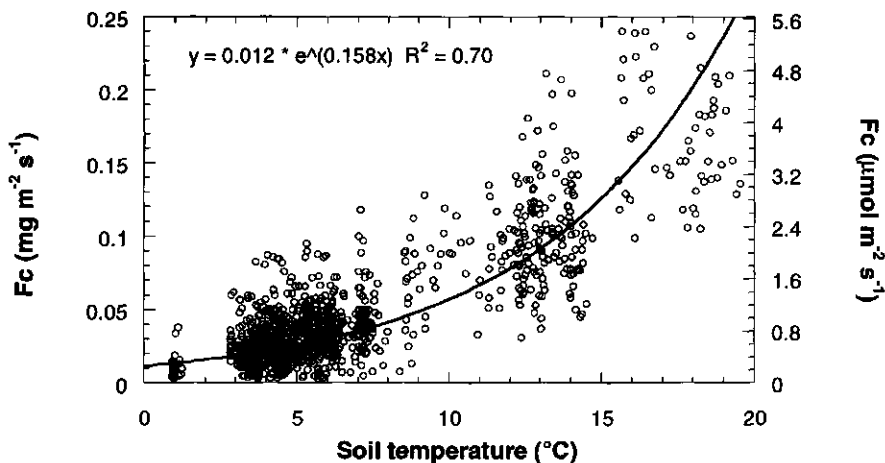


Figure 2.5: The nighttime CO₂ flux density as a function of the soil temperature at 2.5cm for those data where the mean horizontal wind speed $u(8m) > 4 \text{ m s}^{-1}$ and $u_* > 0.2 \text{ m s}^{-1}$. Data are fitted with an exponential function.

from chamber measurements (Chapman & Thurlow, 1996) and $Q_{10} = 2 - 7$ for the ombrotrophic parts of a subarctic mire in Sweden, using a closed vessel and chemical analysis technique (Svensson, 1980).

2.3.4. Effect of light on CO₂ exchange

Figure 2.6 shows the response to light of the vegetation and soil at the Fochtelöer site in the second half of July and August 1995 ($LAI > 1$). The data suggest that at low light intensities, the photosynthetic rate increases more or less linear with increasing irradiance, and that there is a trend towards light saturation after 400 to 500 W m^{-2} . The plot shows that a rectangular hyperbola (e.g. Ruimy *et al.*, 1995 or Landsberg, 1977) can be fitted to the data with an initial slope of $0.0026 \text{ mg CO}_2 \text{ W}^{-1}$ incident global radiation ($0.026 \text{ } \mu\text{mol CO}_2 \text{ } \mu\text{mol PAR}^{-1}$) and a maximum level of about $0.20 \text{ mg CO}_2 \text{ m}^{-2} \text{ s}^{-1}$ ($4.5 \text{ } \mu\text{mol CO}_2 \text{ m}^{-2} \text{ s}^{-1}$) ($R^2 = 0.72$).

Ruimy *et al.* (1995) concluded that for all the investigated vegetation types including: trees, grass and agricultural crops, the relationship between global radiation and canopy photosynthetic rate is far from linear. This is in line with our observation where, despite the low LAI , light saturation is never reached. A similar result was obtained by Beverland *et al.* (1996) in a Scottish peat bog, by Verhoef *et al.* (1996) for natural vegetation in a savannah with a LAI less than 2 and by Kim and Verma (1990) for temperate grassland with LAI less than 3.

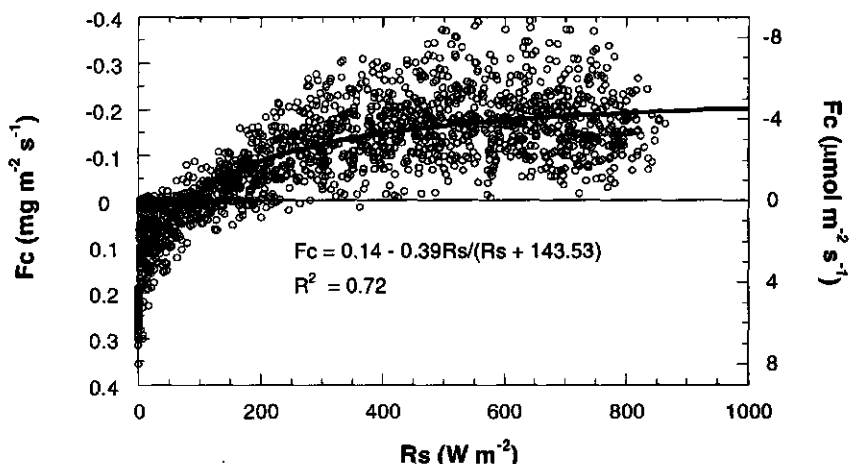


Figure 2.6: The net CO_2 exchange (F_c) as a function of light (R_s) for the disturbed peat bog during the months of July and August 1995. Data are fitted with a rectangular hyperbola relationship.

The light compensation point, the point where the net photosynthesis is zero, is approximately 100 W m^{-2} as estimated from the fitted curve. The intercept of the light response curve represents the respiration rate during night time. The value of $0.14 \text{ mg CO}_2 \text{ m}^{-2} \text{ s}^{-1}$ ($3.2 \mu\text{mol CO}_2 \text{ m}^{-2} \text{ s}^{-1}$), corresponds to the mean value measured in July and August 1995 (see Section 2.3.3.3). The data show significant scatter probably caused on one hand by the changing environmental conditions, like vapour pressure deficit, soil and air temperature and the soil water status during the two months as found by (e.g. Shurpali *et al.*, 1995; Kim & Verma, 1990). Some scatter could also be due to the nature of the eddy covariance method (Baldocchi *et al.*, 1988).

2.3.5. Effect of vapour pressure deficit on CO_2 exchange

Vapour pressure deficit, D , is often observed to be negatively correlated with stomatal aperture (e.g. Lösch & Tenhunen, 1981; Cowan & Farquhar, 1977; Grantz, 1990). The exchange of CO_2 may therefore be reduced at high D . In Figure 2.7, R_s versus F_c is shown again but now a differentiation has been made between data at low D , 0–10 hPa, and at high D , 15–30 hPa. A rectangular hyperbola was fitted to the data with a covariance coefficient, R^2 , of respectively 0.72 and 0.20. The difference in D shows a reduction of the CO_2 uptake by the vegetation of about 50% at high incoming global radiation, indeed indicating a lower conductivity of the leaf's stomata to the transport of CO_2 and water vapour due to the higher

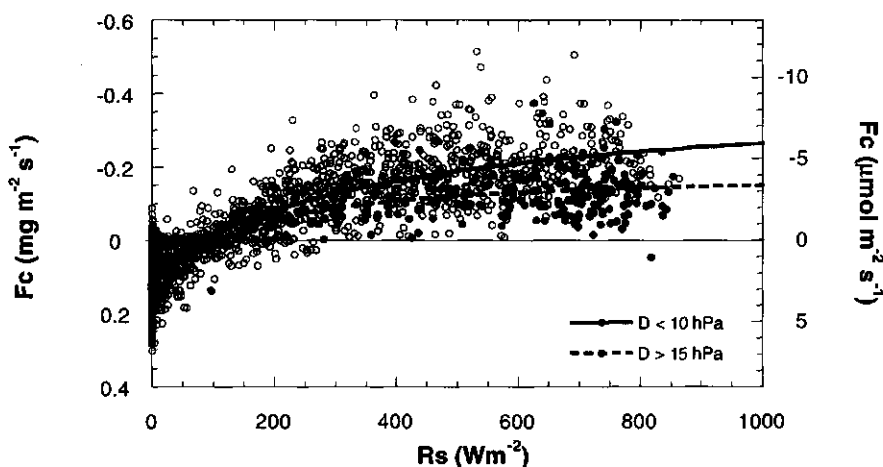


Figure 2.7: The CO_2 flux density (F_c) as a function of the incoming global radiation (R_s) for different classes of D : 1) between 0 and 10 hPa and 2) between 15 and 30 hPa. A best fit (rectangular hyperbola) for both classes is also indicated. Fit 1): $F_c = 0.081 - 0.48R_s/(R_s + 396.4)$; $R^2 = 0.72$. Fit 2): $F_c = 0.18 - 0.36R_s/(R_s + 112.93)$; $R^2 = 0.20$.

D . However a correlation coefficient of 0.20 implies a very weak relation with the incoming global radiation.

At the same time λE showed no significant reduction during periods with high D . An example to illustrate the particular behaviour of the exchange of CO_2 and water vapour in relation to D is given in Figure 2.8; maximum λE exceeded 250 W m^{-2} . Greco & Baldocchi (1996) found similar results for a deciduous forest despite soil water deficits. Note that soil moisture stress, one of the reasons for a lower leaf conductivity (e.g. Grantz, 1990; Kim and Verma, 1990), in our case is unlikely to occur under the extreme wet conditions at the site.

However, the high vapour pressure deficit often coincided with high air temperatures. Calculations from the longwave radiometer demonstrated that the canopy surface temperature was often in the range of 30 to 35 °C. Therefore the canopy temperature may have exceeded the optimum temperature of *Molinia caerulea* for photosynthesis, causing net photosynthesis to diminish. This could either arise from a rapid increase of plant respiration with temperature or a limitation of photosynthetic activity at higher leaf temperatures (Jones, 1992), but probably not from a lower leaf conductivity.

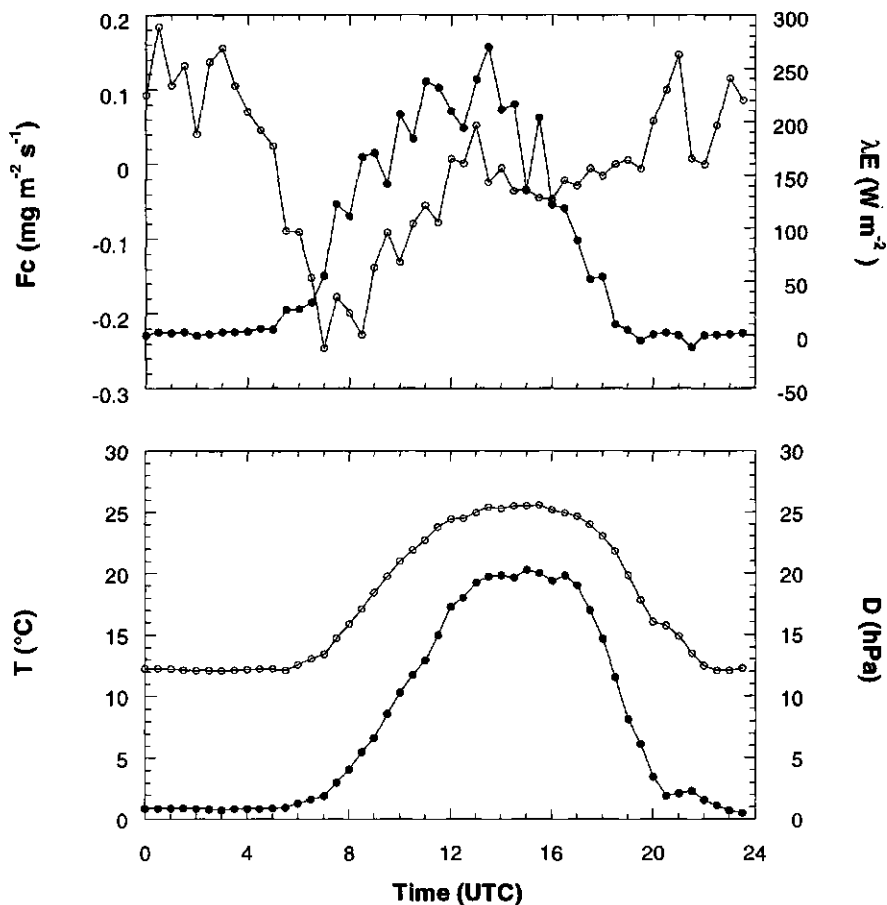


Figure 2.8: The CO_2 flux density (F_c – open circles), the latent heat flux density (λE – solid circles), the 2m air temperature (T – open circles) and the 2m vapour pressure deficit (D – solid circles) on day 181 1995.

2.4. Discussion

The carbon balance presented here shows, like other measurements in peatland ecosystems (e.g. Oechel *et al.*, 1993), a net release of $97 \text{ g CO}_2 \text{ m}^{-2} \text{ y}^{-1}$ ($265 \text{ kg C ha}^{-1} \text{ y}^{-1}$). Following Goulden *et al.* (1996), long-term eddy covariance measurements can be accurate in general up to $\pm 20\%$ ($\pm 19 \text{ g C m}^{-2} \text{ y}^{-1}$) due to random and systematic errors. Taking these errors into account, the area will still show a net release of CO_2 even if the errors were larger. In our case, the net release of CO_2 means that the influence of drainage could still be present. We note that active true raised bogs are expected to be net sinks of CO_2 . Still, due to the inter-annual and intra-annual variability of the environmental conditions, our results may have

given us the impression the peat bog being a source of carbon. The presented carbon balance should therefore be used as an indication of the CO₂ balance of the peat bog ecosystem under the present climate and with the present soil/vegetation characteristics. This emphasises the scientific need for long term and continuous measurements of CO₂ exchange in various ecosystems. Oechel *et al.* (1993), also showed a shift from a net CO₂ sink to source, probably resulting from drainage, while Silvola (1986) showed a 100% increase in CO₂ release due to drainage of reclaimed mires in Finland. Possible future climate changes might induce shifts like these or similar conditions like ours, which have a large impact on the worlds carbon pool.

The soil temperature dependence of respiration is based on a so called Q_{10} response function. This Q_{10} is a useful tool to fill data gaps, but can also simply be used to parameterize soil respiratory processes for peatland ecosystems, like ours, in climate models. CO₂ exchange during the growing season is the result of the total respiration and photosynthesis. While the respiration is mainly a temperature dependent process dynamically, photosynthesis depends on various factors such as LAI, ambient CO₂ concentration, temperature and light. To model net CO₂ exchange at the ecosystem scale, information at the leaf scale has to be scaled up to the canopy level (see e.g. Jacobs, 1994 and Van den Hurk, 1996) by integrating the net CO₂ exchange and leaf surface conductance over the canopy volume. Unfortunately, data collected by the eddy covariance technique is not suited for this purpose.

Our data showed a clear non-linear relation between net CO₂ flux density and the incoming global radiation. High D (>15 hPa) suppressed the flux density by about 50%, but not the evaporation rates. Johnson and Caldwell (1976) also described this poor stomatal sensitivity to humidity as being the main factor allowing survival on extreme sites. High canopy temperatures may cause damage to the vegetation. In places where there is enough soil water evaporation could keep the canopy relatively cool. Johnson and Caldwell (1976) reported that species with poor humidity response were restricted to wet sites.

Acknowledgements

Both Joost P. Nieveen and Cor M.J. Jacobs were financially supported by the Netherlands Organisation for Scientific Research (N.W.O.) under project number 753-06-243 and 09-77-06-243 respectively. We like to thank the technical staff of the Department of Meteorology for their contribution to the field experiment and general logistics.

CHAPTER 3

-
-
-

THE EFFECT OF SURFACE COVER, VAPOUR PRESSURE DEFICIT AND TEMPERATURE ON THE CARBON DIOXIDE AND WATER VAPOUR FLUX DENSITIES OF A DISTURBED RAISED PEAT BOG

JOOST P. NIEVEEN¹, COR M.J. JACOBS² AND JAN GOUDRIAAN³

¹ *Department of Meteorology, Wageningen Agricultural University, Duivendaal 2, NL-6701 AP Wageningen, The Netherlands.*

² *Royal Netherlands Meteorological Institute, PO Box 210, NL-3730 AE De Bilt, The Netherlands.*

³ *Department of Theoretical Production Ecology, Wageningen Agricultural University, Bornsesteeg 65, NL-6708 PD Wageningen, The Netherlands.*

Submitted to *Agricultural and Forest Meteorology*, 1998

3.1. Introduction

Wetlands are major natural sources of carbon dioxide, methane and sulphur compounds and can have high rates of denitrification and nitrogen fixation (Sahagian & Melack, 1998). The surface cover and hydrology have been found to significantly affect the flux densities of carbon dioxide, water vapour and other trace gases such as methane (see e.g. Lafleur, 1990; Shurpali *et al.*, 1995 and Campbell & Williamson, 1997). Various studies have pointed out that evaporation from *Sphagnum* wetlands was reduced remarkably when the water table dropped (see survey by Ingram, 1983). With the presence of vascular plants, evaporation was not only found to be related to the soil water availability but to plant factors as well (Ingram,

1983; Kim & Verma, 1996). Changing hydrological conditions and aeration, possibly due to higher temperatures, have changed many regions in the Arctic tundra from sinks to sources of carbon dioxide (Oechel *et al.*, 1993). With peat in the Northern Hemisphere's wetlands containing about one third of the world's vegetative carbon pool (Gorham, 1991), good understanding of the mass and energy cycles under various climatic, hydrological and ecological conditions is of major importance to survey the effect of possible future climate changes and anthropogenic factors.

The leaves' stomata are the main route for CO₂ and H₂O to transfer between the biosphere and the atmosphere. Micrometeorological, biogeochemical and plant-physiological principles combine the exchange of CO₂ and H₂O and are used in models to describe stomatal behaviour under various environmental and climatic conditions (e.g. Farquhar *et al.*, 1980; Goudriaan *et al.*, 1985; Stewart, 1988 or Jacobs, 1994). To study the effect of physical and physiological factors, Lafleur and Rouse (1990) and later Kim and Verma (1996) used a dual source 'big leaf' (Penman, 1965) model to separate the relative contributions of the vascular and non-vascular (*Sphagnum* spp.) plants to the total evaporation. In this concept, the surface resistance (r_s) represents the control of the diffusion process through the stomatal pore. As r_s is the parallel sum of the stomatal resistances of all the leaves, it depends on the leaf area index (McNaughton & Jarvis, 1983). Besides that, r_s is controlled by plant physiological and environmental conditions, such as: plant and soil water status, CO₂ concentrations, light, leaf temperature or air humidity (see e.g. Lösch & Tenhunen, 1981; Schulze, 1986 or Jacobs *et al.*, 1996). Lafleur & Rouse (1990) assumed r_s to be zero, as the wetland surface with vegetated hummocks and open water was always saturated. In contrast Kim & Verma (1996) pointed out that even in a wetland the *Sphagnum* surface resistance is non-zero. With the presence of vascular plants in wetlands the surface resistance may reach 600 s m⁻¹ (Campbell & Williamson, 1997).

The objective of this study is to describe the effect of the surface cover and the environmental conditions on the surface flux densities of water vapour and carbon dioxide from a disturbed true raised peat bog. To achieve this, a field experiment was executed during a one and a half year period in a disturbed raised peat bog, in the north of the Netherlands. Most raised peat bogs in the Northern Hemisphere dominated by *Sphagnum*. In contrast, peat bogs in the Netherlands are dominated by tussock grass and heather vegetations, e.g. *Molinea caerulea*, *Calluna vulgaris*, *Erica tetralix* (Schouwenaars & Vink, 1990). Until 1980, Dutch peat bogs were used for fuel production and in an extensive part of the Netherlands peat was cut. However, for different reasons some areas were never largely affected, although drainage

had a large impact on all peat bog ecosystems and resulted in the typical tussock grassland vegetation (Schouwenaars & Vink, 1990).

The work was done within the framework of the Surface Layer Integration Measurement and Modelling project (SLIMM) (Vugts *et al.*, 1994). The eddy covariance technique, used in the experiment, allowed the direct measurement of mass and energy transfer at a height above the surface resulting in a spatially integrated flux density. Here the measured flux densities were linked to the environmental conditions with a focus on temperature and humidity, their relationship, and the effect on the water use efficiency. The Penman–Monteith equation was used to deduce the surface resistance, r_s , of which the outcome was compared to values, found for other wetlands throughout the world to study the effect of the typical surface (litter) cover. Moreover, the 'decoupling' concept of McNaughton and Jarvis (1983) offered a diagnostic tool to identify the major controls of evaporation and compare them to other wetland studies.

3.2. Materials and methods

3.2.1. Site description

The experiment was done in a disturbed raised peat bog in the north of the Netherlands (Lat. 53°00'30" N, Long. 6°23'52" W, Alt. +11 m) during a one and a half-year period in 1994 and 1995. The dominating plant species in this tussock–grassland was *Molinia caerulea* (> 75% of the vegetation), but heather species like: *Calluna vulgaris* and *Erica tetralix*, could also be found. In the sections in which the soil was permanently over-saturated *Sphagnum* spp (< 1% of the vegetation) were present (Altenburg *et al.*, 1993). The area taken by the individual tussocks differed from 20 cm² to more than 1 m². The average height of the tussocks was approximately 0.4 m. A dense layer (0.1 m) of dead organic material from the previous growing seasons covered the tussocks and the hollows in between. In these hollows, spots of open water (< 5% of the surface) could be observed sheltered by the surrounding vegetation. Underneath the tussock surface was a saturated dark brown layer of peat. The depth of this layer varied from 0 to 2.5 m. At the measuring site this highly porous layer was about 0.3 m deep and at greater depth, a grey sandy loam was present. Throughout the seasons, the water table varied, depending on the weather, from 0 to 0.2 m below the tussock–soil interface but the soil remained saturated.

The growing season of *Molinia caerulea* lasted from May to October with a maximum

LAI of about 1.7 during mid August. During this period, green shoots grew up to a height (h) of 1.2 m above the tussock. From November until the beginning of May, no green shoots were present. What was left above the tussock was the brownish surface of organic material and some brown shoots standing upright throughout the winter period. For 1995, it was assumed that the LAI followed the same trend, except for a different timing of the onset and end of the growing season and maximum LAI. The periods in which the first shoots became visible (± 1 week), the grass flowered (± 1 week) and the all leaves had turned brown (± 1 week) were recorded for 1995

3.2.2. Instrumentation

A lattice tower was instrumented with an eddy-covariance system installed at a height of 8 m. This system included: a 3-D sonic anemometer (Solent A1012R2, Gill Instruments Ltd., Lymington, UK), a fine wire thermocouple (Dept. of Meteorology, Wageningen Agricultural University) and an inlet tube (Polyethylene 4mm internal diameter) leading to an infrared CO₂ and H₂O gas analyser (LI-6262, LI-COR Inc., Lincoln, Nebraska, USA). The 3-D sonic anemometer and the sampling tube were placed together, at 0.05 m apart.

For all wind directions the fetch was more than one kilometre and between 180–270° the terrain was slightly sloped. The closed path InfraRed Gas Analyser (IRGA) was placed in a box at the base of the mast. A pump was used to draw the air from the inlet to the IRGA at a rate of 10^{-4} m³ s⁻¹. The pump was placed in a way causing the pressure inside the sampling chambers to be slightly below atmospheric, but minimising the chance of condensation of water inside the tube. The IRGA ran in absolute mode and was re-calibrated every week. During this period the analyser's gain typically showed a 2 to 5% drift. The soda lime and magnesium perchlorate used to keep the reference cell free of CO₂ and H₂O, respectively, was changed every week. Every week, dry nitrogen from a cylinder was used as a zero calibration gas for CO₂ and water vapour, while dry air gas (400-ppm CO₂) was used as a second reference. An aspirated psychrometer was used as a second water vapour calibration.

A net radiometer (Funk, Middleton & Company Pty. Ltd., Australia), two pyrgeometers (CG 1, Kipp & Zonen, Delft, The Netherlands) and two pyranometers (CM10, Kipp & Zonen, Delft, The Netherlands) were used to measure net radiation (R_n) and the incoming and outgoing longwave and shortwave radiation respectively. A second 6 m high tower was instrumented with aspirated psychrometers (Dept. of Meteorology, WAU) and sensitive cup anemometers (Dept. of Meteorology, WAU; stalling speed 0.15 m s⁻¹) at 2, 4 and 6 m height

above the soil surface. A soil temperature profile (0.025, 0.2, 0.5 and 1 m) and the soil heat flux density (G) (0.05 m) were measured in the actual peat soil underneath a tussock, but not in the tussock itself.

3.2.3. Data acquisition and –processing

The meteorological instruments were sampled at 0.25 Hz. Every 30 minutes the data were averaged and stored in data loggers (21X, Campbell Scientific Inc., Logan, Utah, USA) for later processing. The sonic anemometer was sampled at 20.8 Hz. Analog signals from the IRGA and thermocouple, connected to the anemometer's interface unit, were sampled at a lower frequency. The resolvable input frequency of these signals was approximately 5 Hz.

The raw data of the eddy covariance system were stored on a PC and processed later, using a first order recursive digital filter with a time constant of 200 seconds (McMillen, 1988). Here a moving average was subtracted from each sample to get the fluctuating values of all the measured components. A software program (Van den Hurk, 1996) performed the necessary corrections, including: co-ordinate rotation (McMillen, 1986), Webb corrections (Webb *et al.*, 1980) and frequency response corrections (Moore, 1986), required for the calculation of the half-hour averaged flux densities. The power and co-spectra of the eddy covariance measurements (not shown) and the ability to close the surface energy balance were

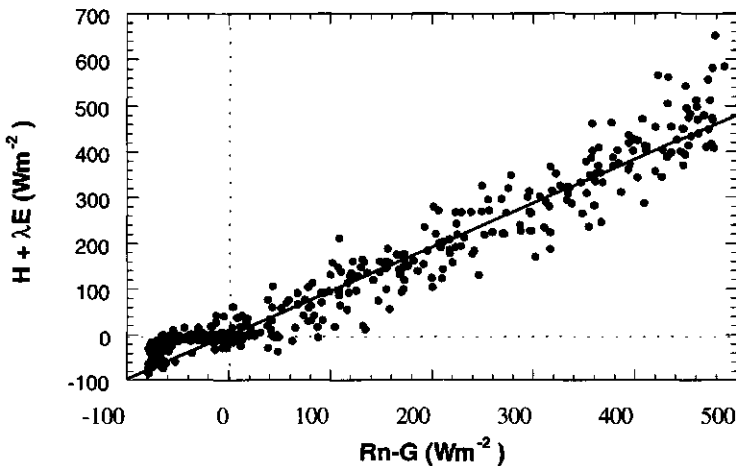


Figure 3.1: The energy balance closure. The half-hourly averaged available energy ($Rn-G$) is plotted against the sum of the partitioning components ($H+\lambda E$) for 10 consecutive days in August 1995. A linear regression line ($Rn-G = 0.96(H+\lambda E)$) could be fitted to the data with a R^2 of 0.94 ($N = 470$).

analysed to test the quality of the data. The available energy ($Rn-G$) versus the sum of the sensible heat (H) and latent heat (λE) flux density were fitted with a linear regression line described by $Rn-G = 0.96 (H+\lambda E)$ [$W m^{-2}$] with a regression coefficient (R^2) of 0.94 ($N = 470$) and is shown in Figure 3.1. This was concluded to be a satisfying quality.

3.2.3. The leaf area index

The course of leaf area index (LAI) was measured during the growing season of 1994. Here three patches in the vicinity of the towers were selected with characteristic features, varying from extremely wet, relatively dry or many pools of shallow open water. These patches were sampled every three weeks. For the measurements only *Molinia caerulea*, the dominant plant species in the area ($> 75\%$ of the vegetation), was considered (Altenburg *et al.*, 1993). To calculate the average leaf area unbiased for a patch, 100 shoots were picked. A hand-held scanner was used to determine the area of every individual leaf using a computer program giving an average leaf area. Furthermore, the average number of leaves from 25 plots of $0.09 m^2$ were used to determine the average leaf density of the patch. The average leaf area was then multiplied by the average leaf density, to obtain the LAI for a particular patch as shown in Figure 3.2.

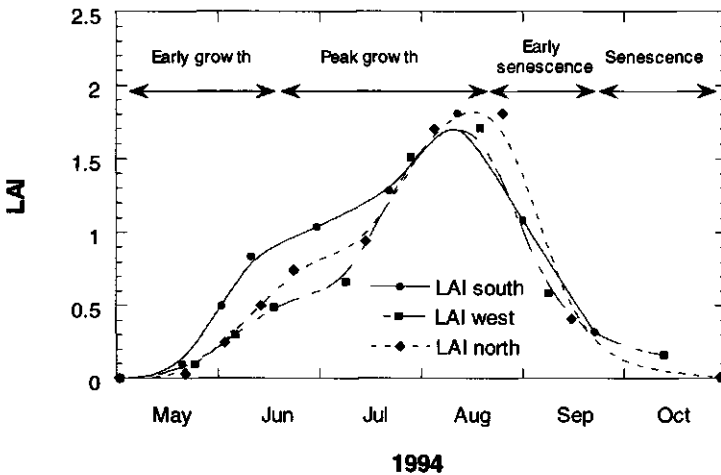


Figure 3.2: Course of the leaf area index (LAI) from three the patches around the experimental site during the growing season of 1994. Also indicated are the growing stages of the dominating vegetation, according to Kim & Verma (1990).

3.3. Results and discussion

3.3.1. Seasonal variation of environmental conditions and LAI

During the one and a half-year period, the daily mean air temperature at the height of 2 m ranged between -6 and 25 °C. The air temperatures for both summers were above the (30 year) climatic mean, with a maximum deviation from this mean in July 1994 of 4 °C. The 0.025 m soil temperatures, during the same period, were below 20 °C with a maximum of 19 °C in August 1994. The daily amplitude of the soil temperature was typically less than 5 degrees (Figure 3.3), half of that of air temperature due to the insulating effect of the dense

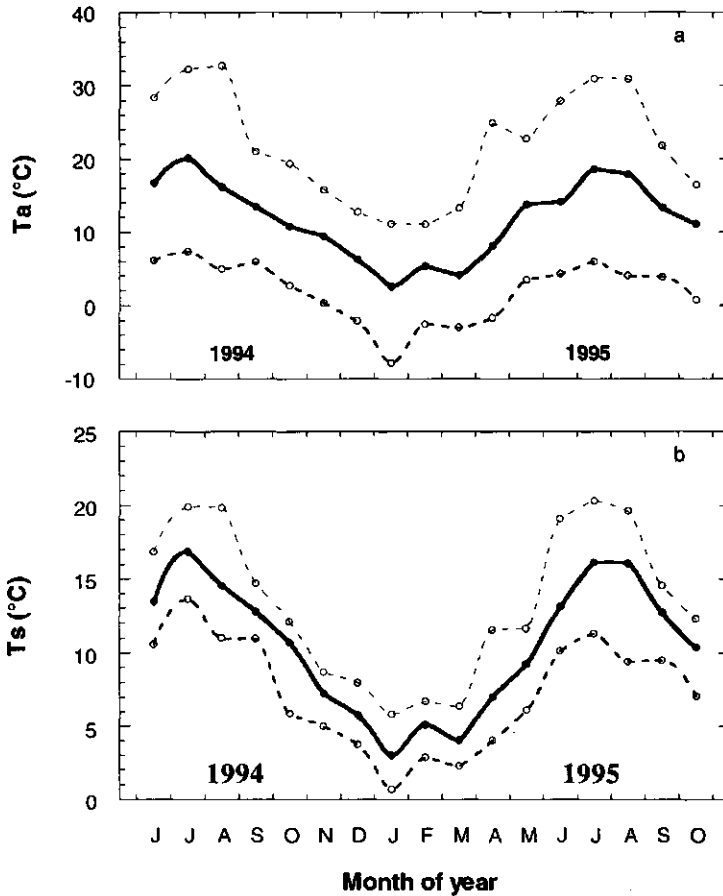


Figure 3.3: (a) Monthly averaged 2 m air temperature during 1994 and 1995. Also indicated are the maximum and minimum temperatures as measured during a particular month; (b) Monthly averaged 2.5 cm soil temperature during 1994 and 1995. Also indicated are the maximum and minimum temperatures as measured during a particular month.

layer of organic material on top of and in between the tussocks. The monthly average 2 m air temperature and the 0.025 m soil temperature are shown in Figures 3.3a and 3.3b, where the solid circles represent the average temperature and the open circles the maximum and minimum temperature measured during that month.

During the summer months, extensive periods of relatively hot weather with high daily maximum temperatures recorded at 2 m (>25 °C) were followed by shorter periods with showers and thunderstorms. The amount of precipitation was on average 25% less than the long-term climatic mean during this period, except for September 1994 and 1995, which were about 50% wetter. The water table dropped during the relatively hot and dry summers. During autumn and winter, precipitation was more regularly distributed and higher than on average.

3.3.2. Variation of CO₂ and latent heat exchange due to the local climate and vegetation

A monthly averaged diurnal course of the CO₂ and latent heat flux densities may help to give us a better understanding of the effect of climate and plant related factors have on the exchange of CO₂ and latent heat from the surface to the atmosphere. Here every half-hourly flux density value in a particular month and at a particular time is averaged to get the monthly averaged diurnal course. Such a representation of measurements will smooth random errors in the measurements and extreme weather events. Below we present the monthly averaged CO₂ flux density (F_c) and λE during different stages of the vegetation, from early spring until late summer irrespective of the measurement year. A negative flux density is directed towards the surface, while a positive flux density is directed away from the surface. Following other recent literature, we use the terms 'peak' or 'maximum' F_c for the largest negative CO₂ flux density (Baldocchi, 1994; Neuman *et al.*, 1994; Verhoef *et al.*, 1996).

Following the growing stages given by Kim and Verma (1990) for a grassland ecosystem, these stages are the early growth stage, peak growth stage, early senescence stage and senescence stage respectively (Figure 3.2). The bars represent the standard deviations of the average flux densities at a particular time of the day.

3.3.2.1. Seasonal variation of diurnal CO₂ flux densities

Figure 3.4 displays the monthly averaged CO₂ flux density for March to September. All data were used here, with the exception of data with apparent errors, such as data measured during short power failures. In Figure 3.4, the absence of green vegetation in March and April (no growth stage) is clear. The average exchange of CO₂ during this month was apparently totally

caused by respiration, resulting in a net release of CO₂ (positive F_c) during the course of the day. In May (early growth stage) the LAI had increased from 0 to 0.2 as seen from Figure 3.2. Despite the presence of green shoots and the associated photosynthetic activity, there was a net release of CO₂ throughout day and night. Soil and plant respiration, in this case, still exceeded photosynthesis. Probably due to a higher soil temperature, respiratory losses were higher than in March.

In the following three summer months (early growth, peak growth and early senescence stages), F_c exhibited a distinct diurnal course. Nighttime efflux of CO₂ varied between 0.05 and 0.1 mg CO₂ m⁻²s⁻¹ (1.1 – 2.3 μmol CO₂ m⁻²s⁻¹). In June, the CO₂ flux density peaked at 11:00 h. with a maximum of -0.18 mg CO₂ m⁻²s⁻¹ (-4.1 μmol CO₂ m⁻²s⁻¹). July, on the other hand, showed a maximum CO₂ flux density around 9:00 h. in the morning of about -0.22 mg CO₂ m⁻²s⁻¹ (-5.0 μmol CO₂ m⁻²s⁻¹). After this, as the day progressed, rates of net CO₂ uptake diminished with time. Similar behaviour has been reported for vegetations suffering from water stress in combination with an increase in air temperature and vapour pressure deficit (see e.g. Greco & Baldocchi, 1996; Neumann *et al.*, 1994; Shurpali *et al.*, 1995; Verhoef *et al.*, 1996). However, in our study area *Molinea caerulea* was never observed to suffer from water stress.

During August (early senescence stage), the daytime course of CO₂ uptake was rather constant during daytime with a maximum of about -0.18 mg CO₂ m⁻²s⁻¹ (-4.1 μmol CO₂ m⁻²s⁻¹) and was symmetrical around noon. The period of net uptake of CO₂ was about 2 hours shorter than during June and July. With the start of autumn, green vegetation was still present but started to diminish rapidly. September (senescence stage) therefore showed a diurnal course with significantly lower maximum daytime values for λE and F_c . The period of net uptake of CO₂ was about 2 hours shorter than in August. Despite the higher T_s and LAI during July and August in both 1994 and 1995 (see Figure 3.2), there was no significant increase in nighttime CO₂ efflux in comparison to June and September. This may have been due to the relatively large contribution of 'calm' nights (wind speed at 2 m height < 4 m s⁻¹ and friction velocity < 0.2 m s⁻¹) with negligible measured efflux of CO₂ during July and August.

The months during autumn and winter are not shown here, but demonstrated diurnal patterns similar to March as presented in Figure 3.4. For F_c this meant a net release of CO₂ during night and day depending on the soil temperature. Nieveen *et al.* (1998), earlier found a (2.5 cm) soil temperature dependence for soil respiration, expressed in a Q_{10} of 4.8 for this area. By definition this means that at every 10 degrees increase in temperature, soil respiration is increased by a factor of 4.8. This is in the range of values found by others for wetland

ecosystems (see e.g. Chapman & Thurlow, 1996).

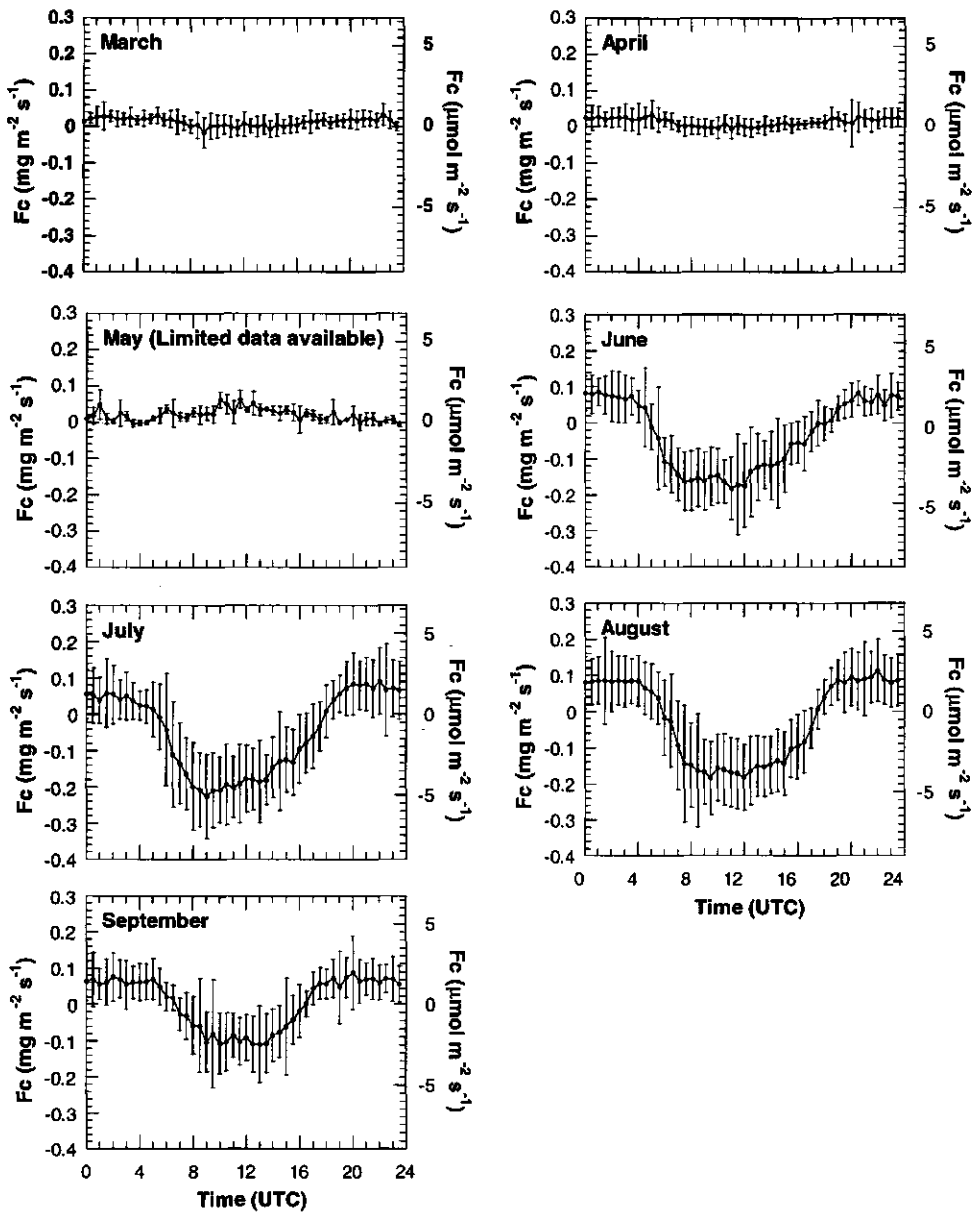


Figure 3.4: Diurnal patterns of monthly averaged half-hourly CO₂ exchange rates from March 1995 until September 1995. Bars indicate the standard deviation of a particular half-hourly mean value.

3.3.2.2. Seasonal variation of diurnal latent heat flux densities

Figure 3.5 shows the monthly averaged diurnal course of the latent heat flux density. Also indicated is the value of the monthly averaged daily evaporation rate in mm per day. The monthly averaged λE in March (no growth yet) showed a maximum of about 20 W m^{-2} during daytime hours and a mean daily evaporation of 0.2 mm d^{-1} . This flux density consisted of soil- and open water evaporation. With a mean daily evaporation of 0.2 mm d^{-1} , April showed a pattern similar to March. Here, in the absence of green vegetation, soil- and open water evaporation were presumably again the main components of λE . In May (early growth stage), the evaporation demonstrated a clear diurnal course, where λE started to increase from 0 W m^{-2} at 06:30 h to a maximum of 95 W m^{-2} at midday. Around 18:00 h, λE had dropped to 0 W m^{-2} and remained constant during nighttime. Soil and open water evaporation could still be the major contributors to the total λE . Transpiration was probably only a minor component, due to the small *LAI* (see Figure 3.2).

During June, July and August (early growth, peak growth and early senescence stages), λE peaked around noon at maximum rates between 170 and 190 W m^{-2} in synchrony with the incoming global radiation. Monthly averaged daily evaporation rates as shown in Figure 3.5, ranged between 1.8 and 2.1 mm d^{-1} , lower values than found in other wetland areas which are mostly dominated by *Sphagnum* species (e.g. Koerselman & Beltman, 1988; Lafleur, 1990; Price, 1991 and Kim & Verma, 1996). Observed evaporation rates compared well with measurements from an *Empodisma minus* dominated raised peat bog with an extremely dense canopy of dead vegetation interwoven with living stems in northern New Zealand (Campbell & Williamson, 1997). They reported a mean evaporation rate of 1.54 mm d^{-1} for a dry canopy with a maximum daily mean of 2.13 mm d^{-1} . As the water table lowered, the insulating layer became thicker and the shallow water pools in the hollows became more sheltered by vegetation. Transpiration was probably the major contributor to the total evaporation.

From September (senescence stage) onwards, the monthly averaged λE showed a rapid decline. The mean daily evaporation rate dropped about 60% to 0.78 mm d^{-1} in comparison to the previous months. The following months, λE continued to diminish to values similar to or smaller than measured in March. Again soil evaporation was probably the only contributor to the total evaporation.

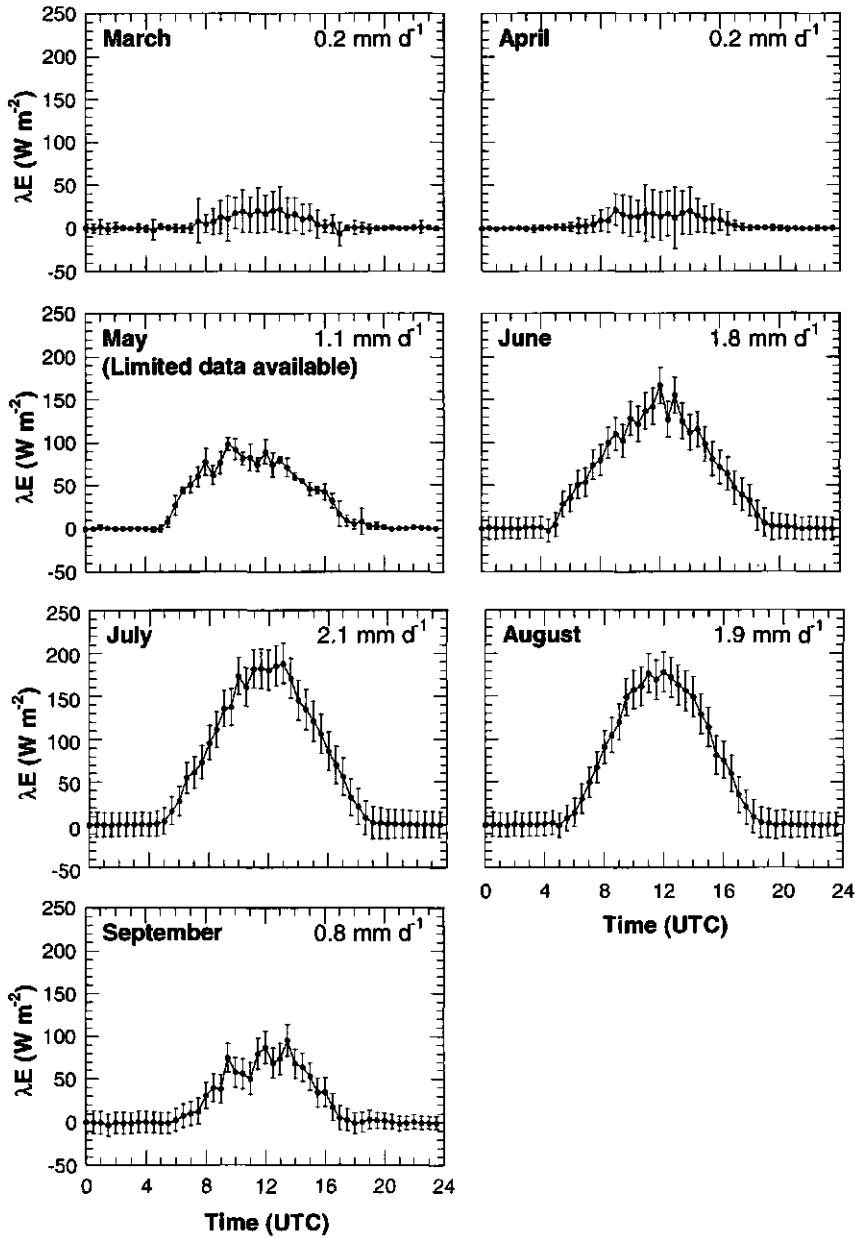


Figure 3.5: Diurnal patterns of monthly averaged half-hourly latent heat exchange rates from March 1995 until September 1995. Bars indicate the standard deviation of a particular half-hourly mean value.

3.3.3. Net CO₂ exchange and transpiration versus stomatal closure and surface temperature

The diurnal course of the CO₂ flux density in July showed a clear mid-morning depression and continuation of this trend towards the evening. This suggests a limitation of photosynthetic activity, which might be due to stomatal closure, high leaf tissue temperatures, or increased respiratory losses induced by high leaf tissue temperatures (Schulze 1986 or Tenhunen *et al.*, 1984). Often midday stomatal closure is associated with soil water stress or a high atmospheric vapour pressure deficit (D) (see e.g. Valentini *et al.*, 1996; Jacobs, 1994; Lösch & Tenhunen, 1981).

Soil water stress as an explanation for stomatal closure is not considered here. Verry (1988) demonstrated that a drop in water table of about 0.2 to 0.3 m had little effect on the total evaporation from an open *Sphagnum* bog with vascular plant cover. A similar result was found earlier by Romanov (1968), who explained an abrupt decline in evaporation by the fact that the water table had dropped below 0.4 m in a raised peat bog with dwarf shrubs. During the summer months, the contribution of vascular plants with an extended root system was relatively high in the Fochteloöer area. The water table dropped to only 0.2 m at most below the actual soil surface underneath the tussocks. This small drop is unlikely to have caused a decrease in evapotranspiration and an associated increase in stomatal closure. This is in large contrast with reports from *Sphagnum* dominated peat bogs, where a slight drop in water table resulted in a substantial decrease in the total evaporation (Ingram, 1983; Kim & Verma, 1996).

What remains, as a possible explanation for stomatal closure, is the vapour pressure deficit. In spite of high D , which stimulates transpiration, the stomatal closure results in a decreased transpiration (Lösch and Tenhunen, 1981; Tenhunen *et al.*, 1987; and Grantz, 1990). In our case, however, a decrease in the total evapotranspiration, synchronised with F_c , was not observed. To further investigate this, we study the behaviour of F_c and λE on four contrasting days.

To demonstrate the relatively small contribution of soil evaporation to the total evapotranspiration, day 123 (3 May 1995) is analysed. On this day, air temperatures at 2 m rose to a maximum of 23 °C with a maximum vapour pressure deficit of 19 hPa. Green shoots started to show on top of the tussock. Throughout day and night there was a net release of CO₂ as shown in Figure 3.6 (daily net exchange = 2.2 g CO₂ m⁻² d⁻¹). Nieveen *et al.* (1998) found a soil respiration (R_d) dependence on soil temperature of $R_d = 0.012\exp(0.16Ts)$ for this area. This would lead to an approximate respiratory flux density of 0.08 mg CO₂ m⁻² s⁻¹

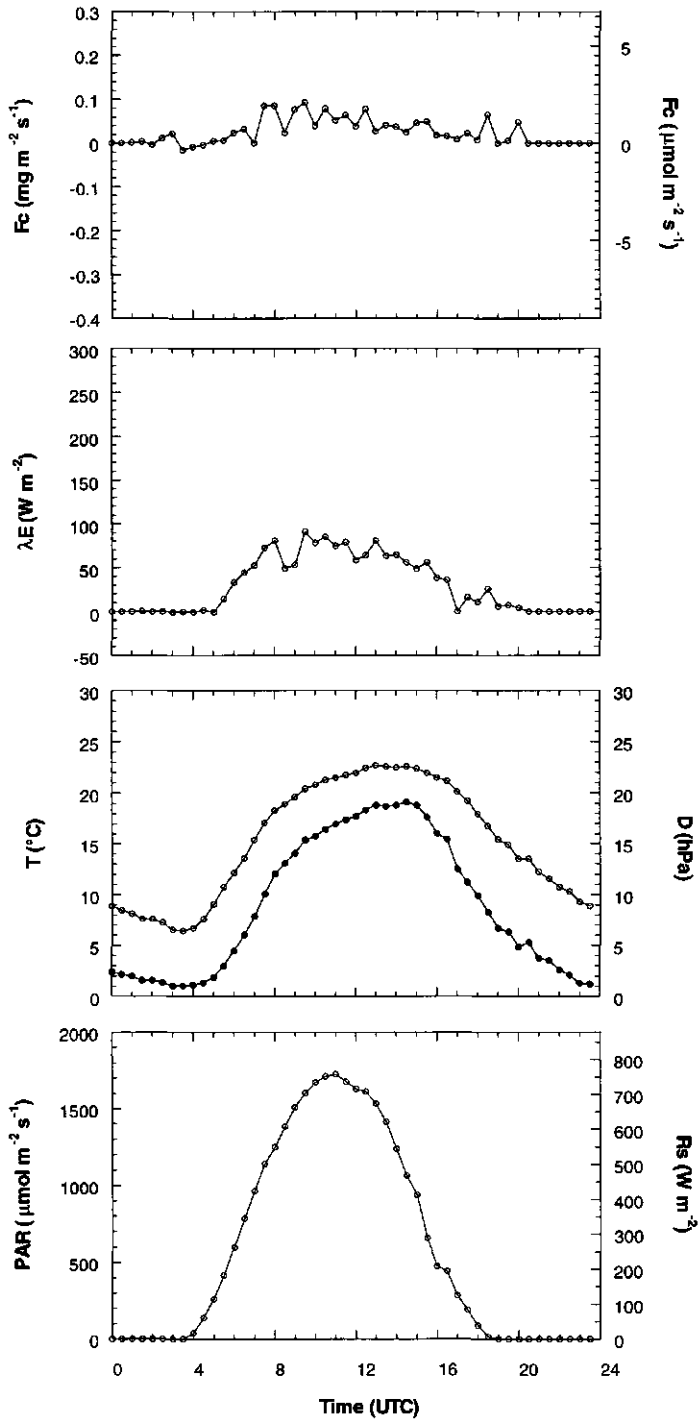


Figure 3.6: Diurnal patterns of canopy CO_2 and latent heat exchange rates, 2 m air temperature, vapour pressure deficit (solid circles) and photosynthetic active radiation for day 123.

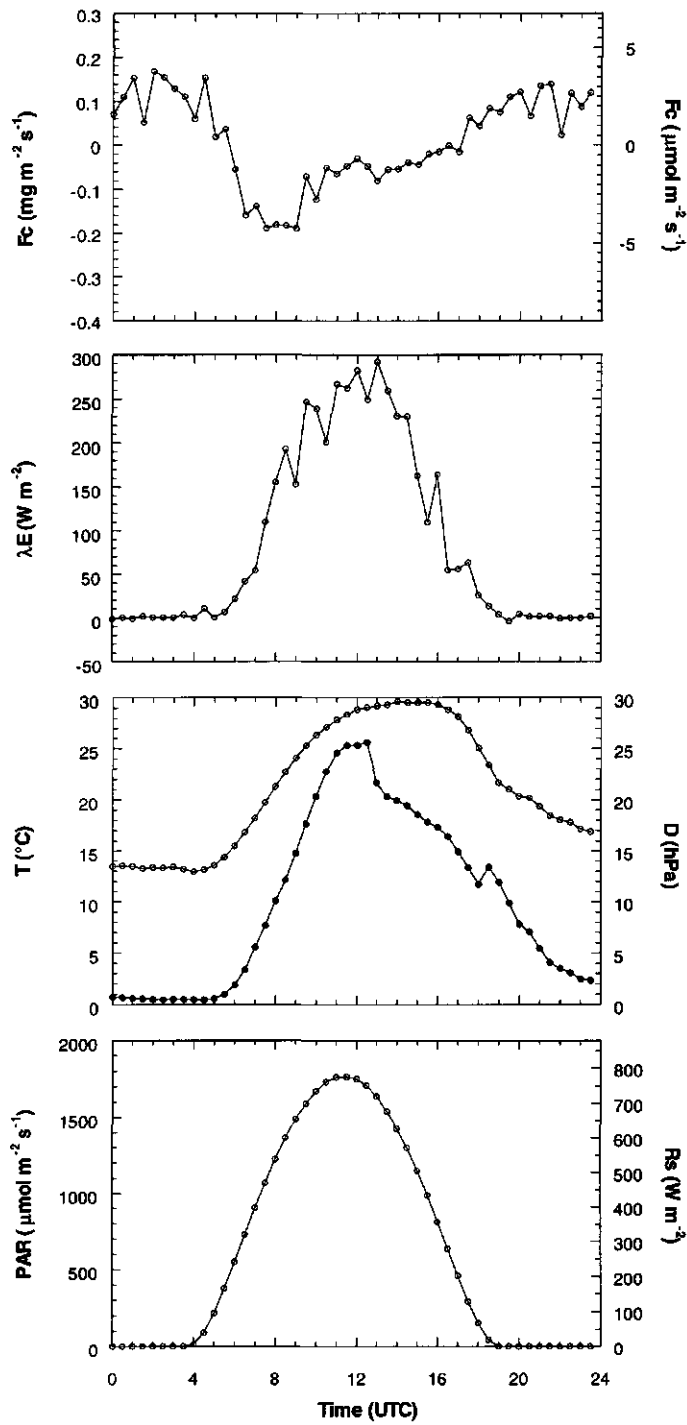


Figure 3.7: Diurnal patterns of canopy CO₂ and latent heat exchange rates, 2 m air temperature, vapour pressure deficit (solid circles) and photosynthetic active radiation for day 223.

at a midday soil temperature at depth 0.025 m of 12 °C, similar to the measured values. This confirms our earlier assessment that the photosynthetic activity at this stage of the growing season contributed little to the CO₂ flux density. At the same time latent heat loss showed a midday maximum of 90 W m⁻² and a daily rate of 1.1 mm d⁻¹. With little green vegetation, this water probably originated solely from the soil which, in this part of the year, was waterlogged and showed numerous shallow puddles. As the growing season progressed the water table lowered and the puddles disappeared or were sheltered by the new shoots, possibly resulting in a smaller contribution of soil evaporation to the total latent heat flux density later in the season.

High *D* has been designated as a possible explanation for decreasing photosynthetic activity during the day. Day 223 (11 August 1995) is an example of a day with high temperature and vapour pressure deficit (Figure 3.7). Maximum *T* reached up to 30 °C and maximum *D* of 26 hPa in the afternoon. During the early morning when the photosynthetically active radiation (*PAR*) was increasing, *F_c* reached a maximum of -0.17 mg CO₂ m⁻² s⁻¹ (-3.8 μmol CO₂ m⁻² s⁻¹). However, after 09:00 h, *F_c* started to decrease while the *PAR* was still increasing to maximum of about 1760 μmol m⁻² s⁻¹ at noon (daily net exchange = +0.98 g CO₂ m⁻² d⁻¹). This mid-morning peak and the decline in uptake was similar to observations made in other *Sphagnum* dominated wetland ecosystems (see e.g. Neumann *et al.*, 1994 and Shurpali, 1995). During the same period, λ*E* did not noticeably reduce and followed more or less the *PAR* trend reaching a maximum of 292 W m⁻² at 13:00 h. (Daily rate 3.1 mm d⁻¹). In comparison to day 123, the environmental conditions on day 223 are quite similar, but with a higher *T* and *D*. We conclude, however, that transpiration is the major contributor to the total evapotranspiration.

As suggested, a possible explanation for the decrease in *F_c* is that high *D* caused the stomatal resistance of the vegetation to increase, as found by Jacobs *et al.* (1996) in a grapevine vineyard in Spain. If this were the case in our study, a stronger reaction of λ*E* to stomatal closure would possibly have been visible. In addition to high *D*, however, high *T* could have negatively affected the photosynthetic activity and/or have increased the soil and plant respiration, as can be seen from Figure 3.8.

Thirteen days earlier in the peak growth stage, on day 210 (29 July 1995), a similar situation as on day 223 occurred. While *PAR* was still increasing towards a maximum of 1685 μmol m⁻² s⁻¹ around noon, net CO₂ uptake reached its maximum of -0.38 mg CO₂ m⁻² s⁻¹ at 07:30 h and continued to decrease as the day progressed (net exchange = -7.8 g CO₂ m⁻² d⁻¹).

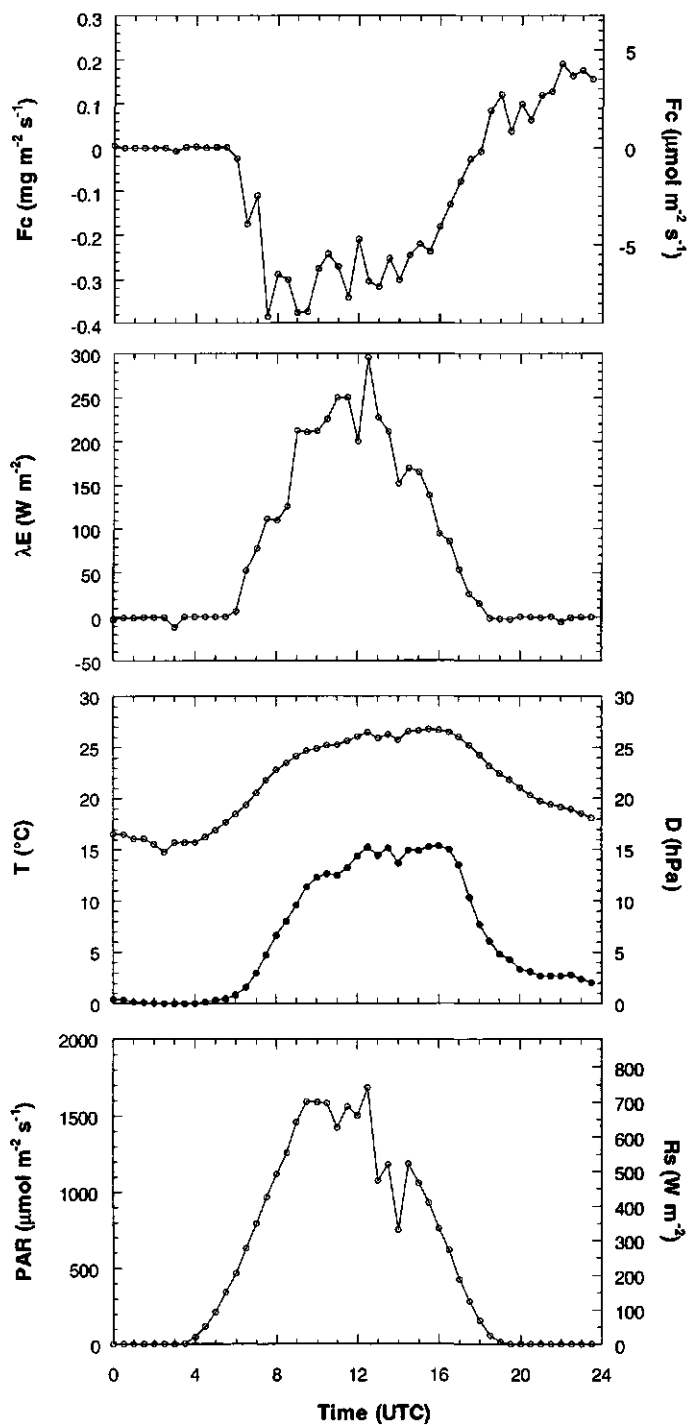


Figure 3.8: Diurnal patterns of canopy CO₂ and latent heat exchange rates, 2 m air temperature, vapour pressure deficit (solid circles) and photosynthetic active radiation for day 210.

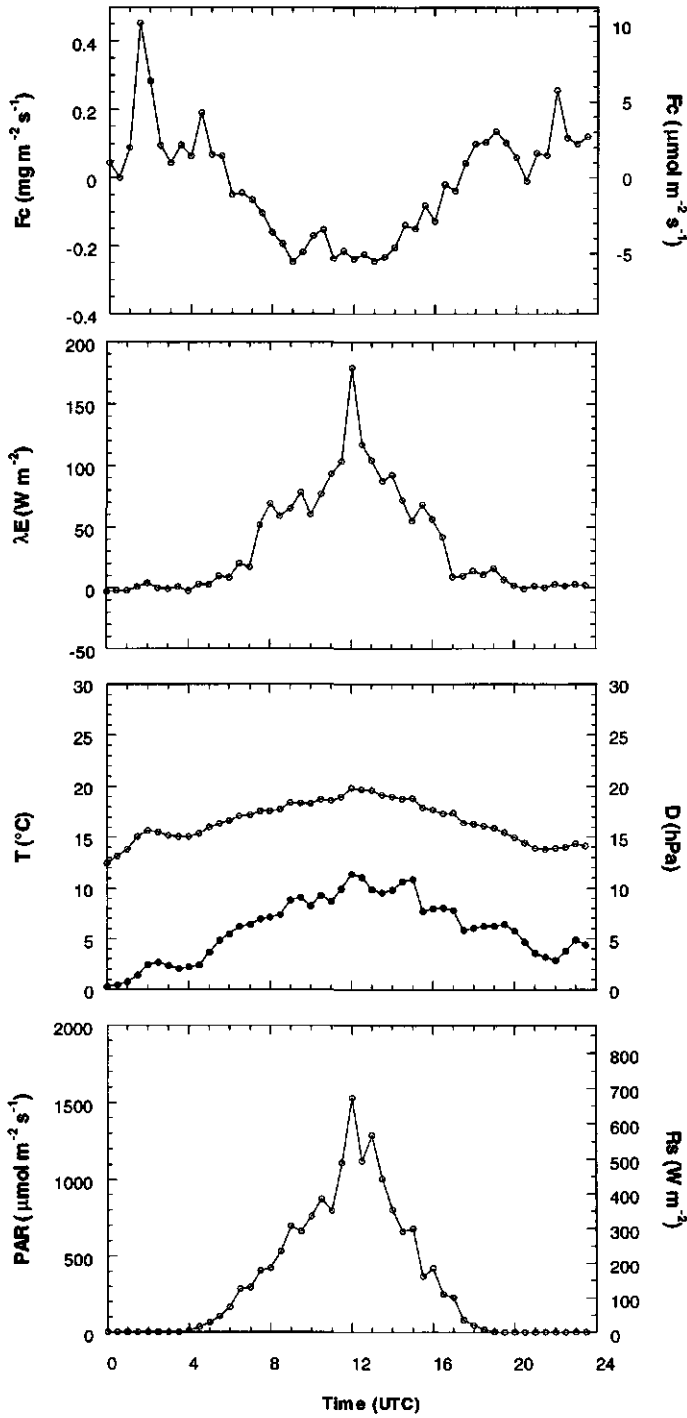


Figure 3.9: Diurnal patterns of canopy CO₂ and latent heat exchange rates, 2 m air temperature, vapour pressure deficit (solid circles) and photosynthetic active radiation for day 219.

The T during the late morning and afternoon was about 3 degrees lower than on day 223, but most importantly D during that period was more than 10 hPa lower with a maximum of about 15 hPa. This indicates that F_c was mainly affected by temperature, reducing the photosynthetic activity and/or increasing the plant and soil respiration, and not by the vapour pressure deficit. The soil temperatures during days 210 and 223 ranged between 14.7 and 17.9 °C with a daily mean of 16.8 and 16.5 °C, respectively. Respiratory losses should therefore be in the same range for both days, assuming the same soil water status. Again λE was not noticeably reduced and followed the PAR trend reaching a maximum of 296 W m^{-2} at 13:00 hours (daily rate 2.7 mm d^{-1}). λE on day 210 was somewhat lower than on day 223, possibly because of a lower D and a reduced evaporative demand of the atmosphere. Due to the earlier discussed mulching effect of the dead organic material (see day 123), transpiration is likely to be the major contributor to the total evapotranspiration.

On day 219 in the early senescence stage (17 August 1995), T reached a maximum of 20 °C while D had a peak of 11 hPa (Figure 3.9). Both moderate values are resulting in a maximum F_c and λE around noon of only $-0.25 \text{ mg CO}_2 \text{ m}^{-2} \text{ s}^{-1}$ and 179 W m^{-2} , respectively. A midmorning depression in F_c was not observed, apart from small reductions in photosynthetic activity probably associated with small depressions in PAR . Both F_c and λE were in synchrony with R_s . Day 219 displayed a net daily uptake of CO_2 of $-1.4 \text{ g CO}_2 \text{ m}^{-2} \text{ d}^{-1}$ and a daily evaporation rate of 1.2 mm d^{-1} , probably induced by senescence.

3.3.4. Relationship between CO_2 flux density and latent heat flux density

The flux densities of CO_2 and water vapour are closely coupled since both water vapour and carbon dioxide diffuse through the same stomata. The behaviour of these stomata is influenced by many environmental conditions and plant related factors, such as: light, soil and air temperature, air humidity, soil water status, plant hormones, leaf age, growth stage, nutrients, and leaf temperature. The data showed that despite a continuing decrease in F_c after the midmorning λE was not greatly reduced. Therefore, high D was rejected as a possible cause for the decrease in F_c . We shall further discuss temperature as a possible explanation of this behaviour as well as some consequences.

3.3.4.1. Relationship between CO_2 flux density and temperature

To investigate the effect of air and canopy temperature on the photosynthetic activity, we selected a period of 14 days in first part of August 1995 with a LAI around the maximum of

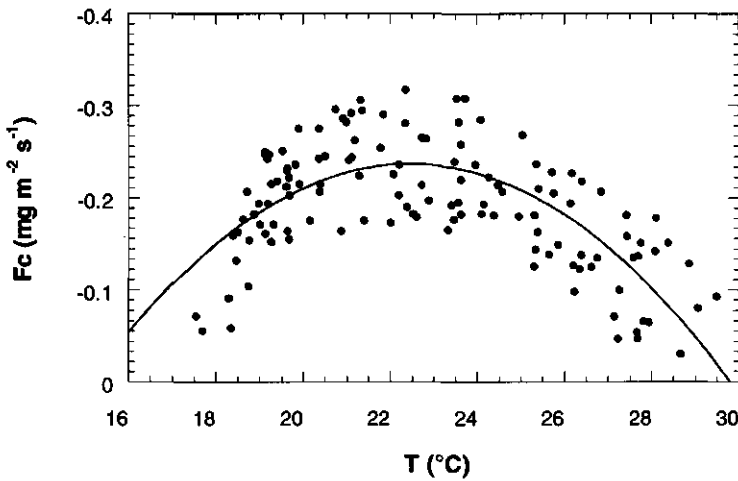


Figure 3.10: The half hourly averaged carbon dioxide flux density between 8:00 and 14:00 h UTC versus the 2 m air temperature for 14 days consecutive in first part of August 1995. Data is fitted with a second order polynomial with a maximum at $T = 22.5^{\circ}\text{C}$.

1.7. Figure 3.10 shows F_c versus T at 2 m for data points measured between 08:00 and 14:00 h. A temperature optimum (T_{opt}) of net CO_2 exchange is evident between 20 and 25 °C. This is in the range found by others for forests and crops (see e.g. Baldocchi *et al.* 1981a, 1981b or Price & Black, 1990). At higher and lower temperatures F_c decreases with temperature, approaching zero at 30°C. The large scatter in the data might be caused by the effect of solar radiation on the photosynthetic activity or plant related factors.

The longwave radiometer showed that the canopy surface temperature was often in the range of 30 to 35 °C (Emission coefficient (ϵ) = 0.98). Therefore the canopy temperature may have exceeded the optimum temperature of *Molinia caerulea* for photosynthesis, causing net photosynthesis to diminish (see days 210 and 223 in section 3.3). This reduction could arise from a rapid increase of soil and plant respiration with temperature or from the inactivation of the assimilation mechanism at higher leaf temperatures (Schulze 1986 or Tenhunen *et al.*, 1984). As λE was not remarkably reduced, lower leaf conductivity can be excluded. The insulating layer of dead organic matter protected the soil from high mean temperatures and strong temperature fluctuations. The highest measured soil temperatures were about 20 °C. Large changes in soil respiration were therefore not considered. However, increased plant respiration remains a possible cause for the reduced CO_2 exchange at high temperatures.

3.3.4.2. Water use efficiency

Water use efficiency [$\text{mg CO}_2 \text{ g H}_2\text{O}^{-1}$] is often expressed as the ratio between the CO_2 and water vapour flux density (F_c/E). Many authors have reported a strong negative correlation between F_c/E and D (e.g. Bierhuizen & Slatyer, 1965; Baldocchi *et al.* 1985; Baldocchi *et al.* 1994 and Verhoef *et al.*, 1996). Figure 3.11 shows the relationship between $|F_c/E|$ and D for the same period of 14 days in first part of August 1995 as used above. Water use efficiency is reported to be sensitive to low levels of irradiance (Baldocchi *et al.*, 1985) and hence only data from periods with $R_s > 300 \text{ Wm}^{-2}$ were used. We found a clear non-linear relationship described by: $|F_c/E| = 165.76 D^{-1.61}$ ($R^2 = 0.72$). Our values were similar to values e.g. found by Baldocchi (1994) for wheat and by Baldocchi *et al.* (1985) for soybeans. Values ranged between 0 and 10 mg g^{-1} indicating that, especially at high D , the peat bog ecosystem was inefficient with water. In comparison, Verhoef *et al.* (1996) found water use efficiencies up to 45 mg g^{-1} at low D for scattered shrubs with a herbaceous understorey in a Sahelian savannah. Obviously, *Molinia caerulea* has no need to be efficient with water, given the abundant availability in the soil. A similar phenomenon was reported by Johnson and Caldwell (1976) for *Dupontia fischeri* and *Deschampsia caespitosa*, tundra species restricted to wet sites with stomata responding poorly to humidity.

Despite the fair correlation between the water use efficiency and D , we suspect T to be the main factor controlling the efficiency. However the individual effects of T and D are difficult to separate due to the temperature dependence of D . High T and moderate D on day

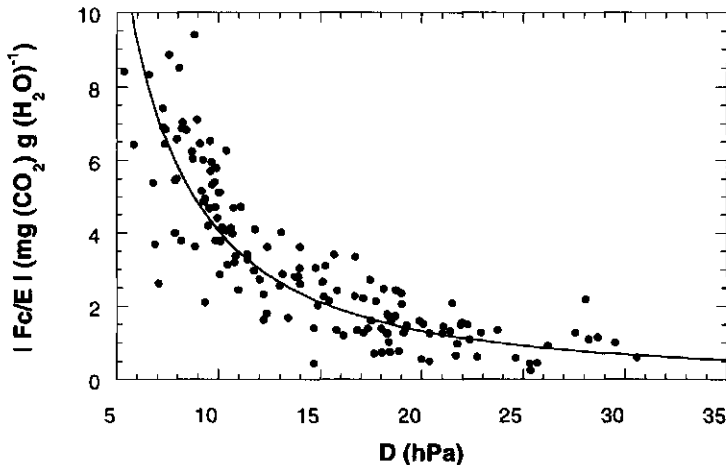


Figure 3.11: Relationship between the water use efficiency ($|F_c/E|$)

210 (see Section 3.3), resulted in a decrease in CO₂ uptake during the course of the day, but no obvious effect on λE . Moderate T and moderate D on day 219 (see Section 3.3), showed no distinct effect for both F_c and λE . This temperature effect probably caused the scatter at low D (Figure 3.11).

3.3.5. Surface resistance

To overcome having to describe the canopy structure in much detail often a simplified 'big leaf' model (Monteith, 1965) is used in which the surface is treated as a single big leaf. A bulk surface resistance [$s\ m^{-1}$], r_s , is introduced to describe the transfer of water vapour from the sub-stomatal cavities to the atmosphere. r_s can be deduced by inverting the Penman-Monteith equation (Monteith, 1965) given by:

$$\lambda E = \frac{s(Rn - G) + \rho C_p D / r_a}{s + \gamma(1 + r_s / r_a)} \quad (3.1)$$

where s is the rate of change of the saturated vapour pressure with temperature [$hPa\ K^{-1}$], ρ is the density of air [$kg\ m^{-3}$], C_p the heat capacity of air at constant pressure [$J\ kg^{-1}\ K^{-1}$], r_a the aerodynamic resistance [$s\ m^{-1}$] and γ the psychrometer 'constant' [$0.67\ hPa\ K^{-1}$ at 293 K]. Following Thom (1975), the aerodynamic resistance to the transport of water vapour is given as the aerodynamic resistance to momentum transport and an excess resistance to the transport of heat and water vapour compared to momentum transfer:

$$r_a = r_{aM} + \frac{1.6}{\kappa u_*} \quad (3.2)$$

Here $r_{aM} = u/u_*^2$ is the aerodynamic resistance to momentum transport [$s\ m^{-1}$], $\kappa = 0.4$ the von Karman constant [-], u the average wind speed [$m\ s^{-1}$] and u_* the friction velocity [$m\ s^{-1}$]. Figure 3.13 shows the mean diurnal variation of r_s as calculated from (3.1) and (3.2) for the period of 14 consecutive days in the beginning of August 1995. The daytime r_s varied 201 and 608 $s\ m^{-1}$, with an average of about 300 $s\ m^{-1}$. Lowest values were found at midday between 10:30 and 12:00 h. The aerodynamic resistance during this period ranged between 20 and 60 $s\ m^{-1}$ with a daytime mean of 30 $s\ m^{-1}$ (data not shown) and is within the range of values found for agricultural crops or grassland (15 – 150 $s\ m^{-1}$). Surprisingly, between 10:30 and 12:00 h. F_c was often found to diminish with time which suggests that F_c is poorly related to the surface resistance. Duyzer and Bosveld (1988) found similar values for r_s for the Fochteloeër

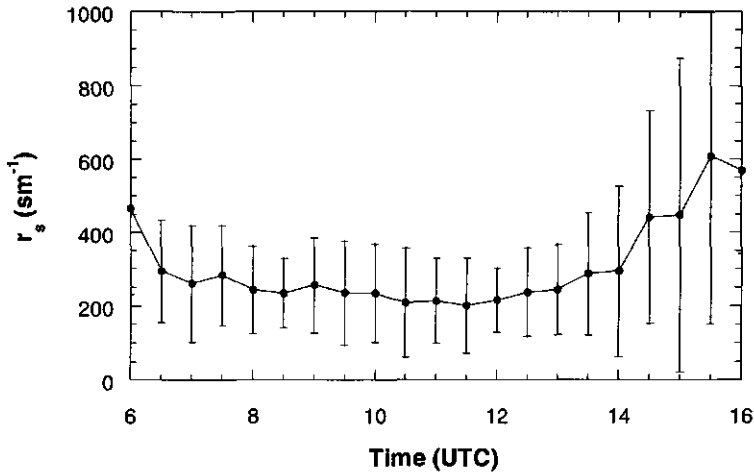


Figure 3.12: Average diurnal pattern of the canopy resistance, r_s , for a period of 14 consecutive days in the beginning of August 1995. Bars indicate the standard deviation of a particular half-hourly mean value.

area in an earlier experiment. These values are rather high compared to values found in other wetlands. Kim and Verma (1996) recently found that values of r_s ranged between 80 and 250 s m^{-1} , with a midday average of 100 s m^{-1} for an open sphagnum fen in north-central Minnesota, USA. Even lower values were found by Lafleur and Rouse (1988) for a subarctic marsh in Canada and by Price (1991) for blanket bog in Newfoundland. Campbell and Williamson (1997), on the other hand, found rather similar values ranging from 150 and 608 s m^{-1} and an overall mean of 320 s m^{-1} for a raised bog in northern New Zealand. Similar to our raised bog, theirs was covered with a dense layer of dead organic material but the vegetation showed a higher *LAI*.

3.3.6. Atmospheric coupling

McNaughton and Jarvis (1983) and Jarvis and McNaughton (1986) rewrote the Penman-Monteith equation, as given in (3.2), to quantify the main forcing variables for transpiration and evaporation for prescribed boundary conditions at a reference level. Here the 'decoupling factor', Ω , is defined by:

$$\Omega = \left[1 + \frac{\gamma}{s + \gamma} \frac{r_s}{r_a} \right]^{-1} \quad (3.3)$$

and (3.1) becomes

$$\lambda E = \Omega \frac{s(Rn - G)}{s + \gamma} + (1 - \Omega) \frac{\rho C_p D}{\gamma r_s} \quad (3.4)$$

The value of Ω ranges between 0 and 1 and is determined by the ratio of r_s and r_a and the temperature at a reference level. In the case Ω is close to 0, the surface is well coupled to the atmosphere and thus λE is mainly controlled by regional conditions. In the case Ω is close to 1, the surface is 'decoupled' from the atmosphere due to insufficient turbulent mixing and λE is dominated by the available energy and the local atmospheric conditions. The use of Ω to describe the coupling between the surface and the vegetation should however be done with caution as Ω can never account for the many non-linear feedback processes encountered in scaling up from the stomatal pore to the region (Jacobs & De Bruin, 1992; McNaughton & Jarvis, 1991). It is recommended to use this approach only for diagnostic purposes.

For the period of 14 days in early August, the calculated values for Ω ranged between 0.11 and 0.68 (6:00 – 16:00 h) with a mean value of 0.29. Within the Ω -concept, this indicates that the λE is strongly coupled to the atmospheric evaporative demand (i.e. D) and the surface resistance and implies negligible dependence of λE on the available energy. However, if we take $(Rn - G) = 500 \text{ W m}^{-2}$, $s / (s + \gamma)$ at $25 \text{ }^\circ\text{C} = 0.74$, $D = 20 \text{ hPa}$, $r_a = 30 \text{ s m}^{-1}$, and $r_s = 300 \text{ s m}^{-1}$, then $\Omega = 0.28$ and the first and second term on the right of (3.4) become 103 and 87 W m^{-2} respectively. Thus the relative contribution of the radiative term is even larger than the aerodynamic term in (4). The calculated Ω 's are low compared to other canopy surfaces discussed in the literature. McNaughton and Jarvis (1983) estimated Ω values of 0.2 and 0.8 for forest and grassland, respectively. Here Ω is mainly determined by a change in the aerodynamic resistance, while in our case, Ω is controlled by the surface resistance.

Lafleur and Rouse (1988) found a median value of 0.64 (0.33 – 0.95) for a subarctic sedge marsh during the growing season. For heather moorland in Scotland, Miranda *et al.* (1984) calculated a median value of 0.32 and values ranging from 0.55 to 0.89 were found by Kim and Verma (1996) for an open *Sphagnum* fen. Campbell and Williamson (1997) calculated a daytime mean Ω of 0.27 with values ranging between 0.21 and 0.36 for a raised bog. Similar to our raised bog, theirs was covered with a dense layer of dead organic matter and showed a slightly smaller surface resistance, but the LAI was about two times higher during the growing season (Campbell & Williamson, 1997).

3.4. Summary and conclusions

We measured the flux densities of carbon dioxide and water vapour from a *Molinia caerulea* dominated raised bog during 1994 and 1995. The growing season lasted from early May till the end of October during which sparse *Molinia caerulea* vegetation developed with a maximum *LAI* of about 1.7. Year round, the tussock grassland was covered with a dense layer of dead organic matter. This and the sparse canopy appeared to have large influence on the exchange of CO₂ and water vapour from the area.

Diurnal courses often showed a single early morning peak in CO₂ uptake, but as the morning progressed, rates of CO₂ uptake continued to diminish with time. Simultaneously, water vapour flux densities seemed unaffected and continued to rise to maximum values around noon in synchrony with incoming global radiation. Results of this study indicated that the observed decrease in the CO₂ flux density was not caused by stomatal closure, such as often associated with soil water stress or a high atmospheric vapour pressure deficit. Soil water stress was excluded as the dominating vegetation rooted in a peat soil permanently close to saturation. Besides, with both high (>25 hPa) and moderate (<15 hPa) *D* it was shown that the CO₂ uptake decreased during the day. High leaf tissue temperatures or increased respiratory losses induced by high leaf tissue temperatures, most likely caused the limitation of the net CO₂ exchange when the 2 m air temperatures and leaf tissue temperatures rose above 25 °C, thereby exceeding the optimum temperature for CO₂ exchange between 20 and 25 °C air temperature.

The daytime mean surface resistance during the peak growing stage of the vegetation was high. Values varied between 200 and 600 s m⁻¹ with a minimum around noon, which is much larger than found in most crops and other wetland studies. The 'decoupling' factor, Ω , ranged between 0.11 and 0.68, despite moderate aerodynamic resistances. Again these values were much lower than found in grassland or wetland studies and indicate a strong coupling to the overlying atmosphere and suggests a strong control of evapotranspiration by *D* and *r_s* and not by the available energy (*R_n*-*G*). However, simple calculation showed an equal contribution of the radiative and the aerodynamic to the total evapotranspiration. In the Ω - concept of Jarvis and McNaughton (1983), the "decoupling factor" Ω is mainly set by the aerodynamic resistance, *r_a*. If *r_a* is relatively small, for example 20 s m⁻¹ in the case of forests, sufficient turbulent mixing causes a coupling of the surface to the atmosphere. If *r_a* is relatively large, for example 80 s m⁻¹ in the case of short grass, insufficient turbulent mixing causes a decoupling of the surface and the overlying atmosphere. In our case, however, Ω is

set by the surface resistance and, thus, inappropriate to use in this approach.

The small *LAI* might be the main reason for the high surface resistance. Besides, the dense layer of dead organic matter probably prevented transfer of water vapour from the soil surface by turbulent mixing and deep penetration of solar radiation, despite the extremely wet conditions. The small *LAI* and the surface litter cover often caused high surface temperatures. High surface temperatures ($T_{surface} > T_{opt}$) led to a reduced net CO_2 exchange, but also induced an increase in *D*. The increased evaporative demand stimulated λE . It appeared that the *Molinia caerulea* vegetation was rather inefficient with water, for example in comparison to natural vegetation under arid conditions. With the abundant availability over water in the root zone, transpiration is not limited and might act as a safeguard against over heating of the plant tissue.

Acknowledgements

Joost Nieveen was financially supported by the Netherlands Organisation for Scientific Research (N.W.O.) under project number 753-06-243. We would like to thank Teun Jansen, Willy Hillen, Frits Antonysen and Bert Heusinkveld of the Department of Meteorology for their contribution to the field experiment and general logistics. We also thank Wim Kohsiek and Alan Green for their helpful comments on this paper. Special thanks go to the management of the Fochteloöerveen (Vereniging tot Behoud van Natuurmonumenten in Nederland), for granting scientific research in the area.

CHAPTER 4

-
-
-

THE SCINTILLATION TECHNIQUE

JOOST P. NIEVEEN

*Department of Meteorology, Wageningen Agricultural University, Duivendaal 2, NL-6701
AP, Wageningen, The Netherlands*

4.1. Introduction

An optical or electromagnetic wave propagating through a turbulent atmosphere exhibits fluctuations in intensity known as 'scintillations' (Lawrence & Strohbehn, 1970). In atmospheric turbulence, fluctuations in temperature, humidity and pressure cause density fluctuation and with it fluctuations in the refractive index (n). These refractive index fluctuations cause random refraction and absorption of electromagnetic (EM) radiation passing through the turbulent atmosphere, changing the characteristics of the wave (Hill *et al.*, 1980). Scintillation of light is related to these phenomena and is experienced at a receiver as fluctuations in the light intensity (e.g. twinkling of stars) caused by interference of refracted light and absorption of the light. Scintillometers measure the turbulent intensity of the refractive index fluctuations of the air from the intensity fluctuations of a received signal expressed in the refractive index structure parameter, C_n^2 [$m^{-2/3}$].

Near-infrared scintillometers are becoming increasingly popular as a means of determining the path-averaged sensible heat flux density. The ability to measure this quantity over distances of more than a kilometre, i.e. the landscape scale, makes it a unique instrument. Many meteorological, agricultural and hydrological applications such as climate models require areally averaged flux densities as input. These data could be obtained from a network of eddy covariance measurements, remote sensing or aircraft measurements, but each of these techniques is either very costly, time consuming or needs a large technical overhead. With the commercial availability of different types of scintillometers, scintillometry offers a relatively

cheap and simple alternative. This is reflected in the increasing number of scientists using the technique over different types of vegetation and landscapes (see e.g., De Bruin et al, 1995 (Vineyard); McAneney *et al.*, 1995 (Pasture); Green & Hayashi, 1998 (Rice paddy); Thiermann & Grassl, 1992 (Bare soil)).

4.2. Atmospheric turbulence

Atmospheric turbulence is generated by large-scale phenomena such as: wind shear and convection. From these events, large scale eddies are generated depending on the local climatology and surface geography. The size of these eddies is assumed to be smaller than some maximum scale size, L_0 [m], often called the outer scale of turbulence. Close to the earth's surface, L_0 is of the order of the height above the ground. The motion of large scale eddies causes the formation of and energy-transfer to smaller eddies. In turn these smaller eddies will generate and transfer energy to still smaller eddies until molecular effects become important and turbulent energy is dissipated into heat. The inner scale of turbulence, l_0 [m], describes the smallest scale of turbulent inhomogeneities (1 mm ~ 1 cm) and marks transition from the inertial range to the viscous dissipation range of eddy sizes. In the range between L_0 and l_0 , often called the inertial subrange of eddy sizes, the turbulence becomes homogeneous and isotropic. The above was originally proposed by Kolmogorov and was expressed in a three-dimensional velocity spectrum, $\Phi_v(K)$ [m^3], which represents the amount of energy of a turbulent eddy at a certain spatial wave number $K = 2\pi l^{-1}$ [m^{-1}], where l is the size of the eddy [m].

Scalar fluctuations were found to obey the same spectral law as velocity fluctuations (e.g. Tartarskii, 1961). As fluctuations in temperature, humidity and pressure cause fluctuations cause fluctuations in the refractive index (Hill *et al.*, 1980), the refractive index spectrum is similar to the velocity spectrum (Tartarskii, 1961). Within the inertial subrange of eddy sizes, this spectrum is given by:

$$\Phi_n(k) = 0.033 C_n^2 K^{-11/3} \quad 2\pi L_0^{-1} \ll K \ll 2\pi l_0^{-1} \quad (4.1)$$

The refractive index structure parameter represents the spatial variation of n over a distance r [m], i.e. a measure of the intensity of the refractive index fluctuations. C_n^2 may be found directly from the structure function, $D_n(r)$ [-] which expresses the turbulent intensity or 'structure' of n over a certain distance or time in the atmosphere (Tartarskii, 1961). Within the inertial subrange of eddy sizes, $D_n(r)$ is defined by:

$$D_n(r) = \overline{[n(x) - n(x+r)]^2} = C_n^2 r^{2/3} \quad l_0 \ll r \ll L_0. \quad (4.2)$$

Here $n(x)$ and $n(x+r)$ are the refractive indexes at the locations x and $x+r$. The overbar represents an average value. It is C_n^2 that connects the propagation of electromagnetic radiation to atmospheric turbulence.

4.3. Propagation of light through a turbulent atmosphere and the Large Aperture Scintillometer

An electromagnetic wave propagating in a straight line between two points (line-of-sight), is distorted by refraction, absorption and diffraction. These cause direct attenuation and fluctuations in the amplitude, phase, angle-of-arrival and polarisation of the wave (Strohbehn, 1968). To study these features theoretically, various solutions (e.g. geometrical optics, the Born approximation and the Rytov solution) have been given for the wave equation. For scintillation measurements we are interested in fluctuations in the intensity or the related amplitude fluctuations. In the geometrical optics approach, intensity fluctuations are attributed to the focusing and defocusing of EM rays caused by turbulent eddies in the propagation path. These eddies may be regarded as a collection of diverging and converging lenses. This approach ignores any diffraction effects and assumes that the optical wavelength λ is much smaller than l_0 (Tatarskii, 1993). As diffraction effects are ignored the diffractive spreading should be small in comparison with l_0 (Tatarskii, 1993). The scale of diffractive spreading is given by the size of the first Fresnel zone $(\lambda L)^{1/2}$.

For weakly refracting turbulence, Tatarskii (1993) showed that for a point source and point receiver eddies of the inner scale size are most effective in producing intensity fluctuations (scintillations) at L in contrast to larger eddies. These inner scale size eddies can be regarded as lenses with small focal lengths giving the largest refraction. The variance of the intensity fluctuations σ_I^2 at a point receiver is proportional to (Tatarskii, 1993):

$$\sigma_I^2 \propto C_n^2 l_0^{-7/3} L^3. \quad (4.3)$$

Summarising, for weakly refracting turbulence where 1) $\lambda \ll l_0$ and 2) $(\lambda L)^{1/2} \ll l_0$ the geometrical optics solution is valid and results in the proportionality given in (4.3).

For a spherical wave originating from a point source, the wavefront is distorted while propagating in a line-of-sight through a turbulent medium. A distortion causes small changes in phase for parts of the wavefront. At a point receiver at a distance L from the emitter,

interference between the different distorted parts of the wavefront leads to intensity fluctuations, considered above as the result of focussing and defocussing lenses. The size and contrast of the interference pattern observed at L are determined by the size l of the eddy, the path position z , the optical wavelength λ and the strength of the refractive index fluctuation Δn (Clifford *et al.*, 1974). An eddy is most effective in producing scintillations at L if the phase difference between distorted parts of the wavefront is $\lambda/2$.

If $(\lambda L)^{1/2} \gg l_0$ due to an increase in L , irregularities less than first Fresnel zone size are not capable of focusing or defocusing the beam and instead cause diffractive spreading. The smallest eddies that can focus or defocus a beam of light are of the size of Fresnel zone itself. For example if we use an infrared light source at $1 \mu\text{m}$ and measure over a distance of 1000 m, the first Fresnel zone is about 3 cm, i.e. larger than the size of l_0 . For this case (4.3) is not valid anymore and is replaced by (4.4) where l_0 is substituted for $(\lambda L)^{1/2}$ to take diffractive effects into account. The variance of the intensity fluctuations σ_I^2 at a point receiver is proportional (Tatarskii, 1993):

$$\sigma_I^2 \propto C_n^2 k^{7/6} L^{11/6} \quad (4.4)$$

where $k (= 2\pi \lambda^{-1})$ is the optical wave number.

When L is getting too large and/or turbulence too intense, the observed intensity fluctuations at the receiver do not continue to increase with increasing L and/or C_n^2 . This phenomenon is called saturation of scintillation and was first reported by Gracheva & Gurvich (1965) and Gracheva (1967). Consequently, the proportionality given in (4.4) will fail. In contrast to the case where $(\lambda L)^{1/2} \ll l_0$ and scintillation at L is assumed to be the result of interference from single diffraction by eddies, the beam is subject to diffraction caused by multiple eddies before it is received at L . Thus, after the wavefront is distorted for the first time by an eddy of first Fresnel zone size, the wavefront is distorted randomly by other eddies in the line-of-sight. The additional distortions are, however, far less effective in causing scintillations and will in fact slightly weaken the scintillation caused by the first distortion (Clifford *et al.*, 1974). Thus measuring intensity fluctuations to obtain C_n^2 using a point source and point receiver is restricted to relatively small pathlengths (~ 100 m) and weak turbulence ($\sigma_I^2 < 0.8$) (Tatarskii, 1993).

One way to overcome the problem of saturation is to increase the size of the transmitting and receiving apertures. Due to the finite aperture of the optics and the size of the light source, the transmitted beam of EM radiation consists of a superposition of incoherent,

spherical waves. The received signal is an average of non-correlated intensity fluctuations originating from multiple incoherent sources (Tatarskii, 1971), where the diffractive effects of the small scale eddies will be averaged out over the receiving aperture. The most effective eddies in causing intensity fluctuations at L are of the size of the aperture, D [m] (see Little, 1951). This principle is used in Large Aperture Scintillometers (LAS) to obtain an saturation-resistant measure for an average C_n^2 for a finite volume in space in both weak and strong turbulence (Wang *et al.*, 1978). For the LAS saturation becomes an issue only when $\sigma_I^2 > 0.03$ (Frehlich & Ochs, 1990).

4.4. From scintillation to the refractive index structure parameter

From the solution of the wave equation, scintillation is expressed as a variance of the logarithm of the amplitude. Since the intensity is the squared amplitude, the variance of the logarithm of the intensity is equal to four times the variance of logarithm of the amplitude (χ):

$$\sigma_{Lnl}^2 = 4\sigma_\chi^2. \tag{4.5}$$

For a LAS, Wang *et al.* (1978) showed that for a spherical wave propagating through a turbulent medium the variance of logarithm of the amplitude is given by:

$$\sigma_\chi^2 = \int_0^L C_n^2(z) W(z) dz. \tag{4.6}$$

where z is the path position $W(z)$ is spatial weighting-function for $C_n^2(z)$ along the propagation path. If turbulence is homogeneous along the path and has a spectrum as given in (4.1), the weighting-function expresses the relative effectiveness of turbulence in producing intensity fluctuations as a function of the position along the path. The weighting function is described by Wang *et al.* (1978) as:

$$W(z) = 4\pi^2 k^2 \int_0^L dK K \Phi(K) \sin^2 \left\{ \frac{K^2 z(L-z)}{2kL} \right\} \tag{4.7}$$

where $\Phi(K)$ is given by (4.1). The weighting-function (4.7) reaches a maximum at the midpoint of the path and drops symmetrically to zero at $z = 0$ and $z = L$. For the LAS this means that D size eddies are most effective in producing scintillation at $z = L/2$.

Substituting (4.1) and (4.7) in (4.6) and solving numerically for the path weighted

average of C_n^2 , Wang *et al* (1978) found for equal transmitting and receiving apertures that:

$$C_n^2 = 4.48 \sigma_X^2 D^{7/3} L^{-3}. \quad (4.8)$$

4.5. The large aperture scintillometer

The LAS is conceived by Wang *et al.* (1978) and first built at the NOAA wave Propagation Laboratory, Boulder Colorado and is aptly described in a NOAA Technical Memorandum (Ochs *et al.* 1980). Our copy of the instrument has a transmitting and receiving aperture of 0.15 m in diameter. At the transmitter, a 7 kHz square wave oscillator modulates a 0.94 μm light emitting, infrared diode (LED) source (TIES 16A, Texas Optoelectronics Inc., Garland TX, USA). The LED is placed in the focal point of a 0.15 m concave mirror. The mirror collimates the light from the LED and transmits it as a uniform beam of incoherent light in a line-of-sight to the receiving aperture. At the receiver, the beam of light is focused by a similar 0.15 m concave mirror on a silicon photodiode detector (UDT-455, UDT Sensor Inc., Hawthorne CA, USA) and processed by analog electronics to provide a direct output of C_n^2 , presented as a scaled, analog voltage.

4.6. Estimation of the sensible heat flux density from C_n^2

While passing through the atmosphere, the characteristics of a beam of EM radiation change due to normal and anomalous dispersion. The normal part is dominant far from any absorption line, whereas the anomalous part may be important when the frequency of an emitted EM wave is close to the resonance frequency (absorption lines) of atmospheric constituents, like water vapour and carbon dioxide. Both parts are a function of the optical wavelength and the temperature, humidity and total pressure of the air. Fluctuations in temperature, humidity and static pressure cause fluctuations in the refractive index of the air (Hill *et al.* 1980). Generally, the contribution of the latter to n is neglected (e.g. Hill *et al.*, 1980).

The measured C_n^2 value is therefore related to the structure parameters of temperature C_T^2 , humidity C_Q^2 and a covariant term C_{TQ} , respectively. The relationship is given by:

$$C_n^2 = A_T^2 \frac{C_T^2}{T^2} + A_Q^2 \frac{C_Q^2}{Q^2} + 2A_T A_Q \frac{C_{TQ}}{T Q} \quad (4.9)$$

Here A_T , A_Q are dimensionless quantities that represent the relative contribution of each term

to C_n^2 depending on λ , mean temperature T [K], mean atmospheric pressure P [Pa] and mean humidity Q [kg m^{-3}]. For visible to near infrared frequencies (0.36–3 μm) A_T, A_Q are given by (Andreas, 1989):

$$A_T = T \left(\frac{\partial n}{\partial T} \right)_{Q=\text{Const}} = -0.78 \times 10^{-6} \left(\frac{P}{T} \right)$$

$$A_Q = Q \left(\frac{\partial n}{\partial Q} \right)_{T=\text{Const}} = -57.5 \times 10^{-6} Q.$$

The numerical values are variables depending only on wavelength and have units of [K Pa^{-1}] and [$\text{m}^3 \text{kg}^{-1}$], respectively. Assuming temperature and humidity are strongly positively or negatively correlated in the inertial subrange, C_{TQ} can be written as (Kohsiek, 1982):

$$C_{TQ} = r_{TQ} (C_T^2 C_Q^2)^{1/2} \quad r_{TQ} = \pm 1. \quad (4.10)$$

By substituting (4.10) in (4.9) and using the above definitions for A_T and A_Q for visible to near infrared frequencies, Wesely (1976) showed that for scintillometers operating at near-infrared wavelengths C_T^2 is related to C_n^2 by:

$$C_T^2 = C_n^2 10^{12} \left(\frac{T^2}{0.78P} \right)^2 \left(1 + \frac{0.03}{\beta} \right)^2. \quad (4.11)$$

Here β is the Bowen ratio and is given by (Wesely, 1976; Kohsiek, 1982):

$$\beta = \left(\frac{\rho C_p}{\lambda} \right) \left(\frac{C_T}{C_Q} \right).$$

Here ρ [$\approx 1.2 \text{ kg m}^{-3}$] is the density of air, C_p [$\approx 1005 \text{ J kg}^{-1} \text{ K}^{-1}$] the specific heat of air at constant pressure and λ_v represents the latent heat of vaporisation [J kg^{-1}]. The need for β reveals a first limitation of the scintillation method, as compromising point measurements of the sensible and latent heat flux are necessary to obtain C_T^2 from (4.11). The Bowen ratio term in (4.11) corrects for the contribution of the combined effect of temperature and humidity fluctuations on C_n^2 . For dry soil conditions β is generally larger than 1 and consequently the Bowen ratio term in (4.11) becomes negligibly small (see e.g. De Bruin *et al.* 1995). However, for β as small as 0.1 the correction term becomes as large as 70% (Green

& Hayashi, 1998).

In the surface layer, C_T^2 can be scaled with the scaling temperature T_* [K] given by:

$$T_* = \frac{-H}{\rho C_p u_*} \quad (4.12)$$

where H [W m^{-2}] is the sensible heat flux density and u_* [m s^{-1}] the friction velocity. Following Wyngaard *et al.* (1971) we write the Monin–Obukhov functional forms of atmospheric stability for normalised C_T^2 as:

$$\frac{C_T^2 (z-d)^{2/3}}{T_*^2} = c_A \left(1 + c_B \left| \frac{(z-d)}{L_o} \right| \right)^{-2/3} \quad \left(\frac{(z-d)}{L_o} \right) \leq 0 \quad (4.13)$$

where z [m] is the height above the zero-plane displacement height (d [m]) and c_A and c_B empirical constants derived from the Kansas data by Wyngaard *et al.* (1971), 4.9 and 7 respectively for unstable conditions. The Obukhov length is defined by:

$$L_o = -\frac{\rho C_p T u_*^3}{g \kappa H_{sc} (1 + 0.07/\beta)} \quad (4.14)$$

for $g = 9.81 \text{ m s}^{-2}$ the gravitational acceleration and von Karman's constant, $\kappa = 0.4$.

Thus, to calculate H_{sc} from (4.14) relies on knowledge of both u_* and $(z-d)/L_o$. Generally, the deficiency in the available spatial measurement of u_* is overcome by using a point measure of the average wind speed, u [m s^{-1}] and surface roughness, z_o [m]. For unstable conditions, the mean vertical wind speed is given by (Panofsky & Dutton, 1984):

$$u_* = \frac{\kappa u}{\text{Ln} \left(\frac{z-d}{z_o} \right) - \Psi_m \left(\frac{z-d}{L_o} \right)} \quad (4.15)$$

Ψ_m is a universal function of z/L_o . For unstable conditions the integrated stability correction for the diabatic wind profile, Ψ_m , equals (Paulson, 1970):

$$\Psi_m \left(\frac{z-d}{L_o} \right) = \text{Ln} \left[\left(\frac{1+x^2}{2} \right) \left(\frac{1+x}{2} \right)^2 \right] - 2 \arctan(x) + \frac{\pi}{2} \quad (4.16)$$

where $x = (1 - 16(z-d)/L_0)^{1/4}$. Now an iterative procedure is used to solve (4.15) for u_* from an initial guess for $(z-d)/L_0$. T_* is then calculated from (4.13) using the obtained value for C_T^2 from the scintillometer and the initial value for $(z-d)/L_0$. From (4.12), using u_* and T_* , H_{sc} can be calculated and then be used in (4.14) to calculate L_0 . This procedure is repeated until the values for $(z-d)/L_0$ converge.

By using two scintillometers at different heights above the surface, a spatial measurement of L_0 and u_* can be derived without incorporating compromising point measurements of the friction velocity u_* or alternatively the average wind speed combined with a measure of the roughness length. The presumption that such measurements are representative of the entire transect usually holds for homogeneous surface cover but may not be valid for patchwork terrain. The two-scintillometer technique, referred to as the C_T^2 -profile method, is the subject of Chapter 5.

4.7. The effect of absorption fluctuations

In a turbulent atmosphere the amplitude of a propagating beam of EM radiation of wavelength λ , can be distorted not only by refraction but also by absorption fluctuations. Generally, the effect of the latter is considered to be too small to be detected. The spectral envelope of the near-infrared light emitting diode (LED) source used by the LAS transmitter, however, encompasses many strong water vapour absorption lines and could cause a significant effect of absorption fluctuations on scintillation.

Refraction is the result of normal and anomalous dispersion as described in section (4.3). If, however, the frequency of the emitted EM wave is close to a resonance frequency (absorption lines) of atmospheric constituents, like water vapour and carbon dioxide, absorption becomes important. To quantitatively describe the combined effect of refraction and absorption, a complex refractive index, C_n^2 , is introduced. Here the phenomenon of absorption is represented by the imaginary part of the refractive index and is solely determined by single absorption lines and their corresponding absorption coefficients (β_i), resulting in a total absorption coefficient for a band of lines (Hill *et al.*, 1980). The absorption line strength is temperature dependent, while the absorption line width is temperature, humidity and pressure dependent.

The contribution of absorption fluctuations to C_n^2 is generally neglected, that means to have a real component only. In reality C_n^2 includes both a real part, C_{nR}^2 , due to refraction and an imaginary part, C_{nI}^2 , attributable to the absorption mechanism, and is defined by:

$$C_n^2 = C_{nR}^2 + C_{nI}^2 \quad (4.17)$$

Any additional source of scintillation such as a contribution from absorption fluctuations could conceivably corrupt the estimation of the sensible heat flux. To decide whether there is significant additional scintillation caused by the absorption mechanism, this subject is studied in detail in chapter 6.

CHAPTER 5

-
-
-

MEASURING SENSIBLE HEAT FLUX OVER PASTURE USING THE C_T^2 - PROFILE METHOD

JOOST P. NIEVEEN¹ AND ALAN E. GREEN²

¹*Department of Meteorology, Wageningen Agricultural University, Duivendaal 2, NL-6701
AP, Wageningen, The Netherlands*

²*Horticultural Research Institute of New Zealand, Kerikeri Research Centre, Kerikeri, Bay of
Islands, New Zealand*

Boundary-Layer Meteorology, 1998 (In press)

5.1. Introduction

Over the past few years the scintillation method to determine the path-averaged sensible heat flux density, H_{sc} [$W m^{-2}$], has increased in popularity (e.g., De Bruin *et al.*, 1995). This trend is reflected by the increase in scientific publications on this subject and the commercial availability of the NOAA-designed large-aperture, infrared scintillometer (Science Technology Inc., Gaithersburg MD, USA) and the Scintec (Model SLS20, Mossingen, Germany) visible diode-laser scintillometer (Thiermann, 1992). There exist other combinations of scintillometers that also provide path-averaged flux density measurements. Of significance is the 'Inner scale meter' utilising the large-aperture infrared and HeNe scintillometers (Hill *et al.*, 1992a) and the 'Biochromatic technique' with HeNe and CO₂ laser scintillometers (Thiermann & Grassl, 1992). The reader is referred to a comprehensive review article on optical scintillation methods (Hill, 1992) for further information.

A first limitation of the current scintillation methods is that none provide kilometre scale path-averaged sensible heat flux without incorporating compromising point

measurements of the friction velocity u_* [m s^{-1}], or alternatively the average wind speed combined with a measure of the roughness length. The presumption that such measurements are representative of the entire transect usually holds for homogeneous surface cover but may not be valid for patchwork terrain. To assert that scintillometers can determine path-averaged flux densities at landscape scales, and for them to successfully characterise surface flux densities over a heterogeneous surface, will require resolution of this issue.

The refractive scintillations, as measured by a scintillometer's receiver, are related to the refractive index structure parameter, C_n^2 [$\text{m}^{-2\alpha}$]. For the inertial subrange scale sizes, C_n^2 expresses the intensity of the refractive index fluctuations encountered by an electromagnetic beam along the propagation path of the scintillometer. Similar to C_n^2 , the temperature structure parameter, C_T^2 [$\text{K}^2 \text{m}^{-2\beta}$], represents the intensity of atmospheric temperature fluctuations (Tatarski, 1961, 1971). For large aperture scintillometers operating at near-infrared wavelengths, Wesely (1976) showed that C_T^2 is related to C_n^2 by:

$$C_T^2 = C_n^2 10^{12} \left(\frac{T^2}{0.78P} \right)^2 \left(1 + \frac{0.03}{\beta} \right)^2, \quad (5.1)$$

provided that the atmospheric temperature and humidity fluctuations are highly correlated. Here, P [Pa] is the average atmospheric pressure, T the average air temperature [K] and β the (Bowen) ratio of sensible to latent heat flux density. The need for β reveals a second limitation of the scintillation method, as compromising point measurements of the sensible and latent heat flux are necessary to obtain C_T^2 from (5.1). The Bowen ratio term in (5.1) corrects for the contribution of the combined effect of temperature and humidity fluctuations on C_n^2 . For dry soil conditions β is generally larger than 1 and consequently the Bowen ratio term in (1) becomes negligibly small (see e.g., De Bruin *et al.*, 1995). However, for β as small as 0.1, the correction term becomes as large as 70% (Green & Hayashi, 1998).

Andreas (1988) published a method to determine the path-averaged Obukhov length, L_o [m], using two matched scintillometers positioned at heights z [m] and propagating over the same pathlength. This method pivoted about C_T^2 being an empirical function of atmospheric stability $f(z/L_o)$ in the lower boundary layer (Wyngaard *et al.*, 1971). Through the measurement of $f(z/L_o)$ at two heights, common constants within this functional expression were eliminated and the functional dependence of L_o was reduced to the accuracy of the measured heights and the scintillometer calibrations. Andreas (1988) made no experimental measurements; this was first undertaken by Hill *et al.* (1992b) who measured C_T^2 at heights of

1.45 and 3.95 m over a propagation path of 606 m using the NOAA designed large aperture scintillometers (Ochs & Cartwright, 1980). The collected data showed reasonable sensible heat flux density comparisons to eddy covariance-determined flux densities for the best meteorological conditions. Hill *et al.* (1992b) believed systematic differences between scintillometers caused undue error in this approach, which was called the C_T^2 -profile method and that reliable flux densities depended on improving instrument performance.

Apart from Hill *et al.* (1992b) no other experimental data have been published using this method. Because of the advantages of a truly path-averaged and long-distance scintillometer system, there is a need to explore the approach further. To this end we present further results of sensible heat flux densities derived using the C_T^2 -profile method compared to those derived using the eddy covariance method. The experiment was conducted over a pasture canopy and data are presented in the form of a continuous time-series of half-hour-averaged flux densities and a direct comparison over several days.

5.2. Theory

In the surface layer, C_T^2 can be scaled with the scaling temperature T_* [K] given by:

$$T_* = \frac{-H_{sc}}{\rho C_p u_*} \tag{5.2}$$

where ρ [kg m^{-3}] is the density of air and C_p [$\text{J kg}^{-1} \text{K}^{-1}$] the specific heat of air at constant pressure. Following Wyngaard *et al.* (1971) we write the Monin-Obukhov functional forms of atmospheric stability for normalised C_T^2 as:

$$f\left(\frac{z}{L_o}\right) = \frac{C_T^2 z^{2/3}}{T_*^2} = c_A \left(1 + c_B \left|\frac{z}{L_o}\right|\right)^{-2/3} \quad \left(\frac{z}{L_o}\right) \leq 0 \tag{5.3}$$

where c_A and c_B are 4.9 and 7 respectively for unstable conditions; empirical constants have been derived from the Kansas data by Wyngaard *et al.* (1971). The Obukhov length is defined by:

$$L_o = \frac{u_*^2 T}{g \kappa T_*}, \tag{5.4}$$

using $g = 9.81 \text{ m s}^{-2}$ the gravitational acceleration, the von Karman's constant, $\kappa = 0.4$ and

neglecting the contribution of humidity fluctuations.

After Hill *et al.* (1992b), the ratio of the functional form of atmospheric stability at a lower and upper height (designated by subscripts L and H) may then be written as:

$$\frac{f(z_H/L_o)}{f(z_L/L_o)} = \left(\frac{C_{TH}^2}{C_{TL}^2} \right) \left(\frac{z_H}{z_L} \right)^{2/3} = R. \quad (5.5)$$

We define r_{sc} as the ratio of the two heights, z_H/z_L , and the geometric mean of z_H/L_o and z_L/L_o as:

$$\xi = \frac{(z_H z_L)^{1/2}}{L_o}. \quad (5.6)$$

Now by substituting L_o from (5.6) into (5.3), then substituting (5.3) into (5.5) and solving for ξ we obtain:

$$\xi = \frac{r_{sc}^{1/2} (R^{3/2} - 1)}{7 (r_{sc} R^{3/2} - 1)} \quad (\xi) \leq 0. \quad (5.7)$$

From the measured values of C_T^2 at z_H and z_L , R and the accompanying ξ can be calculated. One can now find a path-averaged value for L_o using (5.6), which is then used to obtain T_* from (5.3) for either the lower or upper height measurement of C_T^2 . Knowing the path averaged L_o and T_* now allows calculation of a path-averaged u_* , using (5.4). Finally, a path-averaged H_{sc} for the configuration of two scintillometers at two different heights is calculated from the temperature scale T_* as given in (5.2).

5.3. Experimental

5.3.1. Site description and weather conditions

This experiment was an adjunct to a major scintillation experiment exploring the use of a microwave and a large-aperture infrared scintillometer to determine the surface flux densities of sensible and latent heat (Green *et al.*, 1998). Data were collected in summer over several days in February 1996 near Ahipara, a coastal settlement in the far north of New Zealand. The main scintillometer link was established over a 3.1 km distance at a height of 10 m running south-east from the transmitters near the Kaitaia Township oxidation ponds, to the receivers

sited on a cattle farm close by the Kaitaia–Ahipara coast road (midpoint, longitude 173° 15' and latitude 35° 08'). This site was chosen for the homogeneity of surface cover and apparent flatness and is best described as a reclaimed coastal swamp approximately 10 km from the sea. Near the path midpoint a 10-m tower was instrumented with a two-dimensional drag anemometer (Green *et al.*, 1991), 1D sonic–thermometer (Campbell Scientific Inc., Logan UT, USA); Krypton hygrometer (Campbell Scientific Inc., Logan UT, USA); net radiometer (Radiation Energy Balance Systems, Seattle WA, USA), wind vane, sensitive cup anemometer and an air temperature–humidity probe (Vaisala, Helsinki, Finland). Half–hourly eddy covariance calculations of H_{ec} , the latent heat flux density λE_{ec} [W m^{-2}] and u^* were made for the comparison with the path–averaged scintillometer values.

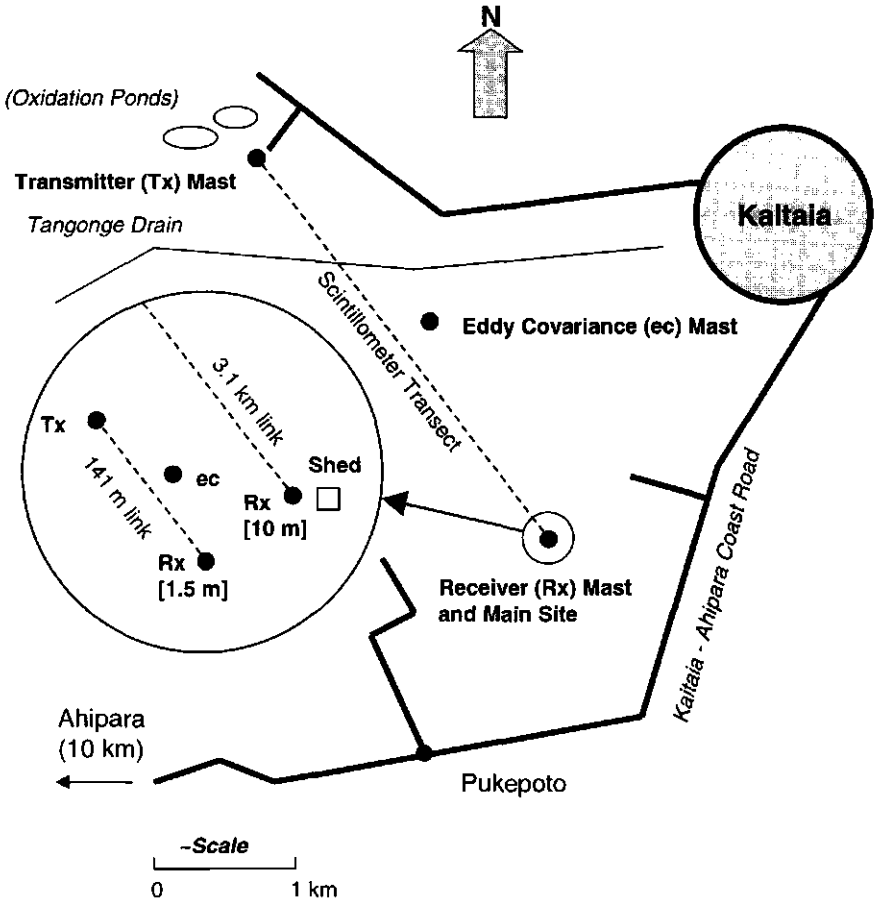


Figure 5.1: Site layout showing the position of the 3.1 km path relative to the shorter 141 m transect.

As these scintillometers were already in place then, another large-aperture scintillometer link at a lower height of 1.5 m was easily installed to specifically investigate the C_T^2 -profile method. This shorter 141 m long link (pasture scale) was sited at the receiver end of the 3.1 km transect (see Figure 5.1). An eddy covariance mast was installed nearby with instruments centred at the same height for surface flux density measurements. This shorter link was a practical compromise in striving for a greater ratio of heights. We could not expect the beam to remain horizontal to the surface and unbroken at 1.5 m close to farm fence and cattle heights over kilometre distances. Besides, signal saturation from refractive turbulence effectively path limited the operation at low heights. In siting the lower scintillometer path in this manner we were effectively assuming homogeneity of terrain and that turbulent flow was consistent over the 3 km distance.

The landscape was bereft of significant obstacles such as buildings, bisecting roads and people, and comprised a collection of paddocks primarily used for grazing cattle with some dairy cows. The surface cover consisted of mainly Kikuyu grass (*Pennisetium clandestinum* Hochst. Ex Chiov) with sporadic Pennyroyal weeds (*Metha pulegium* L.). Drainage ditches, which are dry at this time of year, fractured the surface pattern at intermittent intervals and were confined at their perimeter by clumps of swamp grass. Patches of bulrushes, blackberries and Scotch thistles increased in numbers towards the transmitter end. However, the bell-shaped weighting function associated with the scintillometer path-averaging process (Wang *et al.*, 1978) attributes a lower weighting to changes in ground cover at the ends of the beam. For both scintillometer sites the average surface cover was therefore considered similar.

The experiment started on the 14th of February 1998. The majority of the data, however, were collected on the 27th through to 29th February. During this time the weather typically showed a clear sky early morning, but cloudiness with light winds by midday. This was in contrast to the proceeding period with overcast and some rain. For the measurement period between the 27th and 29th of February, β was larger than 1, making the Bowen ratio correction in (5.1) insignificant.

5.3.2. Data collection and instrumentation

Data were collected using synchronised data loggers (21X, Campbell Scientific Inc., Logan UT, USA) at the receiver ends of the scintillometer links and at the base of the eddy covariance masts. Eddy covariance calculations of the surface flux densities were made for each half-hour period by the loggers using a 10 Hz scan rate. Slower sensors such as the

windvane, net radiometer and the temperature and humidity sensor were logged at 1 Hz, as were the scintillometer signals. The data were downloaded from the loggers in the field to a portable PC for analysis on a spreadsheet.

The scintillometer's transmitting and receiving apertures were 0.15 m in diameter. At the transmitter, a 7 kHz square wave oscillator modulated a light emitting, infrared diode source. At the receiving end of the scintillometer, the signal was processed by analog electronics to provide a direct output of C_n^2 , presented as a scaled, analog voltage. The bandwidth of accepted scintillations is set by electronic hardware at 0.03 – 400 Hz with the final output being time-integrated for 2.5 s. Another micrologger (21X) was used to record the data at a 1 Hz sampling rate, which were averaged for 30 minutes.

5.4. Results and discussion

5.4.1. Scaling C_T^2 with height

Measurements of C_T^2 at $z = 1.5$ m and 10 m using data taken from displaced scintillometers provided an opportunity to observe the scaling behaviour of C_T^2 with height. From (5.5) we write:

$$R \cdot \left(\frac{C_{TL}^2}{C_{TH}^2} \right) = \left(\frac{z_H}{z_L} \right)^{2/3} \quad (5.8)$$

Wyngaard *et al.* (1971) showed that C_T^2 decreases with height as $z^{-2/3}$ for unstable to near neutral conditions, where both $|z_H/L_0|$ and $|z_L/L_0|$ approach zero. From (5.3) and (5.5), R therefore becomes close to unity and (5.8) reduces to $C_{TL}^2 \approx 3.5 C_{TH}^2$ (for heights of 1.5 and 10 m). Note that this is not the case for very unstable conditions where $|z_H/L_0|$ and $|z_L/L_0| \gg 1$ and $R < 1$ cannot be neglected in (5.8). In fact, C_T^2 decreases with height as $z^{-4/3}$ under these conditions (Wyngaard *et al.*, 1971).

The measured values of C_T^2 are collected within a range of stabilities ($-0.2 \leq z_H/L_0 \leq -0.01$). For the outer limit of this stability range ($z_H/L_0 = -0.2$) we first calculate R from (5.5) and substitute this ratio into (5.8) written as:

$$C_{TH}^2 = \frac{1}{R} \left(\frac{z_H}{z_L} \right)^{2/3} C_{TL}^2 = 1.6 \left(\frac{z_H}{z_L} \right)^{2/3} C_{TL}^2, \quad \text{for } \left(\frac{z_H}{L_0} \right) = -0.2, \quad (5.9)$$

reducing further to:

$$C_{TL}^2 = 5.6 C_{TH}^2 \quad (5.10)$$

for the displaced scintillometers at heights 1.5 and 10 m. Presented on a log-log graph (Figure 2) where C_T^2 varies over two orders of magnitude ($0.001 \leq C_T^2 \leq 0.1$) the half-hourly data points are scattered about and between the lines representing $C_{TL}^2 = 3.5 C_{TH}^2$ (neutral conditions) and the stability-corrected expression (5.10) $C_{TL}^2 = 5.6 C_{TH}^2$. With 60 data points the regression line has an intercept of zero and a slope given by:

$$C_{TL}^2 = 3.84 (\pm 0.22) C_{TH}^2.$$

This relationship defines (5.8) for neutral conditions where $R = 1$, multiplied by the average ratio of $(1+7|z/L_0|)^{-2/3}$ at the two heights. It suggests that C_T^2 decreases with height as $z^{-2/3}$ for unstable to near neutral conditions. A correlation coefficient, $R^2 = 0.68$, indicates a larger spread of data about the regression line than is apparent on logarithmic axes. Despite the large difference in propagation pathlengths, and the possibility that C_T^2 may differ at the same height across the 3.1 km transect, the scintillometers appear to be observing the same strength of refractive turbulence when appropriately scaled by their displaced height. This implies a degree of homogeneity of turbulent flow across the transect and that the surface is horizontally homogeneous.

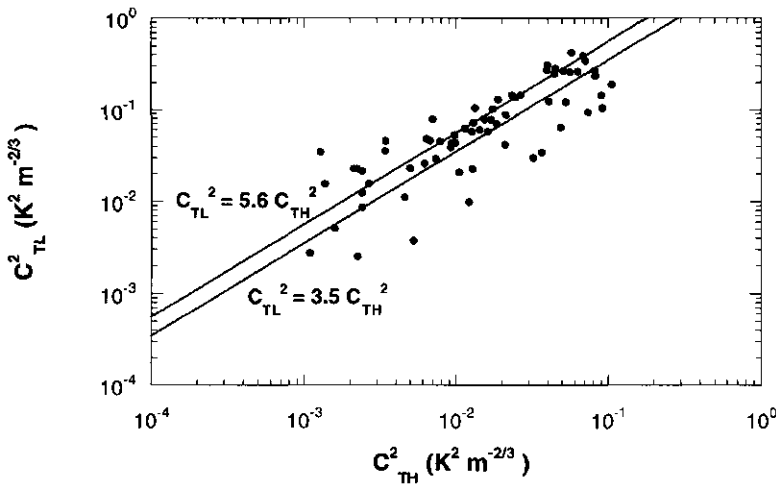


Figure 5.2: Comparison of C_T^2 measured at heights of 10 m (C_{TH}^2) and 1.5 m (C_{TL}^2). Lines indicate equation (5.6) for the outer limits of the measured stability region.

All surface flux density determination techniques have limitations (Thiermann & Grassl, 1992) and mention should be made of the concern expressed by Hill *et al.* (1992b) as to the systematic differences found between the large aperture scintillometers. Their scintillometer, positioned at $z = 1.45$ m and compared indirectly to wire-thermometer pairs, gave systematically 4% lower values of C_T^2 than at $z = 3.95$ m. Such errors will affect the ratio R and the final calculated value of H_{sc} . According to Hill *et al.* (1992b), the systematic error due to non-uniform illumination over the transmitter and receiver apertures is the main reason for this difference. Although we did not compare our scintillometers at the two heights we did compare the signals received at $z = 10$ m for two adjacent receiver units sharing the same transmitter and pathlength (Green *et al.*, 1998). Despite the careful opto-electronic calibration of the receiver scintillometers in the laboratory, and field alignment for maximum signal strength one scintillometer systematically underestimated the other by more than 5% ($R^2 = 0.92$) for a sample of 107 averaged half-hourly values of C_T^2 . This is an error in R of at least 10% assuming both heights are precisely measured.

Andreas (1988) performed a sensitivity analysis for this method taking into account the uncertainty in measuring the signal outputs and the vertical separation of the scintillometers. Not wishing to measure closer to the surface than 1 m, and ensuring the mechanical stability of the scintillometer at greater heights, Andreas showed the best sensitivity is obtained for $r_{sc} = 10$. Further, if the scintillometers agreed to within 5% after calibration and if r_{sc} could be measured to within 2% for an $r_{sc} = 10$, Andreas demonstrated the best sensitivity for this method occurred for a stability range of $-3 \leq (z/L_0) \leq -0.015$. The calculated value of L_0 should be accurate to within a factor of 2. Our data set lies within this range with values spread about $(-0.2 \leq (z_H/L_0) \leq -0.01)$ and a ratio, $r_{sc} = 6.7$, near to the optimum configuration. For very unstable conditions, Andreas showed this method to be not particularly accurate. However, this is not a serious limitation since during free convective conditions C_T^2 becomes independent of mechanical transport so a measure of u_* is not required (Panofsky & Dutton, 1984). H_{sc} can then be calculated directly from either scintillometer using:

$$H_{sc} = 0.5\rho C_p (z-d) \left(\frac{g}{T} \right)^{1/2} (C_T^2)^{3/4}. \quad (5.11)$$

5.4.2. Comparing the profile and eddy covariance methods

A comparison of data obtained for half-hourly calculated H_{sc} versus H_{ec} ($z = 10$ m) is presented for the days, 27th, 28th and 29th February 1996 (Fig. 5.3). The linear regression

at two heights suggest to scale as $z^{-2/3}$ in the surface layer for a range of unstable conditions, $-0.2 \leq (z/L_o) \leq -0.01$. The result further supports Wyngaard *et al.* (1971) describing C_T^2 as a function of atmospheric stability, $f(z/L_o)$. Furthermore, our observations suggest that the large difference in absolute pathlengths and their relative positioning was not necessarily detrimental to this sensible heat flux density comparison. It also implies the experimental site and atmospheric conditions probably met the criteria of homogeneous terrain, flatness of surface and homogeneity of turbulent flow as required by similarity theory.

The comparison of the two scintillometer receivers at $z = 10$ m showed a systematic difference between half-hourly averaged C_T^2 by at least 5%, close to the indirectly determined value of 4% described by Hill & Ochs (1992). It is realistic to expect this instrument difference to be consistent when using the vertically displaced scintillometers and to be reflected in an error in the ratio R of 10%. Despite having taken particular care in optimising the opto-electronics and instrument alignment we can offer no explanation for this discrepancy other than to accept Hill's explanation of non-uniform aperture illumination. There is an obvious need to reduce this uncertainty if the C_T^2 -profile method is to improve determination of the sensible heat flux density, H_{sc} .

The time series of half-hour flux density measurements using the eddy covariance and C_T^2 -profile methods were generally consistent in magnitude and followed the same temporal trend. Without wishing to downplay obvious discrepancies between some half-hour values of H_{sc} and H_{ec} , after scrutiny of the data set some irregularities were explainable by wind shifts causing shadowing of the sonic anemometer. Some disagreement is also attributable to the difference in the flux density determining methods themselves. The C_T^2 -profile method incorporates path-average measurements made over two different pathlengths, whereas the eddy covariance instruments deduce the flux density at the midpoint of the 3 km transect and are susceptible to local effects. In the final comparison of half-hourly values of H_{sc} and H_{ec} the best-fit regression agreement is within 10%. However, there is an even scatter about the 1:1 line (less than for the C_T^2 comparison) suggesting no particular bias for either method.

Future research requires further experimental data for a tighter statistical comparison and effort made to reduce instrument uncertainties. The advantages this offered by this method warrant further improvements in instrumentation and methodology.

Acknowledgments

Funding for this work was supported by the New Zealand Foundation for Research Science

and Technology, Contract CO6641 and the Netherlands Organisation for Scientific Research under project number 753-06-234.

We wish to thank Mark Astill (HortResearch) for his technical assistance with both the field experimentation and general logistics. Bert Heusinkveld and Willy Hillen (Wageningen Agricultural University, The Netherlands) constructed the short pathlength, large-aperture scintillometer and opto-electronics.

CHAPTER 6

-
-
-

USING A LARGE-APERTURE SCINTILLOMETER TO MEASURE ABSORPTION AND REFRACTIVE INDEX FLUCTUATIONS

JOOST P. NIEVEEN¹, ALAN E. GREEN² AND WIM KOHSIEK³

¹ *Dept. Meteorology, Wageningen Agricultural University, Duivendaal 2, 6701AP
Wageningen, The Netherlands*

² *The Horticultural Research Institute of New Zealand, Kerikeri Research Centre, P.O. Box
23, Kerikeri, Bay of Islands, New Zealand*

³ *Royal Netherlands Meteorological Institute, P.O. Box 201, 3730 AE De Bilt, The
Netherlands*

Boundary-Layer Meteorology, 87, 101–116, 1998

6.1. Introduction

Near-infrared scintillometers are becoming increasingly popular as a means of determining the sensible heat flux density (De Bruin *et al.*, 1995). The application of these instruments requires careful evaluation of their ability to produce reliable measurements of the scattering process due to refractive index fluctuations, as the sensible heat flux is derived from the line-integral of the refractive index structure parameter. Any additional source of scintillation such as a contribution from absorption fluctuations, could conceivably corrupt the scattering information were it of appropriate energy and frequency and with that the sensible heat flux.

Scintillometers typically have an operating bandwidth to span the frequency of refraction scintillations. The lower cut-off frequency is generally chosen to be an order less

than the lowest frequency of interest. This removes any gradually varying offsets such as the changing absolute source intensity.

In a lossy atmosphere the amplitude of a propagating beam of electromagnetic (EM) energy of wavelength λ , can be distorted by refraction and absorption fluctuations. To quantitatively describe the combined effect of refraction and absorption, a complex refractive index, C_n^2 , is introduced. The real component, C_{nR}^2 is due to scattering and the imaginary part, C_{nI}^2 attributable to the absorption mechanism.

Tatarskii (1961) produced much of the original work on the propagation of EM waves in a turbulent atmosphere but did not consider the effect of absorption on the signal fluctuations. Gurvich (1968) computed the two-dimensional spatial, spectral density of the logarithmic amplitude fluctuations of a plane wave propagating in a turbulent absorbing atmosphere. He noted that the significance of absorption fluctuations increases for small wave numbers ($k = 2\pi\lambda^{-1}$), attributable to large-scale atmospheric inhomogeneities. From numerical estimates Kanevskii (1972) found that atmospheric absorption can lead to increases in sub-millimetre radio wave amplitude fluctuations. Andreyev and Chernaya (1978) performed calculations and made experimental observations for amplitude fluctuations of millimetre waves propagating in a turbulent absorbing atmosphere and concluded that less than 1% of the total scintillations were due to the imaginary component of the refractive index. Ott (1977) and Ott and Thompson (1978) extended Gurvich's work to demonstrate an enhancement at the low frequency end of the temporal spectral density of the log amplitude fluctuations $W\chi(f)$ for plane radio waves. Here f is the temporal scintillation frequency (Hz). Hill *et al.* (1980) investigated the variance of the logarithmic amplitude (σ_χ^2) of infrared light and found that the absorption fluctuations were small compared to the refractive effect. In his paper Hill also suggested that the effect of absorption fluctuations would be increased relative to refractive scintillations using spatially large transmitting and receiving apertures. Medeiros Filho *et al.* (1983), also working in the time domain, presented a detailed theory and experimental observations for millimetre wave amplitude fluctuations in an oxygen absorbing region, validating the results of Ott and Thompson (1978). Cole (1986) used the work of Medeiros Filho *et al.* (1983) to provide an example of the effect of oxygen absorption on amplitude scintillations. Kagawa *et al.* (1996) calculated $W\chi(f)$ using an infrared, tuneable diode laser centred around a water absorption line and obtained similar results to the millimetre wavelengths.

The spectral envelope of the near-infrared light emitting diode (LED) source used by

the large aperture scintillometer's (LAS) transmitter encompasses many strong water vapour absorption resonances. By isolating a band of these lines using an optical filter we can investigate the effect of scintillations in this absorption region.

This study looks at $W\chi(f)$ in a lossy medium to decide whether there is significant additional enhancement at low frequencies due to the absorption mechanism. Under such conditions it would be advisable to either operate scintillometers at wavelengths outside absorption regions or modify the scintillation low cut-off frequency to exclude absorption effects.

6.2. Theory

Due to the finite aperture of the optics and the size of the LED, the transmitted beam of EM radiation consists of a superposition of incoherent, spherical waves. While passing through the atmosphere, fluctuations in temperature, humidity and static pressure cause fluctuations in both the C_{nR}^2 and C_{ni}^2 resulting in random refraction and absorption of the beam (Hill *et al.* 1980).

Normal dispersion and anomalous dispersion determine the real part of the refractive index. The first effect is dominant far from any absorption line, whereas the latter effect may be important when the frequency of the emitted EM wave is close to the resonance frequency (absorption lines) of atmospheric constituents, like water vapour and carbon dioxide, resulting in enhanced scattering of the beam. Here we consider only the contribution of water vapour resonances. If the frequency of the EM wave is close to a resonance frequency of water vapour, part of the energy of the wave will be absorbed. This phenomenon is represented by the imaginary part of the refractive index and is solely determined by single absorption lines and their corresponding absorption coefficients (β_i), resulting in a total absorption coefficient ($\beta = \sum\beta_i$) for a band of lines (Hill *et al.*, 1980). The absorption line strength is temperature dependent, while the absorption line width is temperature, humidity and pressure dependent. In the case of the spectral envelope of the LED, there are many water vapour resonance frequencies (absorption lines) contributing to the total anomalous refraction and absorption. The refraction remains dominated by normal dispersion, though. As a result, the refractive scintillations are related to the refractive index structure parameter, C_{nR}^2 , and the absorption fluctuations to the structure parameter of the imaginary part of the refractive index, C_{ni}^2 .

Both C_{nR}^2 and C_{ni}^2 are related to the structure parameters of temperature C_T^2 , humidity C_Q^2 and pressure C_P^2 . The contribution of the latter, however, is negligible. C_{nR}^2 and C_{ni}^2 are

respectively given by (Hill *et al.*, 1980):

$$C_{nR}^2 = A_T^2 \frac{C_T^2}{T^2} + A_Q^2 \frac{C_Q^2}{Q^2} + 2A_T A_Q \frac{C_{TQ}}{TQ} \quad (6.1)$$

$$C_{nI}^2 = B_T^2 \frac{C_T^2}{T^2} + B_Q^2 \frac{C_Q^2}{Q^2} + 2B_T B_Q \frac{C_{TQ}}{TQ} \quad (6.2)$$

Here A_T and A_Q are determined by the normal and anomalous dispersion, while B_T and B_Q are determined by absorption. T and Q represent the mean atmospheric temperature and humidity.

For visible and near-infrared wavelengths of the LED source, the C_T^2 term is the main contributor to C_{nR}^2 in (6.1), while the contribution of the covariant term is small but not insignificant. The contribution of the C_Q^2 term to C_{nR}^2 , however, appears to be negligibly small (Wesely, 1976). In contrast with C_{nR}^2 , the C_Q^2 term in (6.2) is the main contributor C_{nI}^2 , while the contribution of the covariant term and the C_T^2 term appear to be negligibly small (Hill *et al.*, 1980). This leaves us with a simple expression for C_{nI}^2 , solely determined by C_Q^2 (see Section 6.3).

The LAS measures the variance of the logarithmic amplitude fluctuations of the received EM wave and computes C_n^2 directly. The instrument provides a bandpass limited value of σ_χ^2 scaled by its aperture diameter D [m] and the propagation pathlength L [m]. From Wang *et al.* (1978),

$$C_n^2 = 4.48 \sigma_\chi^2 D^{-7/3} L^{-3}. \quad (6.3)$$

This paper deals with observations of the effect of water absorption and refractive scintillations on a beam of EM radiation at a near-infrared wavelength ($943.5 \text{ nm} \pm 4.5 \text{ nm}$). To study this effect, similar to the work of Medeiros Fihlo *et al.* (1983) and Kagawa *et al.* (1996), $W\chi(f)$ has to be analysed for the case of finite transmitting and receiving apertures and incoherent spherical waves.

Clifford (1971) derived an equation for $W\chi(f)$ for the case of a spherical wave. This equation can be extended to include the spatially incoherent transmitting and receiving optics by filter factors from Wang *et al.* (1978). The temporal spectral densities of the logarithmic amplitude fluctuations caused by the real and imaginary parts of the refractive index are given

by:

$$W\chi_{,R}(f) = 0.528\pi^2 k^2 C_{nR}^2 \int_{2\pi f/\nu}^{\infty} dK \int_0^L dz K^{-8/3} \sin^2 \left\{ \frac{K^2 z(L-z)}{2kL} \right\} \times \left\{ (K\nu)^2 - (2\pi f)^2 \right\}^{-1/2} \left\{ \frac{2J_1(y_r)}{y_r} \right\}^2 \left\{ \frac{2J_1(y_t)}{y_t} \right\}^2 \quad (6.4)$$

$$W\chi_{,I}(f) = 0.528\pi^2 k^2 C_{nI}^2 \int_{2\pi f/\nu}^{\infty} dK \int_0^L dz K^{-8/3} \cos^2 \left\{ \frac{K^2 z(L-z)}{2kL} \right\} \times \left\{ (K\nu)^2 - (2\pi f)^2 \right\}^{-1/2} \left\{ \frac{2J_1(y_r)}{y_r} \right\}^2 \left\{ \frac{2J_1(y_t)}{y_t} \right\}^2 \quad (6.5)$$

Where $y_r = R_r K z L^{-1}$ and $y_t = R_t K z L^{-1}$ are dimensionless quantities, K is the two-dimensional spatial wavenumber [m^{-1}] of turbulent eddies, z the position along the propagation path [m], R_t and R_r the radius of the transmitter and receiver [m] and k the wavenumber of the EM wave [m^{-1}]. R_t and R_r are taken equal here and will be referred to as $R_{r,t}$. The factors containing the Bessel functions, J_t , describe the damping effect of the finite apertures of the LAS. In the above expression it is assumed that the three dimensional spatial power spectrum of the refractive index follows the Kolmogorov $K^{-11/3}$ or inertial range power law behaviour (e.g. Monin & Yaglom, 1975). This assumption will break down at some low wavenumber, depending on stability, and a high wavenumber, depending on the inner scale of turbulence. Here we are especially interested in the behaviour of the scintillation spectrum at low wavenumbers. For the present we will assume that the Kolmogorov region extends to our lowest frequency of interest, 0.01 Hz (as usual, wavenumber and frequency are related by the wind speed while invoking the frozen turbulence hypothesis).

The total $W\chi(f)$ as measured by the LAS receiver is a combined spectrum where absorption and refractive index fluctuations are both active. Figure 1 shows the combined theoretical spectra for values of $C_{nR}^2 = 10^{-13} \text{ m}^{-2/3}$ and $C_{nI}^2 = 10^{-24} \text{ m}^{-2/3}$ and for $\nu = 1$ (solid line) and $\nu = 4 \text{ ms}^{-1}$ (dashed line). At low frequencies, $W\chi_{,R}(f)$ is constant, but at high frequencies it shows a sharp drop-off. This behaviour is quantitatively similar to the one reported by Clifford (1971) who studied the case of a spherical wave. However, the level of the plateau of $W\chi_{,R}(f)$ is different as is the slope at high frequencies. Whereas Clifford found

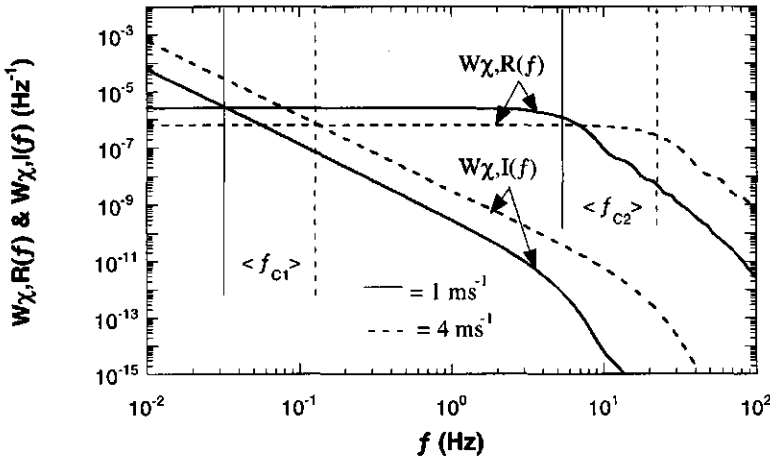


Figure 6.1: The theoretical temporal spectral densities ($W_{\chi,R}(f)$ & $W_{\chi,I}(f)$) of the logarithmic amplitude fluctuations caused by the real and imaginary part of the refractive index for a 1 m s^{-1} (Solid line) and 4 m s^{-1} (Dashed line) transverse windspeed, $C_{nR}^2 = 1 \cdot 10^{-13} \text{ m}^{-2/3}$, $C_{nI}^2 = 1 \cdot 10^{-24} \text{ m}^{-2/3}$, an inner scale (l_0) of 0.5 cm and a 200 m pathlength. The refractive index spectrum includes the so-called Hill bump (Hill & Clifford, 1978).

a $-8/3$ behaviour for $f \gg \nu ((2\pi\lambda L)^{-1/2})$, our numerical calculations show a more or less $-12/3$ dependence as demonstrated in Figure 6.1. The reason for this is the damping effect of the apertures (see e.g. Mandics *et al.*, 1973). If the radius of the receiving and transmitting aperture is larger than the first Fresnel zone $(\lambda L)^{-1/2}$, the transition between the frequency independent part and the dependent part of $W_{\chi,R}(f)$ is determined by $R_{i,r}$ rather than $(\lambda L)^{-1/2}$. At frequencies $f \gg \nu ((2\pi\lambda L)^{-1/2})$ the slope gets steeper than $-8/3$ due to the combined effect of the apertures and the first Fresnel zone. The transition frequency, or *upper corner frequency*, as referred to by Medeiros Fihlo *et al.* (1983), now scales with the ratio of transverse wind speed ν and the diameter of the transmitter and receiver. From the numerical calculations, we found that for

$$f_{C2} = \frac{\nu}{1.25D} \quad (6.6)$$

the spectrum had dropped to half of its value at low f . The frequency independent part of the spectrum is derived from the numerical integration as:

$$W_{\chi,R}(f) = 0.0389 L^3 D^{-7/3} C_{nR}^2 \nu^{-1}. \quad (6.7)$$

Note that $W_{\chi,R}(f)$ is independent of the optical wavenumber k . This is typical for the LAS as

long as the condition $D \gg (\lambda L)^{-1/2}$ is fulfilled.

$W\chi_{,1}(f)$ shows a $f^{-8/3}$ dependence (see Figure 6.1). The cases of spherical wave, plane wave and finite apertures are identical at low frequencies because only the largest eddies contribute to the amplitude spectrum. Here the spectrum for the lower frequencies (<1 Hz) is (Clifford, 1971):

$$W\chi_{,1}(f) = 0.0326 k^2 L C_{nl}^2 v^{5/3} f^{-8/3}. \quad (6.8)$$

Note that $W\chi_{,1}(f)$ is independent of the aperture diameters D , but depends on the optical wavenumber k .

The transition in the total spectrum ($W\chi(f)$) between the contribution of absorption fluctuations in the low frequency part and the frequency independent part of the refractive index fluctuations is defined by $W\chi_{,R}(f_{C1}) = W\chi_{,1}(f_{C1})$. From (6.7) and (6.8) it follows that

$$f_{C1} = 0.936 \left(\frac{k}{L} \right)^{3/4} D^{7/8} v \left(\frac{C_{nl}^2}{C_{nR}^2} \right)^{3/8}; \quad (6.9)$$

f_{C1} is the *lower corner frequency* as referred to by Medeiros Fihlo *et al.* (1983) and is indicated in Figure 1. Note that f_{C1} shifts to higher frequencies with increasing D , whereas f_{C2} shifts to lower frequencies, thus reducing the extension of the frequency independent region from both sides.

6.3. The calculation of C_{nl}^2 and C_Q^2

Knowing C_{nl}^2 permits calculation of f_{C1} from (6.9), as C_{nR}^2 is effectively the LAS output and v is known from a drag anemometer (see Section 6.4.3). C_{nl}^2 can be calculated from (6.2). Following Hill *et al.* (1980), B_Q is given by:

$$B_Q = \left(4\pi \frac{1}{\lambda} \right)^{-1} \left[\sum_i \langle \beta_i \rangle \langle b_{Qi} \rangle + 2 \langle \beta_c \rangle \right], \quad (6.10)$$

where λ is the wavelength of an absorption line and $\langle \beta_c \rangle$ the continuum absorption. The dimensionless coefficient, b_{Qi} , expresses the relation between the absorption line shape and the humidity; if this effect is neglected than $b_{Qi} = 1$; if also the continuum absorption is neglected, the resulting expression for B_Q is than given by:

$$B_Q = \left(4\pi \frac{1}{\lambda} \right)^{-1} \sum_i \beta_i. \quad (6.11)$$

Here $\sum \beta_i$ denotes the sum over only those absorption lines close to a central wavelength (λ), i.e. the absorption lines in the spectral envelope of the optical filter around 943.5 nm. The value $\sum \beta_i$ is determined from tables of the HITRAN database (Hill, pers. comm., 1996) for the optical filter window used in the experiment (9 nm) and result in a value for B_Q of 3.75×10^{-11} .

The humidity structure parameter C_Q^2 , in a dimensionless form, is found to be a universal function of $(z-d)/L_o$. Here z is the height, d the zero-plane displacement height and L_o the Monin-Obukhov length. If all conserved scalars obey Monin-Obukhov similarity theory scaling, all structure parameters are equal as discussed by Hill (1997) and, following Wyngaard *et al.* (1971):

$$\frac{C_Q^2 (z-d)^{2/3}}{Q_*^2} = 4.9 \left[1 - 7 \frac{(z-d)}{L_o} \right]^{-2/3} \quad (6.12)$$

for unstable conditions and

$$\frac{C_Q^2 (z-d)^{2/3}}{Q_*^2} = 4.9 \left[1 + 2.75 \frac{(z-d)}{L_o} \right] \quad (6.13)$$

for stable conditions. Here $Q_* = -Eu_*^{-1}$ in which E is the evaporation rate and u_* the friction velocity. Now, the eddy correlation measurements (see Section 6.4) allow C_Q^2 to be calculated from (6.12) and (6.13) and from this C_{nl}^2 and finally f_{Cl} .

6.4. Experimental

6.4.1. Site description

The experiment took place for several days in early summer 1996 over a flat, exposed pastoral site on the Purerua peninsula (Lat. 35°16'S; Long. 173°55'E). The pasture was green with moist soil surface conditions. The pasture sward was variable in height with a mixture of recently grazed grass types and patches of bare soil. Bowen ratios were typically small and seldom larger than 0.3, reflecting the greater amount of latent versus sensible heat flux. Conditions were generally breezy with high clouds or clear skies. During the mid-morning a

sea breeze would often develop from the North and persist until the late afternoon. Average air temperatures ranged from nighttime means of 15 °C to daytime maximums of about 22 °C.

The LAS link was established along a distance of 248 m in an East–West direction. The LAS receiver and transmitter were each mounted on interleaved concrete blocks at a beam height of 2 m and enclosed with plywood covers to protect against wind vibration and rain. A 3 m lattice meteorological tower was mounted at the midpoint of the propagation path with eddy correlation instruments. All instruments were battery operated.

6.4.2. Large aperture scintillometer

The LAS is a copy of the instrument conceived by Wang *et al.* (1978) and built at the NOAA wave Propagation Laboratory, Boulder Colorado and is aptly described in a NOAA Technical Memorandum (Ochs *et al.* 1980). The only modification to the original design has been to place a 1.25 cm diameter, optical narrow bandpass filter (Andover Corp., Salem, NH USA) in the front of the receiver photo diode. This optically discriminates for a 9 nm wide band of water absorption lines centred at 943.5 nm, present within the bandwidth of the LAS near-infrared source. In this configuration the received signal is more sensitive to the effect of absorption scintillations than it would be for the entire source spectral envelope. The NOAA designed electronics measure the fluctuations in the received light intensity and output a value for C_n^2 for a known pathlength and beam diameter following (6.3). The scintillation bandwidth for refractive turbulence is set to the range 0.03 to 400 Hz by active filters and the final scaled output of the logarithmic amplitude signal variance is integrated for 2.5 s, representing an average of all the scintillations occurring over this interval. This design presumably eliminates any low frequency signal drift beyond 0.03 Hz and as mentioned previously, the effect of absorption scintillations.

6.4.3. Instrumentation and data collection

On the meteorological tower at the LAS beam height eddy correlation instruments included, a 2D drag anemometer (HortResearch); a 1D sonic anemometer, fine wire thermocouple and Krypton Hygrometer (Campbell Scientific Ltd., Logan UT, USA); a sensitive cup anemometer (HortResearch), a net radiometer (Radiation Energy Balance Systems, Seattle WA, USA) and a naturally ventilated humidity–temperature sensor (Vaisala, Helsinki, Finland). A portable datalogger (21X, Campbell Scientific Ltd., Logan UT, USA) with

sampling intervals of 0.1 s and 60 s, calculated 30 minute averages of the sensible and latent heat fluxes, the friction velocity, the streamwise and lateral wind speed components, wind direction, cup wind speed, net radiation, relative humidity and air temperature. The drag anemometer was oriented perpendicular to the scintillometer beam so that its streamwise component represented v .

At the LAS receiver C_n^2 was recorded at 1s intervals and averaged for 30 minutes by a similar 21X datalogger. To obtain $W\chi(f)$, the signal was recorded directly at the output of the LAS receiver photodiode. This procedure bypassed any electronic filtering and provided a signal containing both absorption and refractive fluctuations. Two further 21X dataloggers were programmed to compute Fast Fourier Transforms (FFTs) of the unprocessed signal in ranges 0.01 to 1 Hz and 1 to 100 Hz.

6.5. Results and discussion

Figure 6.2 is a time series of half-hourly averages of v , Q and C_n^2 taken from 10:00 to 20:00 hours local time (UTC +12) on day 343. Several wind shifts occur during the day as the morning sea breeze starts to increase by midday and the wind direction reverses as indicated by an increasing negative v (Figure 6.2a). The wet ocean air increases Q , which then remains relatively constant until 16:00 hours when there is another 180-degree wind shift followed by a drop in Q and as the atmosphere approaches stable conditions the average C_n^2 is then seen to rapidly decrease by several orders of magnitude. This sudden drop in C_n^2 at dusk is symptomatic of the change in the atmospheric state as for a brief moment temperature fluctuations cease (Wesely & Alcaraz, 1973). The scintillometer beam is subject to varying cross winds from opposing quadrants with varying densities of wet air but relatively constant values of C_n^2 until 16:00 hours.

$W\chi(f)$ is presented in Figure 6.3 for a period from 11:00 to 20:00 hours (Day 343). The high frequency region is characterised by a $-8/3$ slope out to the 100 Hz Nyquist frequency and is due to refraction of the near-infrared beam. Here fluctuations result from atmospheric inhomogeneities that are smaller than the LAS beam diameter and which transect the path at velocity v . The $-8/3$ slope is inconsistent with the steeper slope due to aperture averaging as predicted by theory.

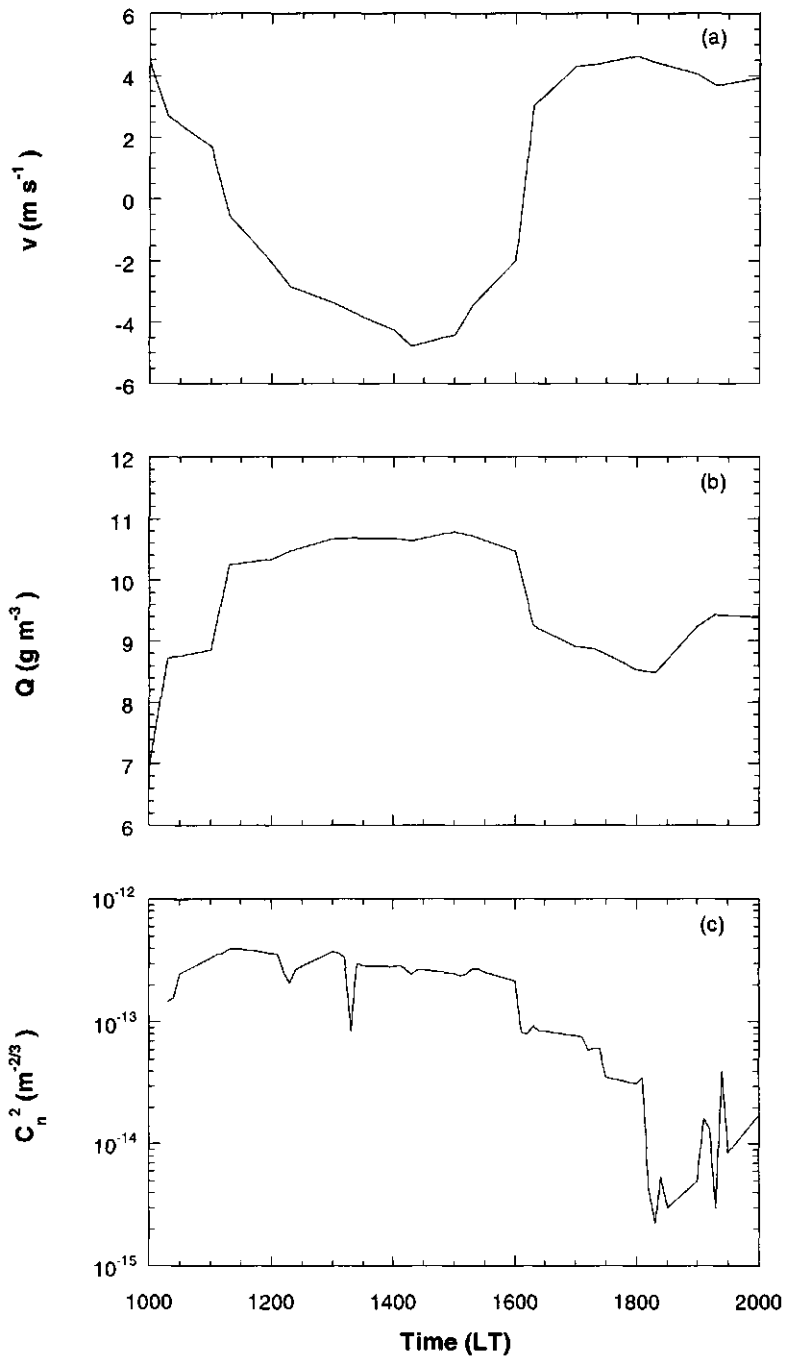
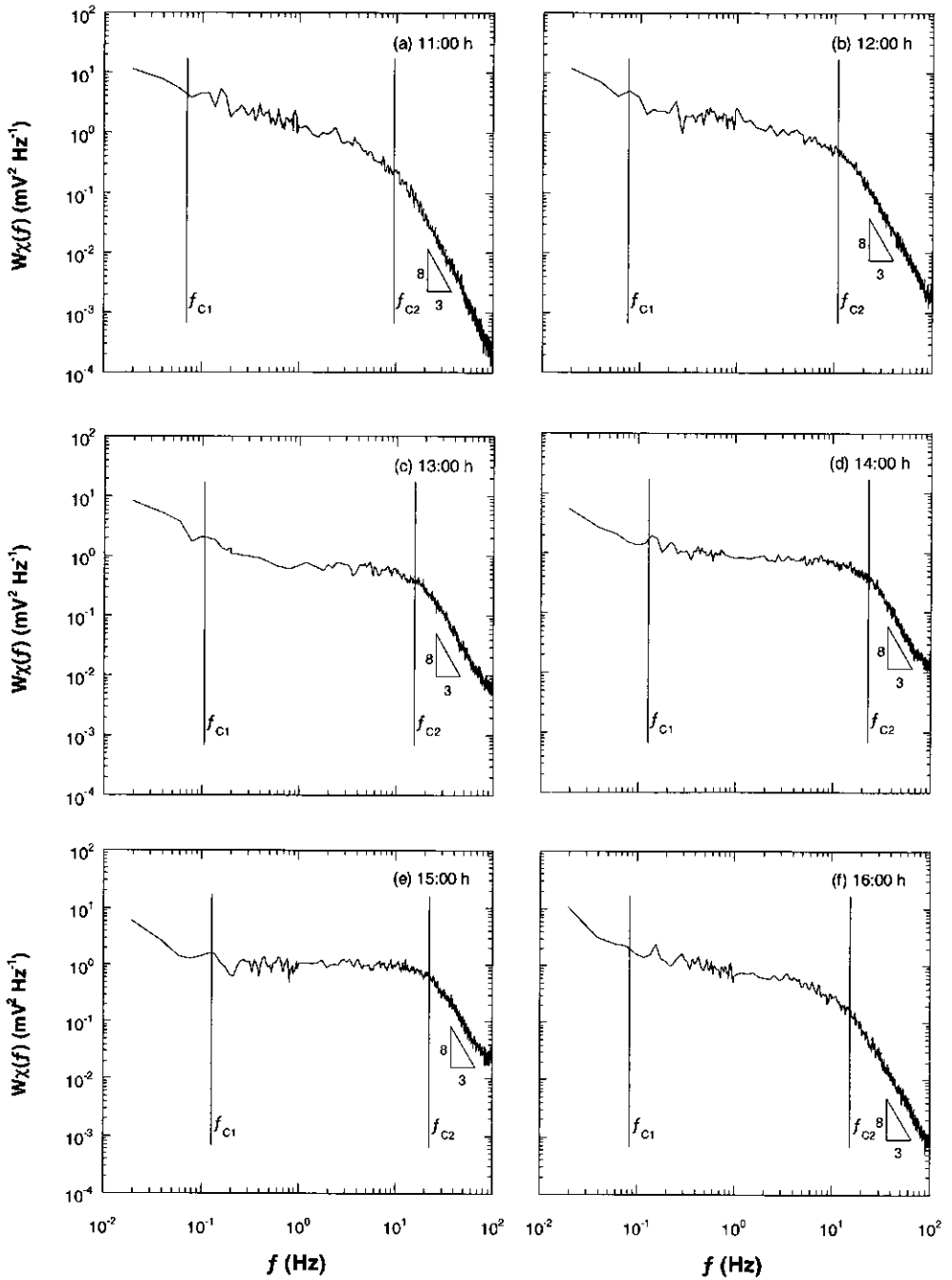


Figure 6.2: (a) Time series of 30 minute averages of the transverse windspeed, (b) the absolute humidity and (c) the refractive index structure parameter for day 343.



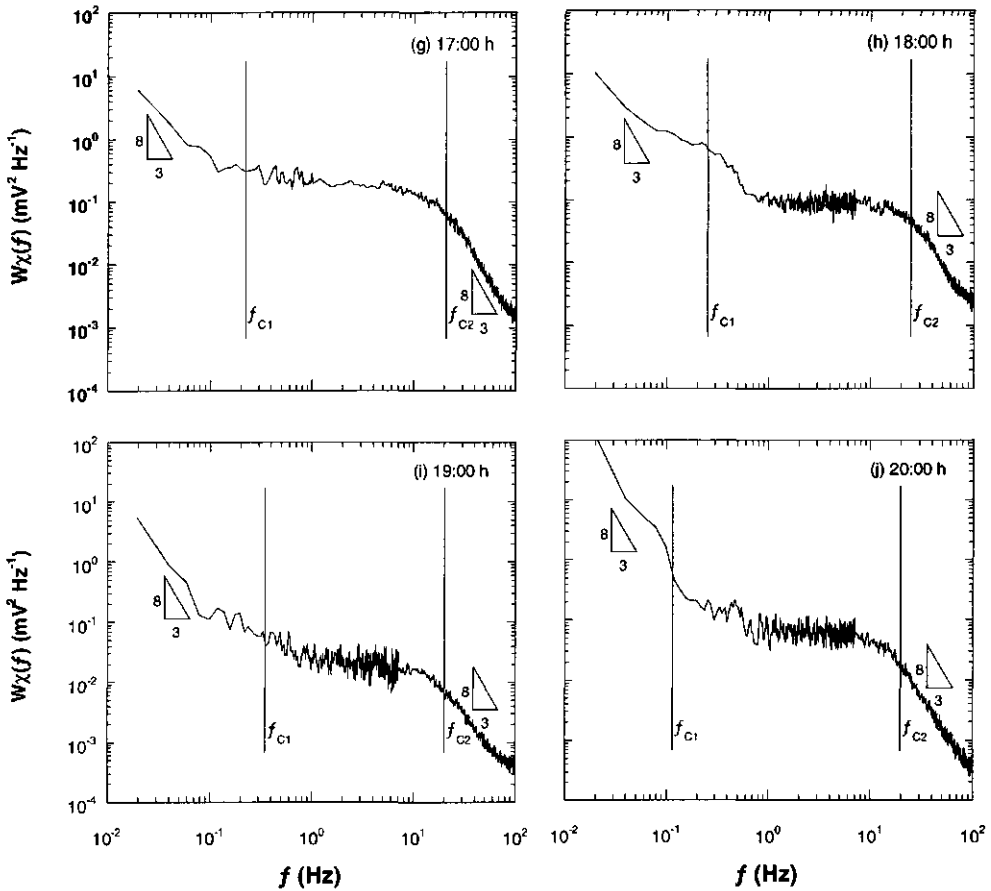


Figure 6.3: The changing temporal spectral density of the logarithmic amplitude fluctuations ($W\chi(f)$) for day 343.

The upper corner frequency, f_{c2} , can approximately be regarded as the point where the declining curve meets the flat region as described by Tatarskii (1971). The indicated positions of f_{c2} in Figure 6.3 are the calculated values from (6.6) (see also Table 6.1). As shown, any change in ν is imitated by the calculated and observed upper corner frequency having a minimum at 11:00 hours and a maximum value at 1800 hours.

As dusk approaches the spectral plateau lowers reflecting the decrease in the magnitude of C_{NR}^2 and creating a well defined break between the low frequency absorption and higher frequency refractive scintillations. Although theory predicts a $-8/3$ slope for the low frequency portion of the spectrum (assuming a Kolmogorov spectrum) this was not clearly observable until 17:00 hours. In retrospect, it would have been preferable to extent the low

frequency limit (Kagawa *et al.* (1993) used 10^{-3} Hz).

Table 6.1: Calculated values of the imaginary part of the refractive index structure parameter (C_{ni}^2) from the eddy correlation measurements and the calculated upper (f_{C1}) and lower (f_{C2}) corner frequencies on day 343.

Time	ν	H	LE	z/L_0	C_{ni}^2	C_{nR}^2	C_{ni}^2/C_{nR}^2	f_{C1}	f_{C2}
H	$m\ s^{-1}$	$W\ m^{-2}$	$W\ m^{-2}$	-	$m^{-2/3}$	$m^{-2/3}$	-	Hz	Hz
1100	1.7	98.6	243.5	-1.60E+00	7.00E-24	2.35E-13	2.97E-11	0.071	9.1
1200	-2.1	8.7	293.4	-1.04E-02	7.82E-24	3.81E-13	2.05E-11	0.076	11.2
1300	-3.3	67.6	290.2	-5.17E-02	4.13E-24	3.07E-13	1.35E-11	0.105	17.6
1400	-4.3	95.4	360.9	-2.51E-02	3.42E-24	2.91E-13	1.17E-11	0.127	22.9
1500	-4.4	91.1	318.9	-2.66E-02	2.76E-24	2.60E-13	1.06E-11	0.127	23.5
1600	-2.0	39.5	274.1	-9.97E-02	7.67E-24	2.45E-13	3.13E-11	0.086	10.7
1700	4.3	61.5	268.6	-3.02E-02	4.13E-24	8.22E-14	5.02E-11	0.220	22.9
1800	4.6	37.5	218.5	-1.35E-02	2.65E-24	4.06E-14	6.35E-11	0.262	24.5
1900	4.0	18.7	131.6	-7.88E-03	9.42E-25	4.30E-15	2.19E-10	0.361	21.3
2000	3.9	-37.7	60.0	1.04E-02	2.49E-25	1.81E-14	1.37E-11	0.125	20.8

From the data presented in Figure 6.3, f_{C1} is seen to increase with decreasing C_{nR}^2 . A 10 fold decrease in C_{nR}^2 from 13:00 to 18:00 hours results in approximately a 2.5 fold increase in f_{C1} . Here the indicated lower corner frequencies are the calculated values and are shown in Table 6.1. For midday conditions, the calculated lower corner frequency lies between 0.07 and 0.13 Hz. However, in the late afternoon and beginning of the evening, f_{C1} reaches even higher values. During this period C_{nR}^2 has dropped one or two orders of magnitude (10^{-13} to 10^{-15}) while C_{ni}^2 is still of the same magnitude (10^{-24}). After 19:00 hours C_{ni}^2 is also decreasing towards 10^{-25} , resulting in a shift of f_{C1} towards the lower frequencies again. Thus, absorption scintillations will effect the position of f_{C1} but by a small amount compared to C_{nR}^2 , which dominates by varying many orders of magnitude throughout the day. When C_{nR}^2 decreases in magnitude towards the evening, the effect of C_{ni}^2 is more clearly seen with an increase in f_{C1} and a clearly definable $-8/3$ slope attributed to the absorption mechanism. Provided C_{nR}^2 remains fairly constant ν can also be observed to influence f_{C1} .

As previously discussed the LAS electronics have a low scintillation cut-off frequency of 0.03 Hz. Referring to Figure 6.3 and Table 6.1, most of the time the effect of the absorption scintillation is seen to exceed this lower frequency limit and one wonders whether this transgression corrupts the measurement of C_n^2 . Until 18:00 hours the variance associated with the absorption scintillations is insignificant compared to the refraction, but by 20:00 hours

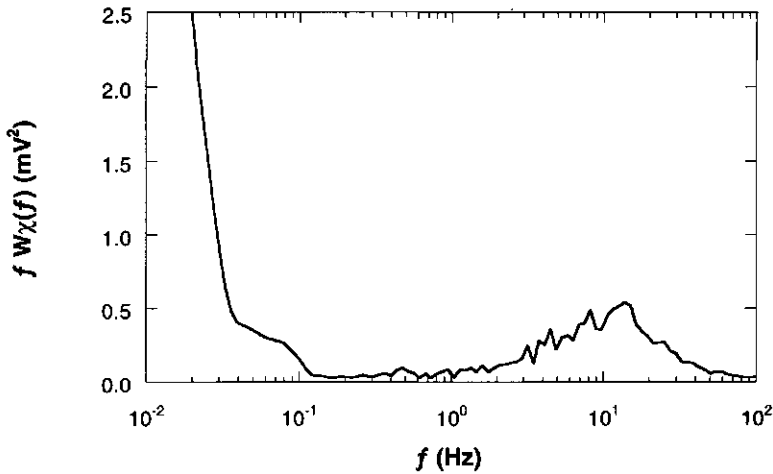


Figure 6.4: The temporal spectral variance at 20:00 hours for day 343.

contribute significantly within the LAS transmitting bandwidth (Figure 6.4). Calculations show that around this time absorption scintillations contribute about 3 to 5% to the total variance σ_χ^2 .

6.6. Conclusions

We analysed the contributions of the refraction and absorption fluctuations to the measured scintillations using a LAS. To do so, the temporal spectral density of the logarithmic amplitude fluctuations ($W_\chi(f)$) was studied and compared with the theoretical description. The observed refraction spectra show a $f^{-8/3}$ decay. This contradicts the theory, which predicts a steeper slope due to the effect of the finite aperture sizes. So far, no explanation has been found for this phenomenon and will be subject of further study. The experimental absorption spectra are less well defined, but nevertheless seem to be in accordance with the theoretical $f^{-8/3}$ slope. However, mind that the $K^{-11/3}$ behaviour may be questionable.

The observed upper corner frequency corresponds with the theoretical predictions. It varies between 10 and 25 Hz depending on the transverse wind speed. During daytime the lower corner frequency is hard to observe due to the limited bandwidth of the spectra. Towards the evening, however, there is significant decrease of the plateau of the refractive spectrum and the lower corner frequency becomes clearly visible. The calculated lower corner frequency varies between 0.071 and 0.36 Hz depending on C_{ni}^2/C_{nr}^2 and the transverse wind

speed and fits well in the observed spectra.

Nocturnal refractive scintillations are typically one order of magnitude or less lower than daytime values and scintillometers used for the determination of the sensible heat flux from the surface are generally only used during daytime. Should measurements of flux densities be attempted for near neutral and stable conditions, it may be prudent to take precaution to avoid corruption by absorption fluctuations by either extending the LAS lower cut-off frequency to 0.5 Hz in order to cut out any absorption or operate the scintillometer at a wavelength outside water vapour absorption regions.

Note: The experiment was repeated in December 1997 using different spectral analysis techniques. It was found that the high frequency drop-off of the spectrum was indeed steeper than $f^{-8/3}$. Spectra were simultaneously observed with the 21X datalogger and kept disagreeing. It is tentatively concluded that the high frequency drop-off is not correctly calculated by the 21X in our application.

Acknowledgements

The authors would like to acknowledge the technical assistance of Mark Astill, Bert Heusinkveld, Frits Antonysen and Willy Hillen in the construction of the scintillometer mechanics, opto-electronics and for assistance in field experimentation. We are most grateful for the helpful comments made by R. Hill, NOAA.

This research was supported by the Netherlands Organisation for Scientific Research under project number 753-06-234, and the New Zealand Ministry of Research and Technology ISAC Programme Grant (94/04) and Research Contract Number C06641.

CHAPTER 7

-
-
-

GENERAL CONCLUSIONS AND RECOMMENDATIONS

7.1. Introduction

For wetlands, the surface cover, local climate and hydrology have been found to significantly affect the flux densities of water vapour, carbon dioxide and other trace gases such as methane. The long-term eddy covariance technique provides a powerful tool to estimate the net annual ecosystem exchange of CO₂ and H₂O. These type of measurements over whole ecosystems will also in future be of major importance to improving our understanding of global mass and energy cycles. Knowledge of the interaction mechanisms at various time and spatial scales becomes significant, as point measurements have to be integrated to the larger landscape, regional and global scale. This is of particular importance in addressing the problem of the missing carbon sink. The development of remote sensing techniques, such as the scintillation technique, to measure areally averaged flux densities could have great potential.

7.2. Eddy covariance measurements

During a one and a half-year period in 1994 and 1995, eddy covariance flux density measurements were made over a disturbed raised peat bog. Annually, the area released about 97 g CO₂ m⁻² to the atmosphere. The major part originates from biochemical oxidation of organic matter, i.e. soil respiration, highly influenced by the temperature of the soil. The observed soil temperature dependence expressed as a $Q_{10} = 4.8$, can be used for recovery and interpolation of the annual cycle, but also for parameterisation of soil respiratory processes of wetland ecosystems in climate models. Net CO₂ exchange during the growing season is the result of the total respiration and photosynthesis. While respiration is mainly a temperature dependent process, photosynthesis depends on various factors such as *LAI*, temperature and

light.

Our data showed a clear non-linear relation between net CO₂ flux density and the incoming global radiation. High vapour pressure deficit (>15 hPa) suppressed the flux density up to about 50 percent. However, at the same time the evaporation rates were not greatly reduced. The observed decrease in the CO₂ flux density was not caused by stomatal closure, such as often associated with soil water stress or a high atmospheric vapour pressure deficit. Soil water stress as a cause can be excluded as the dominating vegetation rooted in a peat soil permanently close to saturation. It was found that the surface litter and the small amount of leaf area often led to surface temperatures exceeding the optimum temperature for photosynthesis. Therefore, long-term measurements of water vapour exchange are necessary to understand the biological and climate processes and surface- and boundary layer feedback mechanisms that control whole ecosystem CO₂ exchange. For wetland ecosystems in particular, water table measurements are of major importance to understand the exchange of greenhouse gases and are therefore highly recommended.

To understand the global mass and energy cycles, long-term eddy covariance measurements from different ecosystems are of crucial importance. Data can be used to quantify and explain the spatial and temporal differences in CO₂ and water vapour exchange under various climatic conditions. However, to study the effect of climate on the inter-annual and intra-annual net ecosystem exchange, a one and a half-year period is too short. Furthermore, data could increase our knowledge of the interaction mechanisms at various time and spatial scales. This is essential, as eddy covariance point measurements have to be integrated to the larger landscape, regional and global scale. To assess a larger pool of data with better certainty, a continuation of long term eddy covariance CO₂ measurements is recommended. Therefore, I highly advocate continuation and extension of long-term eddy covariance measurements projects such as SLIMM, over various ecosystems.

7.3. Scintillation measurements

Over the past few years the scintillation method to determine the path-average sensible heat flux density has increased in popularity. A limitation of the current scintillation methods is that none provide kilometre scale path-averaged sensible heat flux without incorporating compromising point measurements of the friction velocity and the Bowen ratio. The presumption that such measurements are representative of the entire pathlength of the large aperture scintillometer usually holds for homogeneous surface cover but may not be valid for

patchwork terrain. In addition, the application of these types of instruments requires careful evaluation of their ability to produce reliable measurements of the refractive index structure parameter. Any additional source of scintillation such as a contribution from absorption fluctuations caused by water vapour enhances the value of the refractive index structure parameter and with the sensible heat flux density.

The C_T^2 -profile method has been shown to offer a means of providing spatially averaged values of the stability and heat and momentum flux densities without incorporating point measurements of the wind speed or friction velocity. In the comparison of half-hourly values of sensible heat flux density calculations from the scintillation respectively eddy covariance technique agreement was within 10%. The comparison of two scintillometer receivers at $z = 10$ m, one scintillometer systematically underestimated the other by more than 5%, despite the careful opto-electronic calibration of the receiver scintillometers in the laboratory, and field alignment for maximum signal strength. Future research requires further experimental data for a tighter statistical comparison and effort made to reduce instrument uncertainties. The advantages this method offers, warrants further improvements.

In a turbulent atmosphere the amplitude of a propagating beam of electromagnetic (EM) energy of wavelength λ , can be distorted by refraction and absorption fluctuations. To quantitatively describe the combined effect of refraction and absorption, a complex refractive index, C_n^2 , is introduced. The real component, C_{nR}^2 is due to scattering and the imaginary part, C_{nI}^2 attributable to the absorption mechanism. The temporal spectral densities of the logarithmic amplitude fluctuations caused by the real and imaginary parts of the refractive index as measured by a Large Aperture Scintillometer's receiver is a combined spectrum where absorption and refractive index fluctuations are both active. The contribution of absorption shows as an enhancement at the low frequency end of the temporal spectral density of the log amplitude fluctuations. The transition absorption and refraction is known as the *lower corner frequency*.

The calculated lower corner frequency varies between 0.071 and 0.36 Hz depending on the ratio of the imaginary and real part of the refractive-index structure parameter and the transverse wind speed. These frequencies fit well in the observed spectra. Nocturnal refractive scintillations are typically one order of magnitude or less lower than daytime values. If absorption is ignored, this may have consequences for calculating nocturnal surface fluxes. During unstable, daytime conditions the large aperture scintillometer is most sensitive to refractive scintillations. But also under these conditions, the low frequency absorption part of the spectrum is observable. Consequently, should measurements of fluxes be attempted for

unstable conditions it may be prudent to take precaution to avoid corruption by absorption fluctuations by either extending the LAS lower cut-off frequency to 0.1 Hz for unstable conditions and to 0.5 Hz for near neutral and stable conditions in order to cut out any absorption or operate the scintillometer at a wavelength outside water vapour absorption regions.

SUMMARY

-
-
-

Introduction and objectives

Good comprehension of the energy and mass cycles and their effect on climate dynamics is crucial to understanding, predicting and anticipating ecological changes due to possible future climate perturbations. Here direct and long-term flux density measurements of greenhouse gases from various ecosystems provide means to supply such fundamental knowledge. For the global water vapour and carbon cycles, however, the interactions between different spatial scales become important, where extrapolating from canopy flux density measurements to global budgets lead to practical and theoretical problems. This thesis focuses on the direct and long-term measurement of surface flux densities and interaction processes at the canopy (< 1 km scale) within the framework of the Surface Layer Integration Measurements and Modelling (SLIMM) project. Furthermore, some characteristics and limitations of the scintillation technique are studied in two field experiments in New Zealand.

As indicated in Chapter 1, the *first objective* of this project was the direct and continuous long-term measurement of the surface flux densities of radiation, momentum, heat, water vapour and carbon dioxide (CO₂) to study the effect of biological and climatic processes that regulate carbon dioxide exchange of this ecosystem at the canopy scale. At the same time these data were used to study the effect of plant related and environmental conditions on the interaction of carbon dioxide and water vapour exchange, to satisfy the *second objective* of the thesis. The *third objective* focussed on the prospect of obtaining both the spatial averaged sensible heat flux density and momentum flux density from scintillation measurements. Generally, a compromising point measurement of the mean horizontal wind speed or friction velocity is used to calculate the sensible heat flux density from the temperature structure parameter. By using two scintillometers at two heights, point measurements to obtain the atmospheric stability can be omitted. The *fourth objective* of this

thesis was to study the influence of absorption fluctuations on the average sensible heat flux density derived from the scintillation technique.

Carbon dioxide exchange and the effect of biological and climatic processes

Carbon dioxide exchange was measured, using the eddy covariance technique, during a one and a half-year period in 1994 and 1995. The measurements took place over a former true raised bog, characterised by a shallow peat layer and tussock vegetation dominated by *Molinia caerulea*. Peat soils in the Northern Hemisphere's wetlands contain about one third of the world's carbon pool. Many regions in the arctic tundra, however, have changed from sinks to sources for CO₂ over the past decade but this can not simply be generalised.

The growing season extended from May until late October, with a maximum *LAI* in August of 1.7. The carbon balance showed a net release of 97 g CO₂ m⁻² y⁻¹ (265 kg C ha⁻¹ y⁻¹) from the peat bog ecosystem to the atmosphere. During June, July and August there was net consumption of CO₂, while during the rest of the year there was net production of CO₂. The maximum daytime net exchange rates were about -0.5 mg CO₂ m⁻² s⁻¹ (-11.3 μmol CO₂ m⁻² s⁻¹) with an average peak exchange rate of -0.2 mg CO₂ m⁻² s⁻¹ (-4.5 μmol CO₂ m⁻² s⁻¹), in a period where the *LAI* ranged between 1 and 1.7. A high vapour pressure deficit (>15 hPa) corresponding with high temperature was found to reduce the net CO₂ exchange rate by on average 50%. Apart from these factors, *LAI* and the soil temperature co-determined the net exchange of CO₂. The total nocturnal respiration during the growing season was within the same order as the average daytime net photosynthetic rate. Temperature was found to be the main factor controlling soil respiration, with a *Q*₁₀ of 4.8.

The effect of plant related and environmental conditions on the interaction of CO₂ and H₂O exchange

The tussock grassland, dominated by *Molinia caerulea*, was covered with a dense layer of dead organic material from the previous growing seasons. During the summer months, the daytime carbon dioxide uptake often showed a single early morning maximum and a decline in uptake during the rest of the day. Surprisingly, maximum water vapour flux densities were not greatly reduced. The surface cover and the small value of the leaf area index were the main reasons for this phenomenon.

The layer of dead organic material acted as an insulating blanket to the transport of water vapour from the soil to the atmosphere. Furthermore, the canopy was far from closed

with a peak leaf area index of 1.7 in early August. For both low vapour pressure deficit (< 15 hPa) and high vapour pressure deficit (> 20 hPa) at high surface temperatures, the vegetation showed similar behaviour resulting in a clear reduction of the daytime CO₂ uptake. Temperature was therefore inferred to be main the reason for a reduction in CO₂ exchange. The response of the stomata to atmospheric humidity was deduced to be small possibly due to the abundant availability of soil water. Instead transpiration increased with increasing vapour pressure deficit. The latter was stimulated by the surface temperature, which often exceeded the optimum temperature for photosynthesis and led to an increase in the atmospheric evaporative demand.

The scintillation technique

An optical or electromagnetic wave propagating through a turbulent atmosphere exhibits fluctuations in intensity known as 'scintillations'. In atmospheric turbulence, fluctuations in temperature, humidity and pressure cause density fluctuation and with it fluctuations in the refractive index (n). These refractive index fluctuations cause random refraction and absorption of electromagnetic (EM) radiation passing through the turbulent atmosphere, changing the characteristics of the wave. Scintillation of light is related to these phenomena and is experienced at a receiver as fluctuations in the light intensity caused by interference of refracted light and absorption of the light. Scintillometers measure the turbulent intensity of the refractive index fluctuations of the air from the intensity fluctuations of a received signal expressed in the refractive index structure parameter, C_n^2 .

The measured C_n^2 value is related to the structure parameters of temperature C_T^2 , humidity C_Q^2 and a covariant term C_{TQ} , respectively. To calculate the sensible heat flux density from C_n^2 compromising point measurements of the Bowen ratio, β , and friction velocity, u_* , are necessary. Generally, the deficiency in the available spatial measurement of u_* is overcome by using a point measure of the average wind speed, u and surface roughness, z_0 , but the necessity for β often remains unresolved.

By using two scintillometers at different heights above the surface, a spatial measurement of the Obukhov length, L_o , and u_* can be derived without incorporating compromising point measurements of the friction velocity or alternatively the average wind speed combined with a measure of the roughness length. The presumption that such measurements are representative of the entire transect usually holds for homogeneous surface cover but may not be valid for patchwork terrain. The two-scintillometer technique is referred

to as the C_T^2 -profile method.

Refraction is the result of normal and anomalous dispersion. If, however, the frequency of the emitted EM wave is close to a resonance frequency (absorption lines) of atmospheric constituents, like water vapour and carbon dioxide, absorption becomes important. To quantitatively describe the combined effect of refraction and absorption, a complex refractive index structure parameter, C_n^2 , is introduced. Here the phenomenon of absorption is represented by the imaginary part of the refractive index and is solely determined by single absorption lines and their corresponding absorption coefficients (β_i), resulting in a total absorption coefficient for a band of lines (Hill *et al.*, 1980). The absorption line strength is temperature dependent, while the absorption line width is temperature, humidity and pressure dependent.

The contribution of absorption fluctuations to C_n^2 is generally neglected, that means to have a real component only. In reality C_n^2 includes both a real part, C_{nR}^2 , due to refraction and an imaginary part, C_{nI}^2 , attributable to the absorption mechanism. Any additional source of scintillation such as a contribution from absorption fluctuations could conceivably corrupt the estimation of the sensible heat flux.

Measuring sensible heat flux density over pasture using the C_T^2 - profile method

Two large aperture scintillometers were positioned at heights (z) of 10 and 1.5 m with beams propagating horizontally over pasture for distances of 3.1 km and 141 m respectively. From each scintillometer a half-hourly average value of the path-averaged, temperature structure parameter (C_T^2) was obtained in unstable atmospheric conditions. The result suggested C_T^2 to scale with height as $z^{-2/3}$. Using the C_T^2 - profile method, a path averaged measure of the Obukhov length (L_o) was calculated for each half hour period. L_o was used to determine the friction velocity and the surface layer temperature scaling parameter, T^* . The scintillometer sensible heat flux density, H_{sc} , was then calculated from $H_{sc} = -\rho C_p u^* T^*$. A time series of half-hourly averaged H_{sc} compared to H_{ec} obtained by the eddy covariance method agreed to within 10%, with $R^2 = 0.67$, for a range of unstable conditions ($-0.2 \leq (z/L_o) \leq -0.01$).

Using a Large Aperture Scintillometer to measure absorption and refractive index fluctuations

The contribution of refraction and absorption fluctuations to the measured scintillation were observed for a near-infrared absorption region using a NOAA designed large aperture scintillometer. The logarithm amplitude spectra were shown to decay with a frequency as $f^{-8/3}$ for both the absorption and scattering mechanism. For the absorption mechanism this is in line with similar observations made at microwave and infrared frequencies. However, for finite transmitting and receiving apertures, theory predicts a stronger decay of the scattering mechanism due to aperture averaging. The spectral shape is characterised by a region of low frequency absorption, higher frequency refraction separated by a flattish transition zone. The upper observed corner frequency (f_{c2}), compared well with the calculated values using the measured transverse wind speed (v) for a known aperture radius. The lower corner frequency (f_{c1}) position was shown to be sensitive to the ratio of the real and imaginary part of the refractive index structure parameter, $(C_{nR}^2/C_{ni}^2)^{3/8}$ and v . The part of the spectrum associated with the absorption scintillations was observed to be much less than that due to refraction until the evening when decreasing C_{nR}^2 caused C_{nR}^2/C_{ni}^2 to decrease and absorption to become significant. If absorption is ignored, this may have consequences for calculating nocturnal surface heat flux densities. During unstable, daytime conditions the large aperture scintillometer is most sensitive to refractive scintillations despite having an infrared source transmitting in a lossy atmosphere. But also under these conditions, the low frequency absorption part of the spectrum is observable.

SAMENVATTING

-
-
-

Introductie en doelstellingen

Om ecologische verandering tengevolge van mogelijke klimaatsveranderingen te kunnen begrijpen, voorspellen en hierop te kunnen anticiperen, is een gedegen kennis van de globale energie- en massakringlopen nodig en de van effecten daarvan op de dynamica van het klimaat. Aan deze fundamentele kennis wordt bijgedragen door langjarige, directe metingen van de fluxdichtheid van broeikasgassen boven een verscheidenheid aan ecosystemen. Echter voor de mondiale hydrologische- en koolstofcyclus gaan interactiemechanismen tussen de verschillende ruimtelijke schalen een belangrijke rol spelen. Extrapolatie van metingen van turbulente uitwisseling op gewasniveau naar mondiale schalen leidt tot praktische en theoretische problemen. Dit proefschrift richt zich op het langjarig, direct meten van oppervlakte fluxdichtheden en interactieprocessen op gewas- (<1 km), locale- (~1 km) en landschapschaal (~1 – 10 km) in het kader van het 'Surface Layer Measurements and Modelling' (SLIMM) project. De landschapschaal heeft vooral aandacht gekregen gedurende twee korte scintillatieexperimenten in Nieuw Zeeland boven beweide grasland. Hierbij zijn enige karakteristieken en beperkingen van deze 'remote sensing' techniek geanalyseerd.

De *eerste* doelstelling van het SLIMM project was het direct en het langjarig continu meten van de fluxdichtheden van straling, impuls, warmte, waterdamp en koolstofdioxide (CO₂). Deze informatie is gebruikt om de effecten van biologische- en klimatologische processen op de uitwisseling van CO₂ op gewasniveau van een verstoord hoogveen te bestuderen. Als *tweede* doelstelling, boden de gegevens de mogelijkheid om de effecten van plant- en omgevingsfactoren te bestuderen op de interactie tussen de uitwisseling van CO₂ en waterdamp. De *derde* doelstelling omvatte de mogelijkheden en beperkingen van de scintillatiemethode. Deze techniek heeft de potentie ruimtelijk gemiddelde impuls- en warmtefluxdichtheid over enkel kilometers te kunnen bepalen. Gewoonlijk is hier naast de

scintillatiemeting ook een puntmeting van de horizontale windsnelheid, u , of wrijvingsnelheid, u^* , voor nodig om de ruimtelijk gemiddelde warmtestroomdichtheid te kunnen bepalen uit de temperatuur structuurparameter. Echter door het gebruik van twee scintillometers op twee hoogten, kan de benodigde puntmeting van de atmosferische stabiliteit achterwegen gelaten worden. De vierde doelstelling van dit proefschrift was het bestuderen van de invloed van absorptiefluctuaties op de warmtefluxdichtheid afgeleid van de scintillatiemethode.

CO₂ uitwisseling en het effect van biologische en klimatologische processen

De uitwisseling van CO₂ werd gemeten met behulp van de eddy-covariantietechniek gedurende een periode van anderhalf jaar in 1994 en 1995. De metingen werden uitgevoerd boven een verstoord hoogveen, gekarakteriseerd door een ondiepe veenbodem met graspollen gedomineerd door een pijpestrootje (*Molinia caerulea*) vegetatie. Eenderde van de mondiale voorraad koolstof ligt opgeslagen in veengebieden op het noordelijk halfrond. In de afgelopen decaden, zijn echter veel veengebieden in de arctische toendra veranderd van koolstofput naar koolstofbron, dat wil zeggen koolstof wordt afgebroken en vrij komt als CO₂. Echter deze resultaten kunnen zomaar gegeneraliseerd worden.

In het Fochtelooërveen in Friesland strekte het groeiseizoen van het pijpestrootje zich uit van mei tot en met oktober, met een maximale dichtheid van het bladoppervlak (*LAI*) van 1.7 in begin augustus. De koolstofbalans liet een netto verlies van 97 g CO₂ m⁻² y⁻¹ (265 kg C ha⁻² y⁻¹) zien van het hoogveen naar de atmosfeer. Gedurende juni, juli en augustus werd er netto CO₂ geconsumeerd door het ecosysteem, de rest van het jaar werd er netto CO₂ geproduceerd. In de periode waarin de *LAI* tussen de 1 en 1.7 lag, werden de hoogste netto fluxdichtheden gemeten van -0.5 mg CO₂ m⁻² s⁻¹ (-11.3 μmol CO₂ m⁻² s⁻¹) met een gemiddelde piekwaarde rond de -0.2 mg CO₂ m⁻² s⁻¹ (-4.5 μmol CO₂ m⁻² s⁻¹). Bij een hoog dampdrukdeficiet (>15 hPa) gecombineerd met hoge lucht- en oppervlakte temperaturen werd de netto fluxdichtheid met gemiddeld 50% gereduceerd. Naast deze omgevingsfactoren, waren de *LAI* en de bodemtemperatuur mede bepalend voor de netto uitwisseling van CO₂.

De nachtelijke uitwisseling was van dezelfde orde van grootte als netto uitwisseling gedurende de dag. Temperatuur was de meest bepalende factor voor de bodemrespiratie, met een temperatuur quotiënt (Q_{10}) van 4.8. Hierbij neemt bij iedere 10 graden stijging in temperatuur de bodemrespiratie dus met een factor 4.8 toe.

Het effect van plant- en omgevingsfactoren op de interactie tussen de uitwisseling van CO₂ en H₂O

De pollenstructuur van de pijpestrootje vegetatie, was afgedekt met een dikke laag dood organisch materiaal afkomstig van de vegetatie van voorgaande jaren. Vaak werd er in de zomermaanden een bepaald patroon in de CO₂ opname waargenomen. Al vroeg in de ochtend kwam het tot een maximum in CO₂ opname door het gewas waarna, gedurende de rest van de dag, de opname langzaam terug liep. Verassend genoeg werd dit patroon niet waargenomen voor de verdamping. Naar bleek waren de organische laag en de geringe hoeveelheid groen bladoppervlak de hoofdoorzaken van dit fenomeen.

Het geaccumuleerde organische materiaal vormde een sterk isolerende laag tegen het transport van waterdamp van de bodem naar de atmosfeer. Bovendien was het gewas verre van gesloten met een maximale LAI van 1.7 in begin augustus. Beide factoren leidden ertoe dat bij hoge temperaturen bij zowel een laag (<15 hPa) als bij hoog dampdrukdeficiet (>20 hPa) een soortgelijk gedrag van de vegetatie optrad. Dit resulteerde in een duidelijke reductie van de CO₂ opname gedurende de dag. De bepalende factor voor de sterke reductie in de CO₂ uitwisseling bleek dus de temperatuur te zijn. De stomataire reactie op de vochthoeveelheid in de atmosfeer werd klein beschouwd, waarschijnlijk door de overvloedige hoeveelheid beschikbaar vocht in de bodem. Daarentegen nam de verdamping toe bij een oplopend dampdrukdeficiet. Dit laatste werd gestimuleerd door een hoge oppervlaktetemperatuur die regelmatig de optimumtemperatuur voor fotosynthese oversteeg en leidde tot een verhoogd dampdrukdeficiet aan het oppervlak.

De scintillatietechniek

Indien een optisch of elektromagnetisch signaal zich voortbeweegt door een turbulente atmosfeer, dan veroorzaakt dit medium fluctuaties in de intensiteit van het signaal dat bekend staat onder de naam 'scintillatie'. Bij atmosferische turbulentie veroorzaken fluctuaties in temperatuur, vochtigheid en druk, dichtheidsverschillen. Deze laatste zorgen voor fluctuaties in de brekingsindex (n) van de atmosfeer. Hierdoor vindt er breking en absorptie van licht plaats dat zich in de atmosfeer voortbeweegt. Dit wordt door een ontvanger waargenomen als intensiteitfluctuaties ten gevolge van interferentie (breking) en absorptie van licht. Scintillometers meten de intensiteit van deze fluctuaties uitgedrukt in de structuurparameter van de brekingsindex, C_n^2 .

De gemeten waarde van C_n^2 is gerelateerd aan de structuurparameters van temperatuur

C_T^2 , vocht C_Q^2 en de co-variantie term C_{TQ} . Om de voelbare warmtestroomdichtheid, H , te bepalen uit C_n^2 zijn puntmetingen van de Bowen verhouding, β , en de wrijvingsnelheid nodig. Gewoonlijk wordt het gemis aan een ruimtelijk gemiddelde u_* opgelost door deze te bepalen uit de horizontale windsnelheid en oppervlakte ruwheid, z_0 . De noodzaak van de Bowen verhouding blijft meestal onopgelost.

Door gebruik te maken van twee scintillometers op twee hoogten kan een ruimtelijk gemiddelde Obukhovlengte, L_0 , bepaald worden zonder hulp van puntmetingen. De aanname dat deze puntmetingen geldig zijn voor het hele pad van de scintillometer is wellicht juist voor homogene oppervlakten. Echter voor heterogene landschappen is dit nog maar de vraag. Deze duo-scintillometer techniek staat bekend onder de naam C_T^2 - profielmethode.

Breking is het gevolg van normale en anomale verspreiding van licht. Als de golflengte van licht in de buurt komt van de eigenfrequentie van atmosferische bestanddelen zoals: waterdamp en CO_2 , wordt naast de anomale spreiding van licht, absorptie van belang. Om het effect hiervan te kwantificeren, is een structuurparameter geïntroduceerd, waarin absorptie weergegeven wordt als het imaginaire deel van de structuurparameter. Deze wordt enkel bepaald door individuele absorptielijnen en hun corresponderende absorptie-coëfficiënten (β_i), resulterend in een totale absorptiecoëfficiënt voor een absorptieband van lijnen. De absorptielijnsterkte is afhankelijk van de temperatuur, terwijl de absorptielijnbreedte afhankelijk is van de temperatuur, de vochthoeveelheid en de luchtdruk.

De bijdrage van absorptiefluctuaties aan C_n^2 wordt gewoonlijk verwaarloosd, dat wil zeggen alleen het reële deel van de complexe structuurparameter wordt in beschouwing genomen. In werkelijkheid heeft C_n^2 naast een reële bijdrage dus ook een imaginair deel. Deze toegevoegde bron van scintillatie zou de bepaling van de voelbare warmtestroomdichtheid danig kunnen verstoren.

Het meten van voelbare warmte boven gras met behulp van de C_T^2 - profielmethode

Twee scintillometers werden horizontaal opgesteld op een hoogte (z) van 10 en 1.5 m. De horizontale padlengten waren respectievelijk, 3.1 km en 141 m. Voor beide scintillometers werd een padgemiddelde halfuur waarde voor de temperatuur structuurparameter (C_T^2) bepaald in onstabiel atmosferische omstandigheden. De resultaten suggereerden dat C_T^2 schaalt met de hoogte als $z^{-2/3}$. Met behulp van deze profielmethode kon een padgemiddelde halfuur waarde voor de Obukhovlengte afgeleid worden, zonder gebruik te maken van puntmetingen van de horizontale windsnelheid of wrijvingsnelheid. L_0 werd gebruikt om de

padgemiddelde u^* en de temperatuur schalingsparameter, T^* , te bepalen. De voelbare warmtestroomdichtheid, H_{sc} , kon daarmee uitgerekend worden met de formule $H_{sc} = -\rho C_p u^* T^*$. H_{sc} tegen H_{ec} gemeten met behulp van de eddy-covariantie techniek, vertoonde een afwijking van slechts 10% met een $R^2 = 0.67$, voor onstabiele omstandigheden ($-0.2 \leq (z/L_0) \leq -0.01$).

Een scintillometer met grote openingshoek, voor het meten van absorptie- en brekingsindexfluctuaties

Met behulp van een scintillometer met een grote openingshoek (LAS) werden de bijdragen van refractie en absorptie aan de gemeten scintillatie vastgesteld. De logaritmische amplitude spectra lieten voor zowel het refractie- als voor het absorptiemechanisme een verval zien met de frequentie (f) als $f^{-8/3}$. Voor het absorptiemechanisme zijn soortgelijke waarnemingen gedaan in het microgolf en infrarode gebied. Echter voor scintillometers met een eindige openingshoek voorspeldt de theorie een sterker verval met de frequentie voor refractiemechanisme ten gevolge van middeling over de openingshoek. De vorm van het spectrum wordt gekarakteriseerd door absorptie aan de laagfrequente kant van het spectrum, refractie aan de hoogfrequente kant van het spectrum gescheiden door een platte overgangszone. Het buigpunt aan de hoogfrequente kant van het spectrum (f_{C2}) stemde goed overeen met de berekende waarden, gebruikmakend van de gemeten windsnelheid (v) loodrecht op het optische pad en de openingshoek. Het buigpunt aan de laagfrequente kant van het spectrum (f_{C1}) bleek gevoelig te zijn voor de verhouding tussen het reële en imaginaire deel van de structuurparameter voor de brekingsindex, $(C_{nR}^2/C_{nI}^2)^{3/8}$ en v . Waarnemingen lieten zien dat de bijdrage van absorptiefluctuaties aan het gecombineerde spectrum gering was ten opzichte van de bijdrage van refractie. Het teruglopen van de bijdrage van refractie, uitgedrukt in het reële deel van de structuurparameter voor de brekingsindex (C_{nR}^2), tijdens de vroege avonduren veroorzaakte een sterke afname van C_{nR}^2/C_{nI}^2 . Hierdoor leverden absorptiefluctuaties een significante bijdrage aan het spectrum. Indien deze bijdrage verwaarloosd wordt bij het berekenen van nachtelijke warmtefluxdichtheden, kan dit tot beduidende fouten leiden. Gedurende onstabiele atmosferische condities is de LAS het meest gevoelig voor refractie scintillaties, ondanks de infrarode lichtbron en een absorberende atmosfeer. Evenwel zijn ook onder deze omstandigheden de laagfrequente absorptiefluctuaties zichtbaar in het spectrum.

REFERENCES

-
-
-

Altenburg, W., Jansen, H., and Veen, W.S. van der: 1993, *Vegetatie ontwikkeling in het Fochteloërveen van de jaren '69 to 1992*, Bureau Altenburg & Wymenga, Rapport 52, Veenwouden, 53 pp. In Dutch.

André, J.C., Goutorbe, J.P. and Perier, A.: 1986, 'HAPEX-MOBILHY: A Hydrologic Atmospheric Experiment for the study of water budget and evaporation flux at the climate scale', *Bull. Amer. Meteorol. Soc.*, **67**, 138-144.

Andreas, E.L.: 1988, 'Atmospheric stability from scintillation measurements', *Appl. Opt.*, **27**, 2241-2246.

Andreas, E.L.: 1989, 'Two-wavelength method of measuring path-averaged turbulent surface heat fluxes', *J. Atmos. Ocean. Tech.*, **6**, 280-292.

Andreyev, G.A. and Chernaya, L.F.: 1978, 'Fluctuations in millimeter-wave beams propagating in a turbulent absorbing troposphere', *Telecom. Radio Eng.*, **33**, 64-74.

Baldocchi, D.D. and Meyers, T.P.: 1997, 'On using eco-physiological, micrometeorological and biogeochemical theory to evaluate carbon dioxide, water vapor and trace gas fluxes over vegetation: a perspective', *Agric. For. Meteorol.*, **90**, 1-25.

Baldocchi, D.D., Hicks, B.B. and Meyers, T.P.: 1988, 'Measuring biosphere-atmosphere exchanges of biologically related gases with micrometeorological methods', *Ecology*, **69**, 1331-1340.

Baldocchi, D.D., Valentini, R., Running, S., Oechel, W. and Dahlman, R.: 1996, 'Strategies for measuring and modelling carbon dioxide and water vapour fluxes over terrestrial ecosystems', *Glob. Change Biol.*, **2**, 159-168.

- Baldocchi, D.D., Verma, S.B. and Rosenberg, N.J.: 1981a, 'Environmental effects on the CO₂ flux and CO₂ – water flux ratio of alfalfa', *Agric. Meteorol.*, **24**, 175-184.
- Baldocchi, D.D., Verma, S.B. and Rosenberg, N.J.: 1981b, 'Mass and energy exchange of a soybean canopy under various environmental regimes', *Agron. J.*, **73**, 706-710.
- Baldocchi, D.D., Verma, S.B. and Rosenberg, N.J.: 1985, 'Water use efficiency in a soybean field: Influence of plant water stress', *Agric. For. Meteorol.*, **34**, 53-65.
- Baldocchi, D.D.: 1994, 'A comparative study of mass and energy exchange rates over a closed C₃ (wheat) and an open C₄ (corn) crop: CO₂ exchange and water use efficiency', *Agric. For. Meteorol.*, **67**, 291-321.
- Beverland, I.J., Moncrieff, J.B., Ónéill, D.H., Hargreaves, K.J. and Milne, R.: 1996, 'Measurements of methane and carbon dioxide from peatland ecosystems by the conditional-sampling technique', *Q.J.R. Meteorol. Soc.*, **122**, 819-838.
- Bierhuizen, J.F. and Slatyer, R.O.: 1965, 'The effect of atmospheric concentration of water vapour and CO₂ in determining transpiration-photosynthesis relationships of cotton leaves', *Agric. For. Meteorol.*, **2**, 259-270.
- Bink, N.J.: 1996, *The structure of the atmospheric surface layer subject to local advection*, PhD Thesis, Dept. of Meteorology, Wageningen Agricultural University, Wageningen, 206 pp.
- Burrows, W. and Milthorpe, F.L.: 1976, 'Stomatal conductance in the control of gas exchange', In: T.T. Kozlowski (Ed.), *Water Deficits and Plant Growth, Vol. IV*, Academic Press, New York, 103-152.
- Campbell, D.I. and Williamson, J.L.: 1997, 'Evaporation from a raised peat bog', *J. Hydrol.*, **193**, 142-160.
- Chapman, S.J. and Thurlow, M.: 1996, 'The influence of climate on CO₂ and CH₄ emissions from organic soils', *Agric. For. Meteorol.*, **79**, 205-217.
- Claussen, M. and Klaassen, W.: 1992, 'On regional surface fluxes over partly forested areas', *Contrib. Atmos. Phys.*, **65**, 243-248.
- Clifford, S.F.: 1971, 'Temporal-frequency spectra for a spherical wave propagating through

- atmospheric turbulence', *J. Opt. Soc. Amer.* **61** (10), 1285-1292.
- Clifford, S.F., Ochs, G.R. and Lawrence, R.S.: 1974, 'Saturation of optical scintillation by strong turbulence', *J. Opt. Soc. Amer.*, **64** (2), 148-154.
- Cole, R.S.: 1986, 'Amplitude and phase scintillations in the oxygen absorption region', *International Conference on Optical and Millimeter Wave Propagation and Scattering in the Atmosphere, Florence*, 157-160.
- Cowan, I.R. and Farquhar, G.D.: 1977, 'Stomatal function in relation to leaf metabolism and environment', In: *Integration of Activity in the Higher Plant, Symposia of the Society for Experimental Biology*, **31**, Cambridge University Press, Cambridge, 471-505.
- Cowan, T.J., Tans, P.P., Waterman, L.S., Thoning, K.W., Kitzis, D.R., Masarie, K. and Zang, N.: 1994, 'Evidence for interannual variability of the carbon cycle from NOAA/CMDL global sapling network', *J. Geophys. Res.*, **99**, 22,831-22,855.
- Coyne, P.I. and Kelley, J.J.: 1975, 'Carbon dioxide exchange over the Alaskan Arctic tundra: Meteorological assessment by an aerodynamic method', *J. Appl. Ecol.*, **12**, 587-611.
- De Bruin, H.A.R., van den Hurk, B.J.J.M. and Kohsiek, W.: 1995, 'The scintillation method tested over a dry vineyard area', *Boundary-Layer Meteorol.* **76**, 25-40.
- Duyzer, J.H. and Bosveld, F.C.: 1988, 'Measurements of dry deposition fluxes of O₃, NO_x, SO₂ and particles over grass/heathland vegetation and the influence of surface inhomogeneity', *MT-TNO*, Report no.: R 88/111, 89 pp.
- Farquhar, G.D., Von Caemmerer, S. and Berry, J.A.: 1980, 'A biochemical model of photosynthetic CO₂ assimilation in leaves of C₃ species', *Planta*, **149**, 78-90.
- Frehlich, R.G. and Ochs, G.R.: 1990, 'Effects of saturation on the optical scintillometer', *Appl. Opt.*, **29** (4), 548-553.
- Garratt, J.R.: 1992, *The atmospheric boundary layer*, University Press, Cambridge, 316 pp.
- Garratt, J.R.: 1993, 'Sensitivity of climate simulations to land-surface and atmospheric boundary layer treatments - A review', *J. Clim.*, **6**, 419-449.
- Goedee, R.: 1995, *Determination of the LAI*, MSc thesis, Dept of Meteorology, Wageningen Agricultural University, Wageningen, 115 pp.

- Gore, A.J.P.: 1983, 'Introduction', In: A.J.P. Gore (Ed.), *Ecosystems of the World 4A, Mires: Swamps, Bog, Fen and Moor, General Studies*, Elsevier Scientific Publishing Company, Amsterdam, 440 pp.
- Gorham, E.: 1991, 'Northern peatlands: Role in the carbon balance and probable responses to climatic warming', *Ecol. Appl.*, **1**, 182-195.
- Goudriaan, J., Van Laar, H.H., Van Keulen, H. and Louwse, W.: 1995, 'Photosynthesis, CO₂ and plant production', In: W. Day and R.K. Atkin (Eds.), *Wheat growth and modelling*, NATO ASI Series, Series A, Vol 86, Plenum Press, New York, 107-122.
- Goulden, M.L., Munger, J.W., Fan, S-M, Daube, B.C. and Wolfsy, S.C.: 1996, 'Measurements of carbon sequestration by long-term eddy covariance: methods and a critical evaluation of accuracy', *Glob. Change Biol.*, **2**, 169-182.
- Gracheva, M.E. and Gurvich, A.S.: 1965, 'Strong fluctuations in the intensity of light propagated through the atmosphere close to the earth', *Radiophys. Quantum Electron*, **8** (4), 511-515.
- Gracheva, M.E.: 1967, 'Investigation of the statistical properties in strong fluctuations in the intensity of light propagated through the atmosphere near the earth', *Radiophys. Quantum Electron*, **10** (6), 424-433.
- Graham, C.E.: 1995, 'Estimation of the ground heat flux and thermal properties of a bog in the Northern Netherlands', MSc thesis, Dept of Meteorology University of Reading, Reading UK, 107 pp.
- Grantz, D.A.: 1990, 'Plant response to atmospheric humidity', *Plant, Cell and Environment*, **13**, 667-679.
- Greco, S. and Baldocchi, D.D.: 1996, 'Seasonal variations of carbon dioxide and water vapour exchange over a temperate deciduous forest', *Glob. Change Biol.*, **2**, 183-197.
- Green, A. E., Judd, M. J., McAneney, K. J., Astill, M. S. and Prendergast, P. T.: 1991, 'A rapid-response, 2-D drag anemometer for atmospheric turbulence measurements', *Boundary-Layer Meteorol.* **57**, 1-15.
- Green, A. E., Astill, M. S. and Nieveen, J. P.: 1998, 'Sensible and latent heat fluxes measured

using a combination of near-infrared and microwave scintillometers', *J. Atmos. Oceanic Tech.* (Submitted).

Green, A.E. and Hayashi, Y.: 1998, 'Using the scintillometer technique over a rice paddy', *Jap. Agric. Meteorol.* **54** (3), 225-231.

Gurvich, A.S.: 1968, 'Effect of absorption on the fluctuation in signal level during atmospheric propagation', *Radio Eng. Elec. Phys.* **13**, 1687-1694.

Heusinkveld, B.G., Van Loon, W. and Jansen, A.: 1992, 'Outdoor technique to estimate the soil heat conductivity for atmospheric use', WMO/TD, No. 642, 205-207.

Hill, R. J.: 1992, 'Review of optical scintillation methods of measuring the refractive-index spectrum, inner scale and surface fluxes', *Waves in Random Media* **2**, 179-201.

Hill, R.J.: 1997, 'Algorithms for obtaining atmospheric surface-layer fluxes from scintillation measurements', *J. Atmos. Oceanic Tech.* **14**, 456-467.

Hill, R.J., Clifford, S.F.: 1978, 'Modified spectrum of atmospheric turbulence fluctuations and its application to optical propagation', *J. Opt. Soc. Amer.* **68**, 892-899.

Hill, R.J., Clifford, S.F. and Lawrence, R.S.: 1980, 'Refractive index and absorption fluctuations in the infrared caused by temperature, humidity and pressure fluctuations', *J. Opt. Soc. Amer.* **70**, 1192-1205.

Hill, R. J. and Ochs, G. R.: 1992, 'Surface-layer similarity of the temperature structure parameter', *J. Atmos. Sci.* **49**, 1348-1353.

Hill, R. J., Ochs, G. R. and Wilson, J. J.: 1992a, 'Measuring surface -layer fluxes of heat and momentum using optical scintillation', *Boundary-Layer Meteorol.* **58**, 391-408.

Hill, R. J., Ochs, G. R. and Wilson, J. J.: 1992b, 'Surface-layer fluxes measured using the C^2 -profile method', *J. Atmos. Ocean. Tech.* **9**, 526-537.

Houghton, J.T., Meira Filho, L.G., Callander, B.A., Harris, N., Kattenberg, A., and Maskell, K (Eds.): 1996, *Climate Change 1995, The science of Climate Change, Contribution of Working Group I to the Second Assessment Report of the Intergovernmental Panel on Climate Change*, Cambridge University Press, Cambridge, 572 pp.

- Ingram, H.A.P.: 1983, 'Hydrology', In: A.J.P. Gore (Ed.), *Ecosystems of the World 4A, Mires: Swamps, Bog, Fen and Moor, General Studies*, Elsevier Scientific Publishing Company, Amsterdam, 67-158.
- Jacobs, A.F.G., Van Boxel, J.H. and Nieveen, J.P.: 1996, 'Nighttime exchange processes near soil surface of a maize canopy', *Agric. For. Meteorol.*, **82**, 155-169.
- Jacobs, C.M.J. and De Bruin, H.A.R.: 1992, 'The sensitivity of regional transpiration to land-surface characteristics: significance of feedback', *J. Clim.*, **5**, 683-698.
- Jacobs, C.M.J., van den Hurk, B.J.J.M. and De Bruin, H.A.R.: 1996, 'Stomatal behaviour and photosynthetic rate of unstressed grapevines in semi-arid conditions', *Agric. For. Meteorol.*, **80**, 111-134.
- Jacobs, C.M.J.: 1994, *Direct impact of atmospheric CO₂ enrichment on regional transpiration*, PhD Thesis, Dept. of Meteorology Wageningen Agricultural University, Wageningen, 179 pp.
- Jarvis, P.G. and McNaughton, K.G.: 1986, 'Stomatal control of transpiration: scaling up from leaf to region', *Adv. Ecol. Res.*, **15**, 1-49.
- Johnson, D.A. and Caldwell, M.M.: 1976, 'Water potential components, stomatal function, and liquid phase water transport resistances of four arctic and alpine species in relation to moisture stress', *Physiologia Plantarum*, **36**, 271-8.
- Jones, H.G.: 1992, *Plants and microclimate*, Cambridge University Press, Cambridge, 428 pp.
- Kagawa, N., Osami, W. and Koga, R.: 1996, 'Calculations of the PSDF of scintillation for a 7 μ m band TDL beam around a water vapour line', *Infrared Phys. Tech.* **37**, 13-19.
- Kaimal, J.C. and Finnigan, J.J.: 1994, *Atmospheric Boundary Layer Flows - Their Structure and Measurement*, Oxford University Press, New York, 289 pp.
- Kanevskii, M.B., 1972: 'The problem of absorption on amplitude fluctuations of submillimeter radio waves in the atmosphere', *Radio Phys. Quantum Elec.* **15**, 1486-1487.
- Kim, J. and Verma, S.B.: 1990, 'Carbon dioxide exchange in a temperate grassland ecosystem', *Boundary-Layer Meteorol.*, **52**, 135-149.

- Kim, J. and Verma, S.B.: 1996, 'Surface exchange of water vapour between a open sphagnum fen and the atmosphere', *Boundary-Layer Meteorol.*, **79**, 243-264.
- Klaassen, W. and Claussen, M.: 1995, 'Landscape variability and surface flux parameterization in climate models', *Agric. For. Meteorol.*, **73**, 181-188.
- Klaassen, W.: 1992, 'Average fluxes from heterogeneous vegetated regions', *Boundary-Layer Meteorol.*, **58**, 329-354.
- Koerselman, W. and Beltman, B.: 1988, 'Evapotranspiration from fens in relation to Penman's potential free water evaporation (E_0) and pan evaporation', *Aquat. Bot.*, **31**, 307-320.
- Kohsiek, W.: 1982, 'Measuring C_T^2 , C_Q^2 and C_{TQ} in the unstable surface layer, and relations to the vertical fluxes of heat and moisture', *Boundary-Layer Meteorol.*, **24**, 89-107.
- Kroon, L.M.J. and De Bruin, H.A.R.: 1993, 'Atmosphere-vegetation interaction in local advection conditions', *Agric. For. Meteorol.*, **64**, 1-28.
- Kruijt, B., Klaassen W. and Hutjes, R.W.A.: 1995, 'Adjustment of turbulent momentum flux over forest downwind of an edge', In: J. Grace and M. Coultts (Eds.), *Wind and trees*, Cambridge University Press, Cambridge, 60-70.
- Kruijt, B.: 1994, *Turbulence over forest downwind of an edge*, PhD Thesis, Dept. of Physical Geography, University of Groningen, Groningen, 156 pp.
- Lafleur, P.M. and Rouse, W.R.: 1988, 'The influence of surface cover and climate on energy partitioning and evaporation in a subarctic wetland', *Boundary-Layer Meteorol.*, **44**, 327-347.
- Lafleur, P.M. and Rouse, W.R.: 1990, 'Application of an energy combination model for evaporation from sparse canopies', *Agric. For. Meteorol.*, **49**, 135-153.
- Lafleur, P.M.: 1990, 'Evapotranspiration from sedge-dominated wetland surfaces', *Aquat. Bot.*, **37**, 341-353.
- Landsberg, J.J.: 1977, 'Some useful equations for biological studies', *Exp. Agric.*, **13**, 273-288.
- Lawrence, R.S. and Strohbehn, J.W.: 1970, 'A survey of clear-air propagation effects

- relevant to optical communication', *Proceedings of the IEEE*, **58(10)**, 1523-1545.
- Little, C.G.: 1951, 'A diffraction theory of the scintillation of stars on optical and radio wavelengths', *Monthly Not. R. Astr. Soc.*, **111**, 289-302.
- Lösch, R. and Tenhunen, J.D.: 1981, 'Stomatal response to humidity - phenomenon and mechanism', In: P.G. Jarvis and T.A. Mansfield (Eds.), *Stomatal Physiology*, Cambridge University Press, Cambridge, 137-161.
- Mandics, P.A., Lee, R.W. and Waterman Jr, A.T.: 1973, 'Spectra of short-term fluctuations of line-of-sight signals: Electromagnetic and acoustic', *Radio Sci.* **8** (3), 185-201.
- Mason, P.J.: 1988, 'The formation of areally averaged roughness lengths', *Q. J. R. Meteorol. Soc.*, **114**, 399-420.
- McAneney, K.G., Green, A.E. and Astill, M.: 1995, 'Large-aperture scintillometry: the homogeneous case', *Agric. For. Meteorol.*, **76**, 149-162.
- McMillen, R.T.: 1986, *A BASIC program for eddy correlation in non-simple terrain*, NOAA Tech. Memo. ERLARL-147, NOAA, Air Resources Lab., Oak Ridge MD
- McMillen, R.T.: 1988, 'An eddy-correlation technique with extended applicability to non-simple terrain', *Boundary-Layer Meteorol.*, **43**, 231-245.
- McNaughton, K.G. and Jarvis, P.G.: 1983, 'Predicting effects of vegetation classes on transpiration and evaporation', In: T.T. Kozłowski (Ed.), *Water Deficits and Plant Growth*, Vol. 7, 1-42.
- McNaughton, K.G. and Jarvis, P.G.: 1991, 'Effects of spatial scale on stomatal control of transpiration', *Agric. For. Meteorol.*, **54**, 279-301.
- Medeiros Fihlo, F.C., Jayasuriya, D.A.R., Cole, R.S. and Helms, C.G.: 1983, 'Spectral density of millimeter wave amplitude scintillations in an absorbing region', *IEEE Trans. Antennas Propagat.* **AP 31**, 672-676.
- Meidner, H. and Mansfield, T.A.: 1968, *Physiology of Stomata*, McGraw-Hill, London, 179 pp.
- Miranda, A.C., Jarvis, P.G. and Grace, J.: 1984, 'Transpiration from heather moorland', *Boundary-Layer Meteorol.*, **28**, 227-243.

- Monin, A.S. and Yaglom, A.M.: 1975, *Statistical fluid mechanics: Mechanics of Turbulence*, Volume 2, translated from Russian by Scripta Graphica, Inc., Ed: J.L. Lumley, The MIT Press, Cambridge, UK, 874 pp.
- Monteith, J.L. and Unsworth, M.H.: 1990, *Principles of Environmental Physics (2nd Ed)*, Arnold, London, 291 pp.
- Monteith, J.L.: 1965, 'Evaporation and environment', *Symp. Soc. Exp. Biol.*, **19**, 205-234.
- Moore, C.J.: 1986, 'Frequency response corrections for eddy correlation systems', *Boundary-Layer Meteorol.*, **37**, 17-35.
- Neumann, H.H., den Hartog, G., King, K.M. and Chipanshi, A.C.: 1994, 'Carbon dioxide fluxes over a raised open bog at Kinosheo Lake tower site during the Northern Wetlands Study (NOWES)', *J. Geophys. Res.*, **99**, 1529-1538.
- Oberbauer, S.F., Tenhunen, J.D. and Reynolds, J.D.: 1991, 'Environmental effects on CO₂ efflux from water track and tussock tundra in Arctic Alaska, U.S.A.', *Arct. Alp. Res.*, **23**, 162-169.
- Ochs, G.R. and Cartwright, W.D.: 1980, 'Optical system model IV for space-averaged wind and C_n² measurements', *NOAA Tech. Memo.*, ERL WPL-52 NOAA, Env. Res. Lab., Boulder, CO, USA, 31 pp.
- Oechel, W.C., Hastings, S.J., Vourlites, G., Jenkins, M., Riechers, G. and Grulke, N.: 1993, 'Recent change of arctic tundra from a net carbon dioxide sink to a source', *Nature*, **361**, 520-523.
- Ott, R.H. and Thompson Jr., M.C.: 1978, 'Atmospheric amplitude spectra in an absorbing region', *IEEE Trans. Antennas Propagat.* **16**, 329-332.
- Ott, R.H.: 1977, 'Temporal radio frequency spectra of multi-frequency waves in a turbulent atmosphere characterized by a complex refractive index', *IEEE Trans. Antennas Propagat.* **AP-25**, 254-260.
- Panofsky, H.A. and Dutton, J.A.: 1984, *Atmospheric turbulence: Models and methods for engineering applications*, John Wiley & Sons, New York, 397 pp.
- Parry, M.L., Carter, T.R. and Konijn, N.T. (Eds.): 1988, *The impact of climate variations on*

agriculture, Volume 1 & 2, Kluwer, Dordrecht.

- Paulson, C.A.: 1970, 'The mathematical representation of wind speed and temperature profiles in the unstable atmospheric surface layer', *J. Appl. Meteorol.*, **9**, 857-861.
- Price, D.T. and Black, T.A.: 1990, 'Effect of short term variations in weather on diurnal canopy CO₂ flux and evapotranspiration of a juvenile Douglas fir stand', *Agric. For. Meteorol.*, **50**, 139-158.
- Price, J.S.: 1991, 'Evaporation from a blanket bog in a foggy coastal environment', *Boundary-Layer Meteorol.*, **57**, 391-406.
- Raupach, M.R.: 1991, 'Vegetation-atmosphere interaction in homogeneous and heterogeneous terrain: some implications of mixed-layer dynamics', *Vegetatio*, **91**, 105-120.
- Romanov, V.V.: 1968, 'Hydrology of Bogs', *Israel Program for Scientific Translations*, Jerusalem, 299 pp.
- Ruimy, A., Jarvis, P.G., Baldocchi, D.D. and Saugier, B.: 1995, 'CO₂ fluxes over plant canopies and solar radiation: A review', *Adv. Ecol. Res.*, **26**, 1-81.
- Schimel, D.S., Kittel, T. and Parton, W.J.: 1991, 'Terrestrial biogeochemical cycles: global interaction with atmosphere and hydrology', *Tellus*, **43B**, 188-203.
- Schmugge, T.J. and André, J.C. (Eds): 1991, *Measurement and parameterization of land surface evaporation fluxes*, Springer Verslag, Tilburg, 424 pp.
- Schouwenaars, J.M. and Vink, J.P.M.: 1990, 'Hydrophysical properties of peat relicts in a former bog and perspectives for sphagnum regrowth', *International Peat Journal*, **5**, 15-28.
- Schulze, E.D. and Hall, A.E.: 1982, Stomatal responses, water loss and CO₂ assimilation rates of plants in contrasting environments, In: O.L. Lange, P.S. Nobel, C.B. Osmond and H. Ziegler (Eds.), *Encyclopedia of Plant Physiology, New Series, Vol. 12B, Physiological Plant Ecology II*, Springer Verslag, Berlin, 181-230.
- Schulze, E.D., Turner, N.C., Gollan, T. and Shackel, K.A.: 1987, 'Stomatal responses to air humidity and soil drought', In: E. Zeiger, G.D. Farquhar and I.R. Cowan (Eds.),

Stomatal Function, Stanford University Press, Stanford, 311-321.

Schulze, E.D.: 1986, 'Carbon dioxide and water vapor exchange in response to drought in the atmosphere and in the soil', *Ann. Rev. Plant Phys.*, **43**, 247-274.

Shurpali, N.J., Verma, S.B., Kim, J., and Arkebauer, T.J.: 1995, 'Carbon dioxide exchange in a peatland ecosystem', *J. Geophys. Res.*, **100**, 14, 319-14,326.

Shuttleworth, W.J.: 1988, 'Macrohydrology-the new challenge for process hydrology', *J. Hydrol.*, **100**, 31-56.

Silvola, J., Martikaine, P. and Nykänen, H.: 1992, 'A mobile automatic gas chromatograph system to measure CO₂, CH₄ and N₂O fluxes from soil in the field', *SUO Mires and peat*, **43**, 263-266.

Silvola, U.: 1986, 'Carbon dioxide dynamics in mires reclaimed for forestry in Eastern Finland', *Ann. Bot. Fenn.*, **23**, 59-67.

Spence, T. and Townshend, J.: 1995, 'The Global Climate Observing System (GCOS). An Editorial', *Clim. Change*, **31**, 131-134.

Stewart, J.B.: 1988, 'Modelling surface conductance of pine forest', *Agric. Meteorol.*, **30**, 111-127.

Strohbehn, J.W.: 1968, 'Line-of-sight propagation through the turbulent atmosphere', *Proceedings of the IEEE*, **56(8)**, 1301-1318.

Svenson, U.: 1980, 'Carbon dioxide and methane fluxes from the ombrotrophic parts of a subarctic mire', *Ecol. Bull. Stockholm*, **30**, 235-250.

Tans, P.P., Bakwil, P.S. and Guenther, D.W.: 1996, 'A feasible Global Carbon Cycle Observation System: a plan to decipher today's carbon cycle based on observations', *Glob. Change Biol.*, **2**, 309-318.

Tatarskii, V.I.: 1961, *Wave Propagation in a Turbulent Medium*, translated from Russian by R.S. Silverman, McGraw-Hill, New York, USA, 285 pp.

Tatarskii, V.I.: 1971, *The Effect of the Turbulent Atmosphere on Wave Propagation*, translated from Russian by Israel Program for Scientific Translation, Rep. N 72-18163, National Technical Information Service, Springfield, Va, USA, 472 pp.

- Tartarskii, V.I.: 1993, 'Review of scintillation phenomena', In: V.I. Tartarskii, A. Ishimaru and V.U. Zavorotny (Eds.), *Wave propagation in random media (scintillation)*, Co-published by the International Society for Optical Engineering and the Institute of Physics Publishing, 2-15.
- Tenhunen, J.D., Lange, O.L., Gebel, J. Beyschag, W. and Weber, J.A.: 1984, 'Changes in the photosynthetic capacity, carboxylation efficiency, and CO₂ compensation point associated with midday stomatal closure and midday depression of CO₂ exchange of leaves of *Quercus suber*.', *Planta*, **162**, 193-203.
- Tenhunen, J.D., Pearcy, R.W. and Lange, O.L.: 1987, 'Diurnal variation in leaf conductance and gas exchange in natural environments', In: E. Zeiger, G.D. Farquhar and I.R. Cowan (Eds.), *Stomatal Function*, Stanford University Press, Stanford, California, 323-351.
- Thiermann, V.: 1992, 'A displaced beam scintillometer for line-averaged measurements of surface layer turbulence', 10th Symposium on Turbulence and Diffusion, Portland, Oregon, American Meteorological Society.
- Thiermann, V and Grassl, H.: 1992, 'The measurement of turbulent surface-layer fluxes by use of bichromatic scintillation', *Boundary-Layer Meteorol*, **58**, 367-389.
- Thom, A.S.: 1975, 'Momentum, mass and heat exchanges of plant communities', In: J.L. Monteith (Ed.), *Vegetation and the Atmosphere*, Vol. 1: Principles, Academic Press, London, 57-109.
- Ting-i Wang, Ochs, G.R. and Clifford, S.F.: 1978, 'A saturation resistant optical scintillometer to measure C_n²', *J. Opt. Soc. Amer.* **68**, 334-338.
- Valentini, R., De Angelis, P., Matteucci, G., Monaco, R., Dore, S. and Scarascia Mugnozza, G.E.: 1996, 'Seasonal net carbon dioxide exchange of a beech forest with the atmosphere', *Glob. Change Biol.*, **2**, 199-207.
- Van den Hurk, B.J.J.M.: 1996, *Sparse canopy parameterizations for meteorological models*, PhD Thesis, Dept. of Meteorology, Wageningen Agricultural University, Wageningen, 271 pp.
- Verhoef, A., Allen, S.J., De Bruin, H.A.R., Jacobs, C.M.J. and Heusinkveld, B.G.: 1996,

- 'Fluxes of carbon dioxide and water vapour from a Sahelian savanna', *Agric. For. Meteorol.*, **80**, 231-248.
- Verhoef, A.: 1995, *Surface energy balance of shrub vegetation in the Sahel*, PhD Thesis, Dept. of Meteorology Wageningen Agricultural University, Wageningen, 247 pp.
- Verry, E.S.: 1988, 'Hydrology of wetlands and men's influence on it', In: *Symposium on Hydrology of Wetlands in Temperate and Cold Regions*, Vol 2., Publication of the Academy of Finland, Helsinki, **5**, 41-61.
- Vugts, H., Jacobs, A.F.G. and Klaassen, W.: 1994, 'SLIMM project', In: S. Zwerver, R.S.A.R. van Rompaey, M.T.J. Kok and M.M. Berk (Eds.), *Studies in Environmental Science 65A, Climate Change Research: Evaluation and Policy Implications*, Elsevier Science B.V., Amsterdam, 674 pp.
- Wang, T. -i., Ochs, G. R. and Clifford, S. F.: 1978, 'A saturation-resistant optical scintillometer to measure C_n^2 ', *J. Opt. Soc. Amer.*, **68**, 334-338.
- Webb, E.K., Pearman, G.I. and Leuning, R.: 1980, 'Corrections of flux measurements for density effects due to heat and water vapour transfer', *Q. J. R. Meteorol. Soc.*, **106**, 85-100.
- Wesely, M.L. and Alcaez, E.C.: 1973, 'Diurnal cycles of the refractive index structure function coefficient', *J. Geophys. Res.* **78**, 483-490.
- Wesely, M.L.: 1976, 'The combined effect of temperature and humidity fluctuations on refractive index', *J. Appl. Meteorol.* **15**(1), 43-49.
- Wieringa, J.: 1986, 'Roughness dependent geographical interpolation of surface wind speed averages', *Q. J. R. Meteorol. Soc.*, **112**, 867-889.
- Wofsy, S.C., Goulden, M.L., Munger, J.W., Fan, S.M., Bakwin, P.S., Daube, B.C. and Bazzaz, F.A.: 1993, 'Net exchange of CO₂ in a mid-latitude forest', *Science*, **260**, 1314-1317.
- Wyngaard, J.C., Izumi, Y and Collins Jr., S.A.: 1971, 'Behaviour of the refractive index-structure-parameter near the ground', *J. Opt. Soc. Amer.* **61**, 1646-165.

CURRICULUM VITAE

-
-
-

Op 26 maart 1968 werd in Arnhem de derde zoon van Jan Gerhard Nieveen en Henderika Nieveen Modder op de wereld gezet. Deze creatie noemden zij Joost Pieter Nieveen. Na zijn lagereschooltijd, doorliep hij van 1979 tot 1986 het Voorbereidend Wetenschappelijk Onderwijs (VWO) aan het Katholiek Gelders Lyceum in Arnhem. Aansluitend verhuisde hij 20 kilometer naar het westen om daar zijn studie Landbouwtechniek te beginnen. In 1991 werd als afstudeeropdracht aan de formatie en droging van dauw gewerkt. Hiervoor werd een veldexperimentje opgezet in een perceel zomergerst en de resultaten vergeleken met een eenvoudig computermodel. Vervolgens werd het tijd eens buiten de grenzen te gaan kijken en was een stage aan het Horticultural Research Institute of New Zealand in Kerikeri het gevolg. Hier werkte hij aan het meten en modelleren van CO₂ uitwisseling van kiwi's en werd hij als mens wat verder bijgeschaafd. Na thuiskomst doorliep hij nog een stage bij Meteo Consult B.V.. In 1993 studeerde hij af in de Landbouwtechniek en de Bodem-Water en Atmosfeer. Dat zelfde jaar begon hij als onderzoeker in opleiding (OIO) in dienst van de Nederlandse Organisatie voor Wetenschappelijk Onderzoek (NWO) zijn promotie bij de toenmalige vakgroep Meteorologie van de Landbouwuniversiteit Wageningen. Het resultaat van die werkzaamheden heeft u in het voorgaande kunnen lezen.

